Multiphase steels: Modelling, parameter identification and optimal control

vorgelegt von
Diplom-Mathematikerin
Nataliya Togobytska
geb. in Dnipropetrowsk (Ukraine)

Von der Fakultät II – Mathematik und Naturwissenschaften
der Technischen Universität Berlin
zur Erlangung des akademischen Grades

Doktor der Naturwissenschaften
Dr. rer. nat.

genehmigte Dissertation

Promotionsausschuss:

Vorsitzender:	Prof. Dr. Martin Skutella
Betreuer/Gutachter:	Prof. Dr. Dietmar Hömberg
Gutachter:	Prof. Dr. Oliver Ernst

Tag der wissenschaftlichen Aussprache: 19. November 2014

Berlin, 2014

Abstract

This thesis is concerned with the mathematical modelling, optimal control and parameter identification of phase transformations in multiphase steels. The main focus is on hot-rolled dual phase steels, which combine good formability properties with high strength. Phase transformations in dual phase steels, which occur during the controlled cooling after hot rolling, play an essential role in the formation of the final microstructure and mechanical properties of the material.

Based on the Leblond–Devaux approach, a mathematical model for the austenite-ferrite phase transformation during controlled cooling on the run out table is derived. The ordinary differential equation for the growth of ferrite includes the factor that couples the influence of the austenite grain size and the retained strain before the cooling on the formation of ferrite. The mathematical model for the austenite-martensite transformation incorporates the carbon enrichment during the ferrite formation, which influences the martensite start temperature. The derived model has been validated by means of deformation dilatometer experiments, simulating the hot rolling of dual phase steels.

Dilatometer experiments provide complementary information useful for the modelling of phase transformations in steel. Usually, the data is only used to determine the start and end temperatures of the phase transformation during cooling from the high-temperature phase. In this thesis, an inverse problem is considered to identify the complete phase transformation kinetics from the dilatometer measurements of the temperature and the length change of the steel samples. The inverse problem under investigation is a parameter identification problem for the one-dimensional thermo-elasticity system, which describes the interaction of temperature, displacement and phase transformations in dilatometer experiments. A global stability estimate for the inverse problem is derived using the tools of semigroup theory. It is shown that, in the case of at most two product phases, the complete phase transformation kinetics, including the final phase fractions, are uniquely determined by the dilatometer data.

For the numerical implementation, the parameter identification problem is formulated as an optimal control problem. The state system is discretized using a finite-difference scheme and the unknown phase functions are approximated by cubic splines. The numerical results are presented for the Mo-Mn dual phase steel and compared with experimental data.

An optimal control problem for the production of dual phase steel is investigated that takes into account phase transformations in the steel slab. The state equations are a semilinear heat equation coupled with the ordinary differential equation, that describes the evolution of ferrite fraction. The time-dependent heat transfer coefficient serves as a control function. This optimal control problem is analyzed. Moreover, the necessary and sufficient optimality conditions are derived. For the numerical solution of the control problem, a reduced sequential quadratic programming method with a primal-dual active set strategy is applied. The numerical results are presented for the optimal control of a cooling line in the production of hot-rolled Mo-Mn dual phase steel. The optimal control approach has been verified in hot rolling experiments at the pilot hot rolling mill at the Institute for Metal Forming of the TU Bergakademie Freiberg.

Zusammenfassung

Das Thema dieser Arbeit ist die mathematische Modellierung, Optimalsteuerung und Parameteridentifikation für die Phasenumwandlungen in Mehrphasenstählen. Dabei liegt der Schwerpunkt auf den Dualphasenstählen, die eine gute Umformbarkeit mit einer hohen Festigkeit kombinieren. Phasenumwandlungen in Dualphasenstahl während einer kontrollierten Abkühlung nach dem Warmwalzen spielen eine entscheidende Rolle für die Einstellung der gewünschten Mikrostruktur und mechanischen Eigenschaften des Stahlblechs.

Basierend auf dem Ansatz von Leblond und Devaux, wurde ein mathematisches Modell für die Austenit-Ferrit-Phasenumwandlung entwickelt. Eine gewöhnliche Differentialgleichung für das Wachstum von Ferrit wurde um einen zusätzlichen Faktor erweitert, der den Einfluss der Umformung und Austenitkonditionierung auf die Bildung von Ferrit beschreibt. Das mathematische Modell zur Beschreibung der Austenit-Martensit-Phasenumwandlung berücksichtigt die Kohlenstoffanreicherung des Restaustenits während der ferritischen Phasenumwandlung, was die Martensit-Starttemperatur beeinflusst. Das entwickelte Modell wurde durch Experimente zur Prozesssimulation von Warmwalzvorgängen am Umformdilatometer validiert.

Dilatometerexperimente liefern wichtige Informationen über die Phasenumwandlungen, die für die Modellierung der Gefügekinetik benutzt werden können. Normalerweise werden die Daten nur zur Bestimmung der Anfangs- und Endtemperatur der Phasenumwandlung nach Abkühlung von der Hochtemperaturphase genutzt. In dieser Arbeit wird ein inverses Problem zur Identifikation der kompletten Kinetik der Phasenumwandlungen in Stahl aus Dilatometerdaten untersucht. Ein Parameteridentifikationsproblem für ein eindimensionales quasistationäres Modell der Thermoelastizität wird betrachtet und eine globale Stabilitätsabschätzung für die Lösung des inversen Problems abgeleitet. Es wird gezeigt, dass sich bei maximal zwei Produktphasen, als Funktionen der Zeit die komplette Phasentransformationskinetik eindeutig durch die zeitabhängigen Längenänderungs- und Temperaturmessungen bestimmen lassen. Die numerischen Ergebnisse werden für Mo-Mn-Dualphasenstahl präsentiert und mit experimentellen Daten verglichen.

Ein Optimalsteuerungsproblem für die Kühlstreckensteuerung einer Warmbandstraße zur Produktion von Dualphasenstahl wird untersucht, wobei die Phasenumwandlungen in Stahl berücksichtigt werden. Die Zustandsgleichungen sind eine semilineare parabolische Differentialgleichung für die Temperatur und eine gewöhnliche Differentialgleichung, die die Austenit-Ferrit-Phasenumwandlung in Stahlblech beschreibt. Der zeitabhängige Wärmeübergangskoeffizient trifft als Steuerungsgröße auf. Für dieses Randsteuerungsproblem wird die Existenz einer Lösung gezeigt und die notwendigen und hinreichenden Optimalitätsbedingungen abgeleitet.

Für die numerische Lösung des Optimalsteuerungsproblems wird ein reduziertes SQP-Verfahren (sequential quadratic programming) mit der primal-dualen Aktive-Mengen-Strategie implementiert. Die numerischen Ergebnisse werden für die optimale Steuerung der Kühlstrecke zur Produktion der gewünschten Mikrostruktur für Mo-Mn-Dualphasenstahl präsentiert. Der Steuerungsansatz wurde an der Pilotwalzanlage im Institut für Metallformung der TU Bergakademie Freiberg verifiziert.

Acknowledgments

The research presented in this thesis was carried out during my work at the Weierstrass Institute of Applied Analysis and Stochastics in the project "Simulation, optimization and control of microstructure evolution and mechanical properties during hot rolling of multiphase steels" as a part of the German Research Foundation program SPP1204 "Algorithms for fast, material specific process chain design and analysis in metal forming". My gratitude belongs to numerous colleagues who helped and motivated me during this work.

First, I would like to thank my supervisor, Prof. Dr. Dietmar Hömberg, for his support during all the years and his optimal control of my research work. I greatly appreciate his guidance and encouragement of my attendance at international conferences and summer schools and for giving me the opportunity to collaborate with different experts in the field of steel treatments. I am grateful to Prof. Dr. Masahiro Yamamoto for his valuable comments, suggestions and interesting discussions about the theory of inverse problems. I thank Dr. Marcel Graf from the IMF Freiberg and Dr. Piyada Suwanpiniy from the IEHK Aachen for carring out the various dilatometer and hot rolling experiments, explanations regarding experimental setups and numerous discussions regarding modelling and heat treatment of steel. Many thanks to Jens Seidel from TU Chemnitz for sharing his mathematical knowledge in model reduction, his valuable remarks and ideas during the proofreading of the thesis.

I want to express my gratitude to the colleagues at WIAS, Anke Giese, Konstantin Emich, Kevin Sturm, Dr. Thomas Arnold, Dr. Alfonso Caiazzo, Dr. Marita Thomas, Dr. Daniela Kern, Dr. Oliver Rott, Dr. Lucia Panizzi, Dr. Thomas Petzold, who were always available for discussions. Special thanks go to Swetlana Schyschlowa, Dr. Chantal Landry and Dr. Beatrice Bugert for their moral support, valuable hints and the proofreading of the thesis. I thank Dr. Wolf Weiss for pleasant and constructive working atmosphere and for his support in understanding the concepts of thermomechanics and the physical background of investigated problems. Many thanks to Timo Streckenbach for his practical help and valuable remarks regarding pdelib. Furthermore, I would like to thank Dr. Klaus Krumbiegel for sharing his broad mathematical knowledge of theory and numerical algorithms for optimal control of PDEs.

My sincere gratitude to Svitlana Kolinski and all my friends from Cottbus for their moral support and motivation.

Finally, I would like to thank my family, in particular my parents Daria and Pavel, my sister Tanja and Denis for their support and faith in my abilities in helping me to complete this research. My especial thanks to my husband Yevgen and my son Bogdan for their patience and always motivating and active support of my work.

Contents

Chapter 1

Introduction

> "*In a way, the sense of quality has improved, the status symbol of the small things is gone, and it is acceptable to use stainless steel, even if the neighbour uses silver.*"
>
> Arne Jacobsen

In recent years, numerous new functional materials have been developed. Nevertheless, steel remains the most successful and cost-effective of all materials, with more than a billion tonnes being consumed annually in improving the quality of life. In particular, the increasing steel production has been triggered by the demands of automotive industry. In 1999, a group of 33 international steel producers formed the Ultra Light Steel Auto Body - Advanced Vehicle Concepts (ULSAB-AVC) consortium to pursue a steel-intensive family car, fit for the 21st century, that would be safe, affordable and fuel-efficient. According to the results of the ULSAB-AVC Program, an automotive body could be constructed by utilizing approximately 85 % of so-called "Advanced High Strength Steels" (AHSS), achieving a weight reduction of 25 % compared to a benchmarked "average base model" and without any increase of the manufacturing costs [81].

The AHSS are characterized by their multiphase structures. They have excellent mechanical, forming and even energy absorbing properties. The multiphase AHSS family includes Dual Phase (DP), Transformation Induced Plasticity (TRIP) and complex multiphase steels. Of all currently available types of AHSS, the most commonly used in automotive applications are dual phase steels. Applications of dual phase steels are, for example, wheel disks, wheel webs, B-pillar and longitudinal structural members such as beams and chassis in automobiles (cf. [2, 18]) as shown in Figure 1.1.

The critical part in the manufacturing process of multiphase steels is to control the processing conditions so that the optimal microstructure and, hence, the optimal mechanical properties of the material are achieved. The essential industrial process route for the production of multiphase steels, e.g., DP steel and TRIP steel, consists of the hot rolling and subsequent controlled cooling on the run out table which is located behind the finishing mill. The control of the cooling process allows to adjust the desired final microstructure of steel. Therefore, the mathematical modelling and proper optimal control approaches for a run out table of hot rolling mills are of crucial importance for the industrial production of multiphase steels.

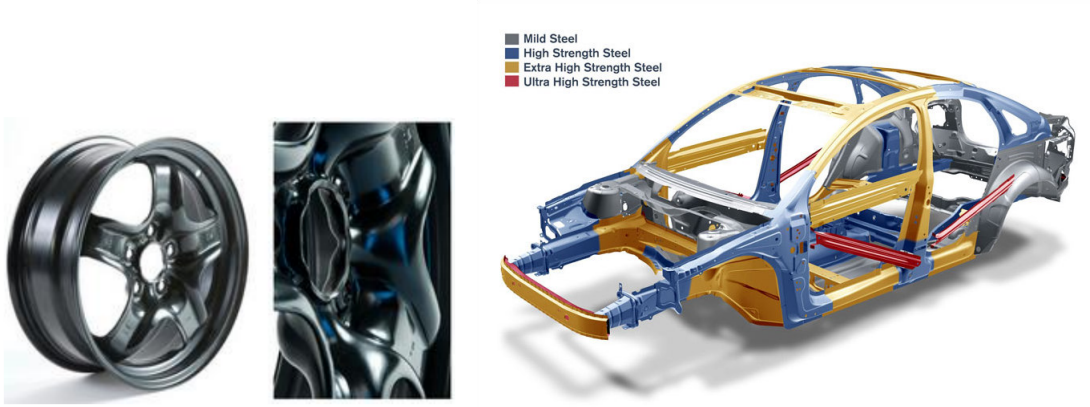

Figure 1.1: Wheel webs in car wheels fabricated by Hayes Lemmerz International, produced from hot-rolled dual phase steel [2] (left). Steel composition in Volvo S40 [18] (right).

1.1 Subject of the thesis

This thesis presents the results that were obtained by research carried out within the project "Simulation, optimization and control of microstructure evolution and mechanical properties during hot rolling of multiphase steels". The project is part of the German Research Foundation program SPP1204 "Algorithms for fast, material specific process chain design and analysis in metal forming". The work on this project benefited from the cooperation between mathematical and engineering institutions, the Weierstrass Institute for Applied Analysis and Stochastics, Leibniz Institute in Forschungsverbund Berlin e. V. and the Department of Ferrous Metallurgy of RWTH Aachen. This project aimed at developing a model for the fast cooling control of a hot strip mill. It comprises the modelling and efficient simulation of the structural transformation as well as the prediction of the mechanical properties of the finish product. Accordingly, this thesis is application-driven and combines mathematical analysis with numerical treatment of a practical task from engineering.

The goal of the thesis is the investigation of multiphase steels from a mathematical point of view, i.e., the modelling and analysis of the kinetics of phase transformations and optimal control of the process parameters in a cooling line for the production of multiphase steels. The main focus is on dual phase steels. The microstructure of these steels which, in turn, defines the mechanical properties of a final product, strongly depends on the phase transformations during the heat treatment. Therefore, studying the kinetics of phase transformations is of crucial importance for the production of dual phase steels.

In this work, a mathematical model for the phase transformations in hot-rolled dual phase steels is developed in close cooperation with the Department of Ferrous Metallurgy of the RWTH Aachen. The model should be the basis for further simulations and the optimal control of the process parameters for the adjustment of a desired dual phase microstructure. Here, the most important impact factors of the hot rolling process on the kinetics of phase transformations should be taken into account. The main focus is on the austenite to ferrite phase transformation. The model involves the acceleration effect of

the retained strain from the last finishing stand as well as of the austenite conditioning before cooling on the austenite-ferrite transformation. It is based on the Leblond–Devaux approach proposed for the first time in 1984 in [50], but is additionally extended by a factor that couples the influence of the austenite grain size and the retained strain before the cooling process on the formation of ferrite. The identification of parameters in the model is carried out by using the data obtained from dilatometer experiments.

In engineering practice, dilatometer experiments are widely used to detect the kinetics of solid-solid phase transformations in steel upon cooling from the high-temperature phase. Usually, the data are only used for measuring the start and end temperatures of a phase transformation. In the case of several coexisting product phases, expensive microscopic investigations have to be performed to obtain the resulting fractions of the different phases. One of the aims of this thesis is to extend the methodology of the evaluation of dilatometer data in order to gain maximum information about the phase transformations. It will be shown that in the case of at most two product phases the complete phase transformation kinetics, including the final phase fractions, can be uniquely determined by the dilatometer data.

The problem of identifying phase transformations from dilatometer measurements is formulated as an inverse problem. It results in a parameter identification problem for the thermo-elasticity system which describes the dilatometer experiment. The key point is the mathematical investigation of the inverse problem. In particular, for the practical employment of the numerical computations, the crucial issue is to investigate the continuous dependence of the solution of the inverse problem on the measurement data. To this end, a global stability estimate for the inverse problem is derived. Numerical results obtained by the solution of the inverse problem confirm the theoretical result.

Another focal point of the work is an optimal control of the process parameters in a cooling line for production of dual phase steels. The standard process route for the production of dual phase steels consists in hot rolling with subsequent controlled cooling to adjust the desired dual phase mixture. Since the process window for the adjustment of the phase composition is very tight, the computation of optimal process parameters is an important task also in practice. Here the most important control parameters are the flow-rate of water in cooling line and the feed velocity of the strip. The controlled cooling of steel is a well-studied topic in engineering science and mathematics. However, the existing optimal control approaches for run out tables up to now solely focus on the evolution of temperature. In this thesis, an optimal control approach is proposed which additionally takes the phase transformations into account.

The optimal control problem consists in obtaining the cooling strategy such that the desired dual phase microstructure in steel is reached most accurately. This problem is a nonlinear boundary control problem, in which the state system consists of a semilinear heat equation coupled with an ordinary differential equation. The latter describes the evolution of the ferrite phase fraction. The time-dependent heat transfer coefficient serves as a control function. The mixed boundary condition and the control of the parameter function, i.e., the heat transfer coefficient function, is challenging with respect to mathematical analysis. The optimal control problem is analyzed and the first-order necessary and second-order sufficient optimality conditions are derived. For the numerical solution of the control problem, the reduced sequential quadratic programming method with a primal-dual active set strategy is applied. The application of the proposed control ap-

proach is validated by experiments performed at the pilot hot rolling mill at the Institute for Metal Forming (IMF) of the TU Bergakademie Freiberg.

1.2 Outline

In **Chapter 2**, some important material properties of steel are introduced. Moreover, the phase transformations in steel during a heat treatment are explained.

The modelling of the phase transformations in dual phase steel is addressed in **Chapter 3**. In the beginning of this chapter, the introduction to multiphase steels and the brief description of the production process for this steels are given. The main objective of this chapter is to derive a mathematical model for austenite-ferrite and austenite-martensite phase transformations. The model for the ferrite growth is based on the Leblond–Devaux approach, modified by a factor which couples the effect of austenite grain size and retained stress on the formation of ferrite. In the modelling of the martensite transformation, the carbon enrichment during the ferrite formation is taken into account. In the last section, the model verification by measurements from the hot deformation dilatometer is discussed.

The aim of **Chapter 4** is a mathematical investigation of dilatometer experiments. Here, the inverse problem for the identification of the phase transformation kinetics by two dilatometer measurements is studied. The interactions between temperature, mechanical behaviour and phase transformations in steel during the dilatometer experiment are described by a one-dimensional thermo-elasticity system. The key point of this chapter is the analysis of the direct and inverse problem. The main result is a global stability estimate for the solution of the inverse problem, which is an important theoretical result for the numerical computations. The numerical identification of two phase fractions from dilatometer measurements is first carried out for the model data of the plain carbon steel C1080. Then, the numerical results for the real dilatometer data of dual phase steel are presented.

Chapter 5 is concerned with the mathematical analysis of the optimal control problem of the heat transfer coefficient for a semilinear parabolic system. The formulation is based on a concrete application, namely on the controlled cooling of dual phase steel in a hot rolling mill. In this control problem, the state system consists of a semilinear heat equation and an ordinary differential equation which describes the kinetics of the austenite to ferrite phase transformation. The control function is a time-dependent heat transfer coefficient. In the first part of this chapter, the state system is analyzed and the existence of a solution of the optimal control problem is investigated. Moreover, the first-order necessary and second-order sufficient optimality conditions are derived. The second part of this chapter contains the description of the numerical implementation. The numerical algorithm applied to the control problem is the reduced sequential quadratic programming method with a primal-dual active set strategy. The numerical test demonstrates the convergence of the applied numerical algorithm.

In **Chapter 6**, the focus is on the optimal control of a cooling line for the production of dual phase steel in a hot rolling process. The aim is to compute the optimal cooling strategy such that the desired dual phase microstructure is achieved most accurately. At the beginning of the chapter the hot rolling process for dual phase steels is introduced. Then,

the modelling of heat transfer in a cooling line is considered. The problem of controlled cooling is formulated as the optimal control problem which is discussed in Chapter 5. Finally, the last section of this chapter is devoted to the numerical implementation of the formulated control problem using the numerical algorithms introduced in Chapter 5. The numerical results are presented for the Mo-Mn dual phase steel.

In the appendix, an overview of the notations and utilized theorems is given.

Remarks on the notation throughout this thesis

The variable c with or without index usually denotes a generic constant. This is the case especially for inequality chains. The variable c_p refers to the specific heat capacity of steel.

Additional to subscripts, also superscript variables and superscript natural numbers usually denote indices and determine the considered component. Superscript 2 and, e.g., p, q could also denote squaring or taking the respective power, but this will be clear from the context.

Chapter 2

Basics of steel

2.1 Material properties

Steel is an alloy that consists mostly of iron and has a carbon content between 0.0002 % and 2.1 % by weight. Carbon is the most common alloying material for iron, but various other alloying elements are used, such as nickel, manganese, chromium, vanadium etc. About 2000 steels are technically relevant and usually have several alloying elements along with the element iron. Varying the amount of alloying elements and the form of their presence in the steel controls qualities such as hardness, ductility, and tensile strength of the resulting steel. Too little carbon content leaves (pure) iron quite soft, ductile, and weak. Cast iron usually has a higher carbon content of around 2.0 mass-% to 4.0 mass-%, and is further processed using casting techniques [8]. Cast iron is very resistant, but has bad forming properties, it cannot be shaped and is prone to damages by breaking.

Heat treatments, i.e., processes of controlled heating and cooling, influence the grid structure, in which iron and carbon atoms are arranged. Depending on temperature and pressure, iron exists in a number of molecular forms (allotropes), where the atoms are bonded together differently. At a temperature above 912 °C, iron possesses a face-centred cubic (fcc) lattice and is called γ-iron. Below 912 °C, iron has a body-centered cubic (bcc) crystal structure known as α-iron (see Figure 2.1).

In transforming between γ- and α-iron or vice versa, the iron passes through an allotropic change, that is, a change in crystal structure. It is important to understand this allotropic change because it is an important part of the foundation for phase transformations in steel. An important aspect of the allotropic change in iron is the accompanying change in volume. For example, in transforming from γ-iron to α-iron, there is an expansion upon cooling, and upon transforming back (heating), there is a contraction. This volume change can be detected by sensitive instruments. In fact, the dilatometer, an instrument found in most steel-related research laboratories, is based on measuring the volume changes that take place during a phase transformation.

The physical properties of steel such as strength, toughness, ductility, hardness and corrosion resistance are strongly influenced by its microstructure. The microstructure of steel is composed of chemically and physically homogeneous microregions that are separated by interfaces and called *phases*. The main phases and phase mixtures in steel are the following:

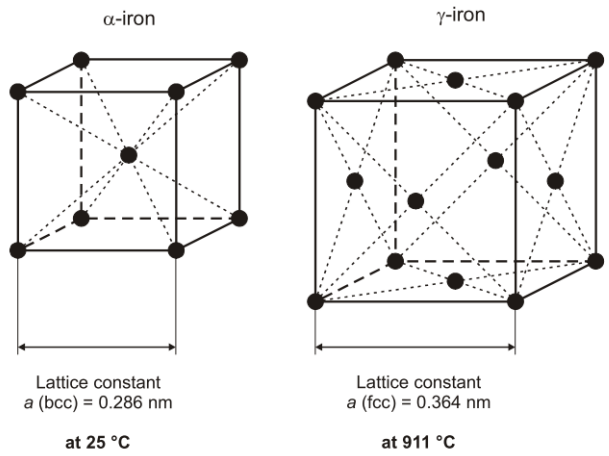

Figure 2.1: Crystal structures of pure iron, from Bleck [8].

- **Austenite** is a solution of carbon in a cubic face-centered iron crystal (γ-iron). The solubility of carbon reaches a maximum of 2.1 % at 1148 °C and decreases to 0.8 % at 727 °C. The carbon atoms are dissolved interstitially, i.e., in the spaces (vacancies) within the crystal lattice of iron, see, e.g., [8]. The term "austenite" is named after Sir William Chandler Roberts-Austen, an early English metallurgist. In most steels, austenite is a high-temperature phase and generally exists only above about 700 °C. However, some steels, for example, the austenitic stainless steels are 100 % austenite at room temperature [12]. Austenite is soft and ductile.

- **Ferrite** (from Latin "ferrum") is a solution of carbon in a body-centered iron crystal (α-iron). The maximum carbon solubility in bcc iron is 0.02 mass-% at 720 °C while the carbon solubility in bbc iron at room temperature is very low (10^{-5} mass-%). In its typical shape, it looks like a sequence of polyhedral-shaped surfaces in the two-dimensional representation of flat metallographic sections, see Figure 2.2A. The microstructure shown in Figure 2.2 is typical for a very low-carbon steel.

- **Cementite** also known as iron carbide (Fe_3C), is a chemical compound of iron and carbon. By weight, it is 6.67 % carbon and 93.33 % iron. The name cementite comes from cementation steel, which was an early process used to produce high-carbon steel through carburization, by which carbon is absorbed into the steel by packing it in charcoal and heating to a high temperature. In steels, cementite is never present as 100 % of a microstructure. It is often associated with ferrite as a constituent of pearlite and bainite. Cementite is extraordinarily hard, it has a lower density than iron and is magnetic at room temperature.

- **Pearlite** is the ferrite-cementite phase mixture. The name "pearlite" comes from the golden yellow sheen often appearing in light microscopy, which resembles mother-of-pearl. The metallographic structure of pearlite is shown in Figure 2.2B. In commercial steels, a fully pearlitic structure is sometimes desirable, as in rail steel and piano wire, because of the hardness, wear resistance (rail), and high strength (piano wire) imparted.

- **Martensite** is a constituent that forms during rapid cooling (quenching) of steel. It is a body-centered tetragonal crystal, hard and brittle. Martensite was named after the German scientist A. Martens (1850–1914), who directed the Royal Materials Testing Office, which was founded in 1904 and was a predecessor to the present Institute for Materials Testing and Research in Berlin (Bundesanstalt für Materialprüfung, BAM). The metallographic structure of martensite is presented in Figure 2.2C. One application of a martensitic steel is in razor blades. In this case, the martensite imparts high strength and hardness, which allows the blade to maintain a sharp cutting edge.

- **Bainite** is a mixture of ferrite and cementite. First described by E. S. Davenport and Edgar Bain, it is one of the decomposition products that may form when austenite is cooled below a critical temperature of 727 °C. Bainite is an intermediate of pearlite and martensite in terms of hardness. The metallographic structure of bainite can be seen in Figure 2.2D.

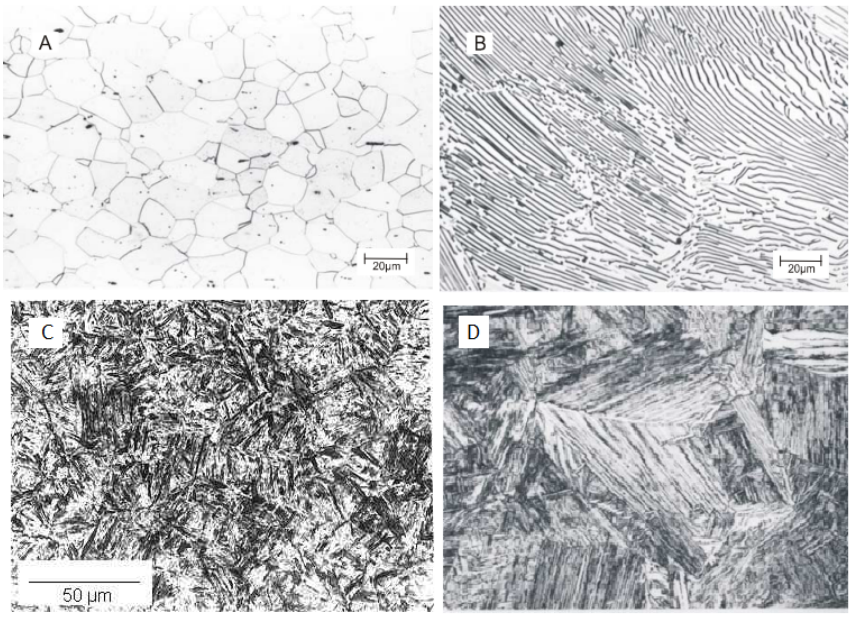

Figure 2.2: Optical microscope photo of ferrite (A), pearlite (B), martensite (C), and bainite (D) microstructure, from Bleck [8].

A study of the microstructure of all steels usually starts with the metastable iron-iron carbide (Fe-Fe_3C) diagram, see Figure 2.3. In this diagram, the correspondence of temperature and carbon concentration to metastable steel phases is presented. For most carbon steels the phase diagram up to 2.06 mass-% carbon is adequate. If the influence of other alloying elements and cooling rates are neglected, the phase diagram for up to 0.8 mass-% carbon is sufficient to describe the near-equilibrium transformations for over 90 % of the steels produced in Germany, cf. Bleck [8].

The iron-carbon phase diagram in Figure 2.3 only represents iron-carbon binary alloys and does not apply to iron-carbon alloys containing other elements such as manganese,

silicon, nickel, chromium, molybdenum, vanadium, and so on. Any of these elements, if added to an iron-carbon alloy, would expand or contract the phase fields shown in Figure 2.3. Nevertheless, for all practical purposes, the iron-carbon diagram can be used as a basic guide to the origin of the microstructure in steels. More information about material properties of steel and iron-carbon phase diagrams can be found, e.g., in Bramfitt and Benscoter [12] and Bleck [8].

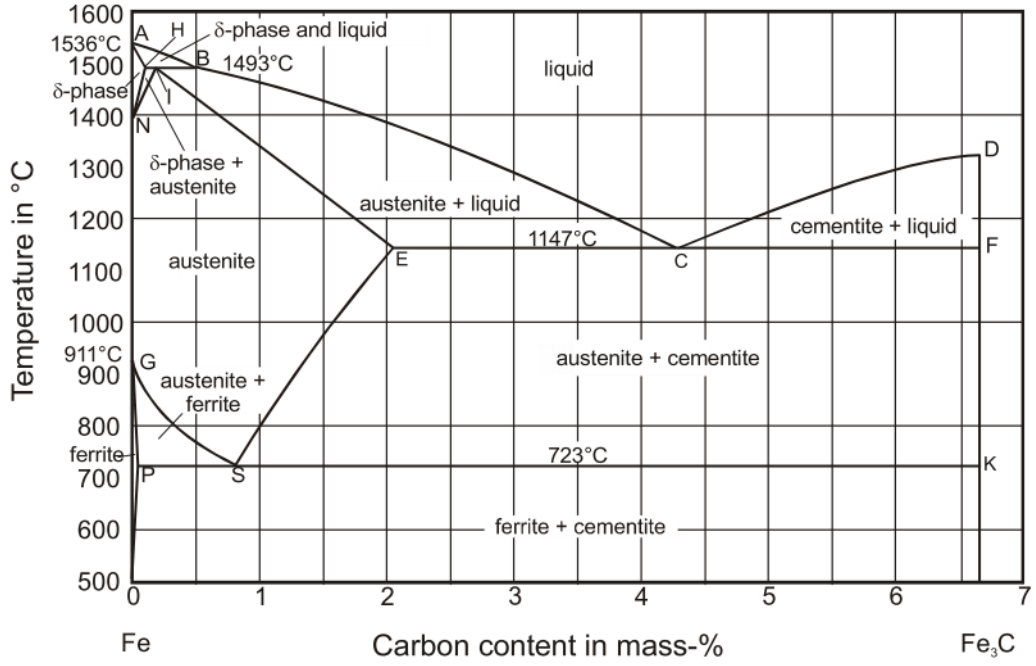

Figure 2.3: Phase diagram of Fe-Fe_3C (metastable equilibrium).

The great variety of properties in steels is primarily due to the possibility of adjusting the microstructures of steels over a wide range. The heat treatment of steels intended to establish a particular microstructure is usually started by heating it into the austenite range, i.e., austenitization. Then, steels are often cooled from austenite to the room temperature. The phase transformations occurring during cooling are discussed in the next section.

2.2 Phase transformations

The phase transformations in steel can be divided into diffusion-controlled and diffusionless transformations. The phases ferrite and cementite, as well as the phase mixture pearlite, are formed by diffusion-controlled processes [8]. During diffusionless phase transformations, atoms move only over distances that are significantly smaller than the length of one lattice space. Therefore, these transformations can also occur at lower temperatures where diffusion is no longer possible. If the transformation occurs without diffusion by means of a shearing process, then the martensitic phase, which forms at high cooling rates below 500 °C, is created as a transformation product [8]. A combination of diffusion-controlled and shear transformation can appear within a wide range of the cooling rate.

Such transformations are called bainitic transformations.

Our main focus is on the phase transformations in multiphase low-carbon steels with a carbon content of less than 0.3 mass-%. The phase transformations that can appear during cooling from the austenitic phase and the resulting microstructures are given in Table 2.4. We consider these phase transformations in more detail.

Characteristic	**Type of phase transformation**			
	I		**II**	**III**
1. Mechanism	diffusion-controlled		bainitic	diffusionless
2. Microstructure	ferritic-pearlitic		bainite	martensite
	equiaxial α + normal pearlite	irregular α + carbide-poor pearlite	granular bainite to upper bainite	lath martensite
3. Parameters:				
3.1 Transformation temperature	approx. 900 to 640 or 510 °C		approx. 640 to 510 °C	below 510 °C
3.2 Cooling rate	very slow up to approx. 160 °C/s		approx. 160 to 3000 °C/s	higher than 3000 °C/s

Figure 2.4: Phase transformations while cooling from the austenitic state of an unalloyed steel with approx. 0.08 mass-% carbon. Source: Bleck [8].

Ferritic-pearlitic transformation

In many technological processes, the austenite-ferrite ($\gamma \rightarrow \alpha$) transformation is of great importance because it occurs at temperatures used in heat treatments and hot deformation processes. We consider a slow cooling from the austenite temperature region to the room temperature. Figure 2.5 shows a part of the iron-carbide diagram and some stages of the microstructural development along the cooling process.

At point a) the alloy is fully austenitic. The transformation of austenite begins when the temperature is reached at point b). Ferrite nucleates on the grain boundaries of austenite. As cooling continues, ferrite grows along the grain boundaries. The growth process is characterized by the diffusion of carbon out of the ferrite into the austenite, since a maximum of 0.02 mass-% carbon is soluble in ferrite. It causes a respective increase in the carbon content on the phase boundaries of the austenite. At point c) a microstructure is present in which ferrite completely covers the austenite grain boundaries. At this point, the microstructure consists of up to almost 40 % ferrite. A further cooling below the eutectoid temperature of 727 °C leads to a transformation of the remaining 60 % austenite into pearlite (point d) [8]. Thus, the final microstructure of the steel consists of ferrite and pearlite.

There are some factors that influence the rate of nucleation and growth of ferrite. Some of these factors are: the nature of the austenite under consideration, the temperature of transformation and the presence of alloying elements. These factors should be taken into

account when modelling the kinetics of the austenite-ferrite phase transformation. In Chapter 3, we will discuss the effect of the austenite conditioning and the amount of deformation on the modelling of ferrite growth in hot-rolled dual phase steels.

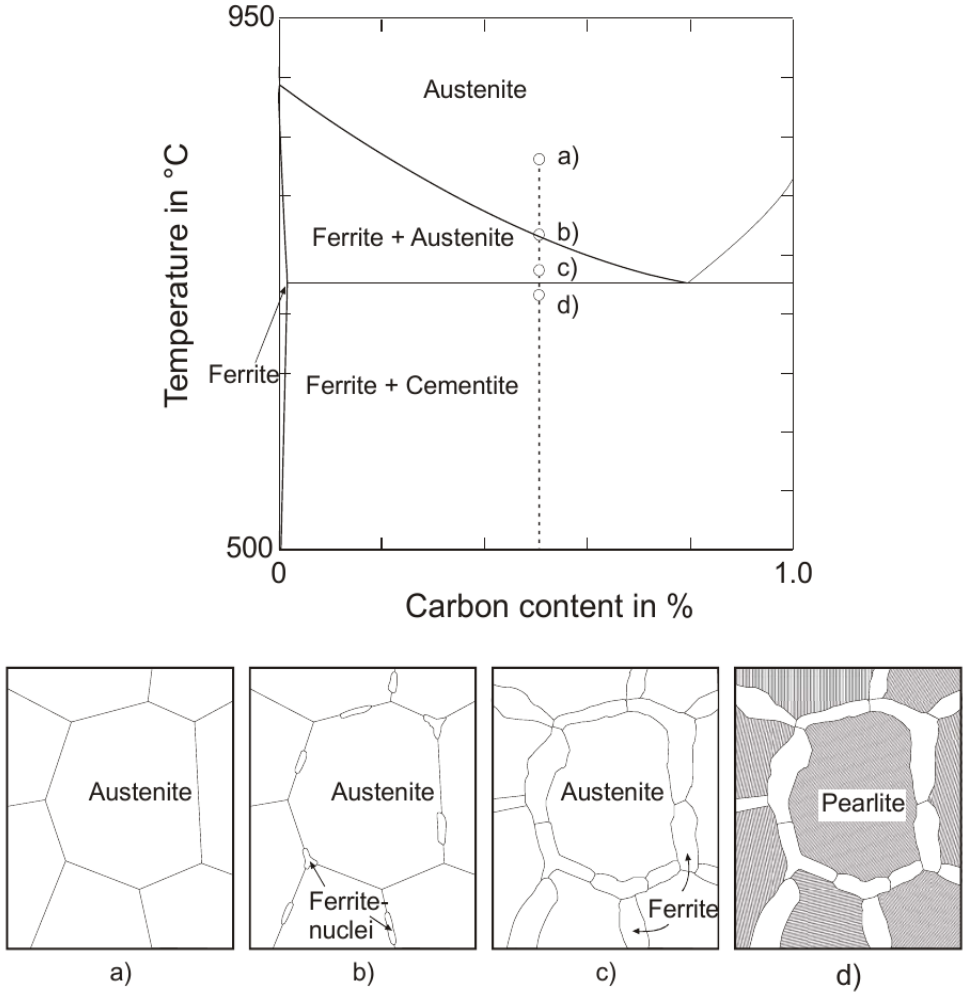

Figure 2.5: Section of the metastable iron-carbon diagram (top). Sketch of the microstructural development from austenite to pearlite for an alloy with 0.5 mass-% carbon (bottom), from Bleck [8].

Martensitic transformation

If the material is cooled down rapidly (quenched), carbon has no time to diffuse and is trapped inbetween the reconfiguring lattice. This results in shifted body-centered tetragonal cubic crystals of martensite. The austenite-martensite transformation is responsible for the outstanding position of steel because it permits the extreme hardenability of the material. This phase transformation has the following characteristic attributes:

- It usually occurs athermally at low temperatures. It begins suddenly when a certain temperature is reached during cooling and proceeds cascade-like in a fraction

of a second when cooling continues. If the cooling is stopped, then the further transformation also stops, although "para"-equilibrium has not yet been reached [8].

- Because of the low transformation temperature and the nevertheless high transformation velocity, the diffusion evidently does not determine the movements of the atoms. Only the type of lattice is changed, by means of a strictly co-ordinated movement of the atoms. The cubic face-centered lattice of austenite shears to the cubic body-centered martensite [8].
- The martensite transformation of a given alloy cannot be suppressed, nor can the martensite start temperature M_s be changed by changing the cooling rate. The temperature range of the formation of martensite is characteristic of a given alloy. Most alloying elements lower the martensite start temperature M_s, with the exception of cobalt and aluminium. The effect of carbon on both martensite start M_s and finish M_f temperatures is shown in Figure 2.6. Note that above 0.7 mass-% carbon the M_f temperature is below room temperature and consequently higher carbon steels quenched into water will normally contain substantial amounts of retained austenite, cf. [12], Chapter 5.6.2.

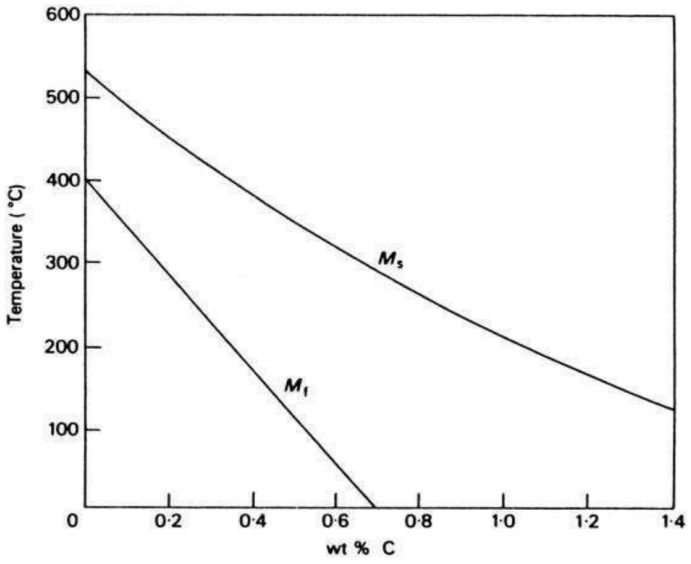

Figure 2.6: The effect of carbon on M_s and M_f, from [12].

Many formulas have been experimentally determined for the dependency of M_s upon composition of steels, cf. [8, 12, 84]. According to [12], one empirical formula is

$$M_s[\mathrm{K}] = 539 - 423(\%\mathrm{C}) - 30.4(\%\mathrm{Mn}) - 17.7(\%\mathrm{Ni}) - 12.1(\%\mathrm{Cr}) - 7.5(\%\mathrm{Mo}). \quad (2.1)$$

The equation applies to a limited class of steels. Thus, the gradient of the curve in Figure 2.6 is different from that implied by the empirical relationship (2.1).

Bainitic transformation

The bainite transformation is intermediate between pearlite and martensite transformations. The kinetics of this transformation and the structures formed exhibit features of

both, the diffusive pearlite transformation and the diffusionless martensite transformation. A mixture of the α-phase (ferrite) and carbide is formed as a result of the bainite transformation. The bainite transformation mechanism involves $(\gamma - \alpha)$ rearrangement of the lattice, redistribution of carbon, and precipitation of carbide. A distinction is drawn between the upper and the lower bainite, which are formed in the upper and lower parts of the intermediate temperature range 550 °C–250 °C. The difference in the structures of upper and lower bainites is attributed to a different mobility of carbon in the upper and lower parts of the bainite temperature range. In upper bainite, carbon-rich components, such as carbide, martensite, and/or retained austenite, appear between the needles of the bainitic ferrite. In the lower bainite, carbides precipitate out within the ferrite plates. Both types of bainite can appear in the microstructure concurrently [78].

For more details on the kinetics and morphology of the phase transformations in steel we refer to Bhadeshia and Honeycombe [6], Bleck [8].

We have seen, for the case of ferritic-pearlitic transformation, how the equilibrium diagram iron-cementite can be used for the description of phase transformations in steel. However, equilibrium diagrams are only valid for infinitely-slow heating or cooling rates. During cooling or heating at rates normally applied in heat treatments, phases and arrangements of phases may form, which do not correspond to the equilibrium diagram, as, for instance, in the case of martensitic transformation. Information about the connection of the cooling rate and phase evolution can be drawn from the Continuous-Cooling-Transformation diagrams described in the next section.

2.3 Time-Temperature-Transformation diagrams

The use of Time-Temperature-Transformation (TTT) diagrams followed the pioneering work of Davenport and Bain (1930) in studying the isothermal transformation behaviour of carbon steels. Davenport and Bain first introduced the isothermal transformation approach, and showed that by studying the reaction isothermally at a series of temperatures, a characteristic time-temperature-transformation or TTT curve can be obtained for each particular steel. In their simplest form, these transformation curves have a well-defined "C" shape (see Figure 2.7), where the nose of the curve represents the temperature at which the reaction proceeds most rapidly, slowing down both at higher and at lower temperatures.

Isothermal transformation diagrams

One of the simplest examples of an isothermal transformation (IT) diagram is that for an eutectoid carbon steel which contains 0.79 mass-% carbon and therefore transforms entirely to pearlite over a range of temperatures well below 727 °C. The IT diagram for this steel is shown in Figure 2.7.

The region marked by "A" represents austenite, whereas "F" represents ferrite, and "C" represents cementite. Here A_s and M_s denote the starting temperatures for the formation of pearlite and of martensite, respectively. Figure 2.7 was produced by fast quenching from the austenitizing temperature to a series of temperatures below 727 °C and subsequent holding at those temperatures. For fixed temperatures, the bold lines

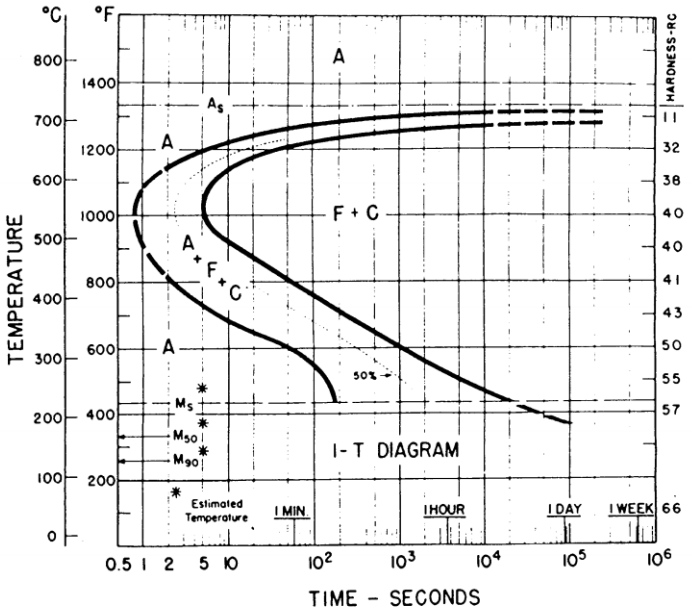

Figure 2.7: The isothermal transformation diagram for the plain carbon steel C1080 (from [3]).

indicate the beginning of the austenite-pearlite transformation, i.e., the time when 1 % of the austenite has been transformed, and the end of the transformation, i.e., the time at which 99 % of the austenite has been transformed. For example, if the steel is held at 400 °C, the austenite will start to transform to ferrite and cementite in about 3 seconds and complete the transformation in about 100 seconds.

Continuous-Cooling-Transformation diagram

Many of the heat treatments performed on steel are carried out by continuous cooling rather than by isothermal holding. As a result, diagrams that represent the transformation of austenite for cooling at various rates have been developed. The latter type of the diagram for a given steel is referred to as a Continuous-Cooling-Transformation (CCT) diagram.

A CCT diagram is developed in the following way. Many small specimens are austenitized and cooled within a dilatometer with different cooling rates. The start and the finish of the transformation of relevant phases with each cooling curve are recorded and then these points are connected to obtain the regions of transformation for the relevant phases (see Figure 2.8).

A CCT diagram can be read only in the way in which it was developed, i.e., along the cooling curves. As can be seen from Figure 2.8, a single-phase structure occurs only in cases of very high cooling rates (martensite) and very slow cooling rates (pearlite). In all other cooling regimes, a mixture of martensite and pearlite phases results. When comparing the curves for the start of transformation in CCT and IT diagrams (Figure 2.7 and Figure 2.8), we find that in the CCT diagram the curves are slightly shifted to longer times and lower temperatures.

Another example is the CCT diagram for Mo-Mn dual phase steel plotted in Figure 2.9. Depending on the cooling rate, the product of ferrite, pearlite, bainite and martensite can be present in the final microstructure of this steel. How much of each phase the microstructure contains can be read in percentage from the numbers along the cooling curve. The numbers at the end of each cooling curve denote the relevant hardness after quenching. For example, as shown on the first cooling curve from the left, a mixture of 70 % bainite and 30 % martensite will result at room temperature, and the hardness after quenching will be 296 HV (Vickers Pyramid Number).

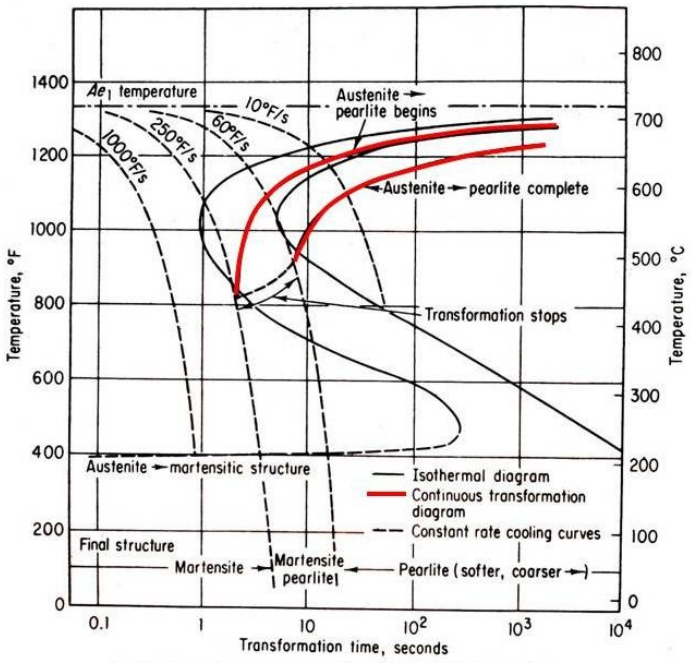

Figure 2.8: Continuous-Cooling-Transformation diagram for the plain carbon steel C1080 (from [86]).

It should be noted that the TTT diagrams are an important tool in the derivation of the model equations for the kinetics of phase transformations in steel. Descriptions of how the parameters of phase equations are derived from TTT diagrams, are given, e.g., in [33, 90].

In Chapter 4 we discuss the problem of how the kinetics of phase transformations can be identified from the dilatometer measurements used for the derivation of the CCT diagram.

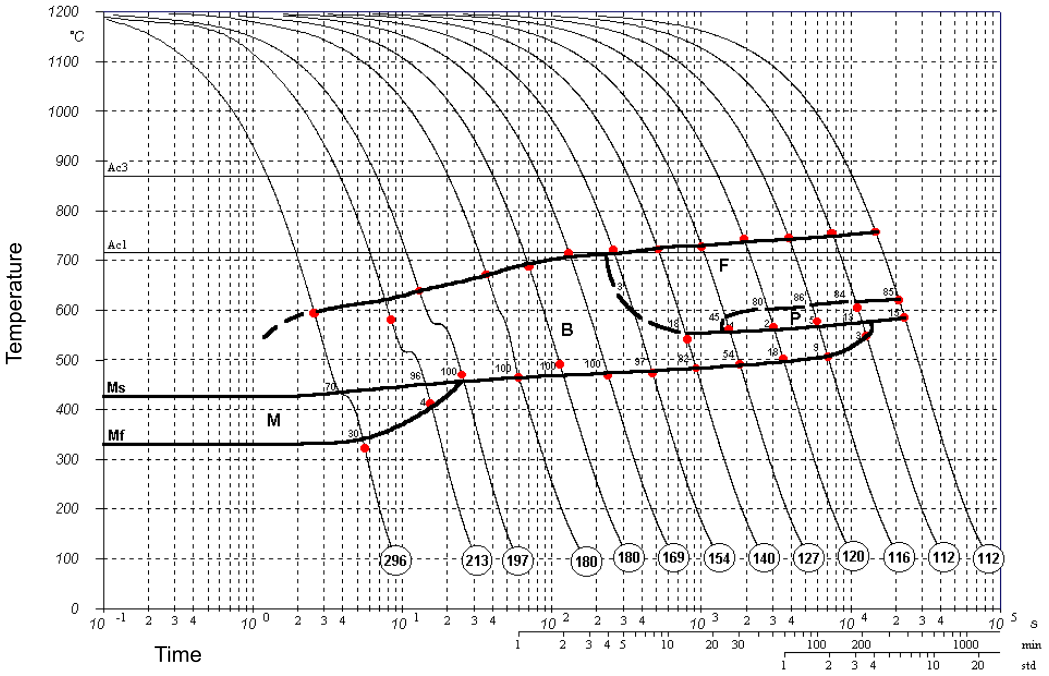

Figure 2.9: Continuous-Cooling-Transformation diagram for Mo-Mn dual phase steel (developed at IEHK Aachen).

Chapter 3

Modelling of phase transformations in hot-rolled multiphase steels

Phase transformations in steel during heat treatment play an essential role in the formation of the final microstructure and the mechanical properties of steel. For this reason, modelling of phase transformations in steel is of great importance for industrial applications and is a wide field of research.

This chapter is concerned with the modelling of phase transformations in multiphase steels, in particular, in hot-rolled dual phase steels. The main focus lies on the evolution of the soft and ductile phase ferrite during isothermal holding of the steel slab on the run out table, and on the formation of hard and brittle phase martensite upon the subsequent quenching. The mathematical model includes the main factors that influence the kinetics of the phase transformations in hot-rolled dual phase steels. These factors are the austenite grain size and the retained strain from the last deformation step before the cooling line that affect the ferrite transformation on the run out table. At the same time, the mathematical model for the austenite-martensite transformation incorporates the carbon enrichment during the ferrite formation that influences the martensite start temperature.

This chapter begins with an introduction to multiphase steels and a brief description of the production process of hot-rolled DP and TRIP steels. Then, in Section 3.2, the mathematical model for austenite-ferrite and austenite-martensite phase transformations is discussed. Finally, Section 3.3 is devoted to the comparison between the simulated and the measured transformation data from deformation dilatometer experiments.

3.1 Multiphase steels

Multiphase steels are new Advanced High Strength Steels, which have been developed for the automobile industry for the purpose of reducing car body weight. These steels contain ferrite, martensite, bainite, and/or retained austenite in quantities sufficient to produce unique mechanical properties. In particular, the multiphase steels offer an excellent combination of high strength and large elongation due to the coexistence of harder and softer phases in their microstructure. The most well-known multiphase steels are Dual Phase (DP) steels and Transformation Induced Plasticity (TRIP) steels.

Figure 3.1 shows the strength and ductility properties for a number of different steel

grades. While classical single phase steels either have good ductility (ferritic steels) or strength (martensitic steels), modern multiphase steels like dual phase or TRIP steels have shown high potential especially for automotive applications. This goes back to their remarkable properties combining high strength and good ductility. As can be seen in Figure 3.1, these steels are located in the middle of the diagram.

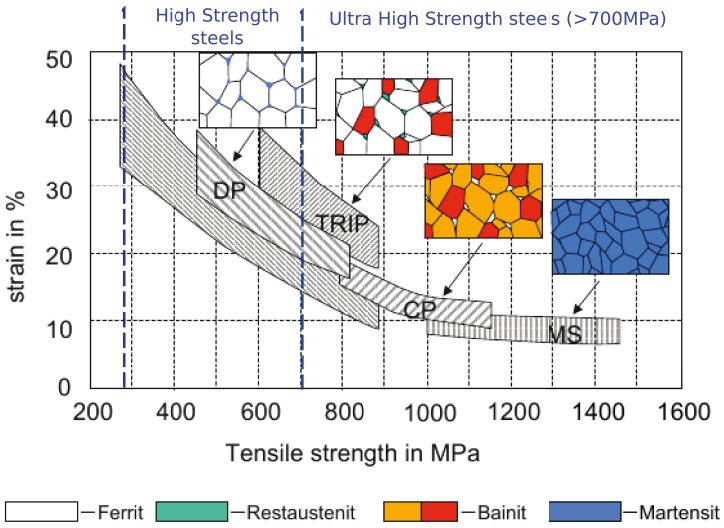

Figure 3.1: Typical combinations of strength and ductility exhibited by different steel grades.

Remark 3.1.1. *Tensile strength (or ultimate tensile strength) is defined as the measurement of the amount of force necessary to tear a piece of steel apart. The amount of strength is typically measured in megapascals (*MPa*). The % of strain shows how much the metal will stretch before it fractures or breaks.*

Dual phase steels are characterized by a microstructure consisting of a fine dispersion of hard martensite particles in a continuous, soft, ductile ferrite matrix (see Figure 3.2). These steels have been thoroughly studied after the early work of Rashid (1976, 1977) who showed that a microstructure consisting of a dispersion of martensite grains in a ferrite matrix can bring about enhanced mechanical properties. The soft ferrite phase is generally continuous, giving these steels excellent ductility. When these steels deform, strain is concentrated in the lower-strength ferrite phase surrounding the islands of martensite, creating the unique high work-hardening rate exhibited by these steels.

DP steels are produced by controlled cooling from the austenite phase (in hot-rolled products) or from the two-phase ferrite plus austenite phase (for continuously annealed cold-rolled products) to transform some austenite to ferrite before a rapid cooling transforms the remaining austenite to martensite. The processing routes are depicted in Figure 3.3.

With the addition of appropriate alloying elements, hardenability of the alloy is adjusted such that the austenite to martensite transformation occurs at cooling rates that are achievable in modern continuous annealing lines for cold rolled products, or on the run out table of a hot mill in the case of hot-rolled products [54].

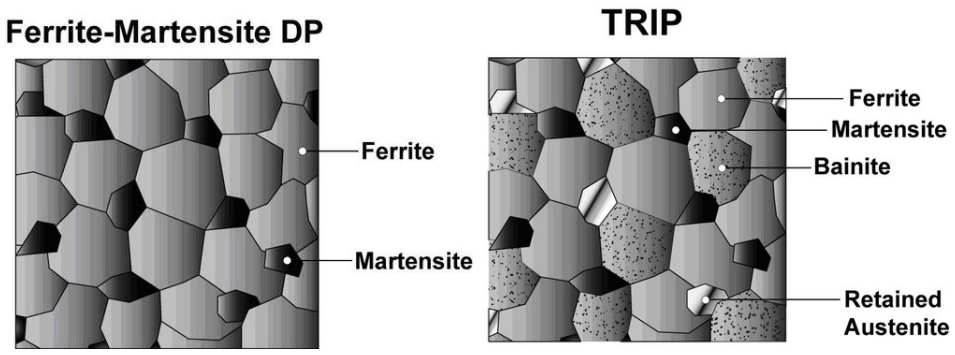

Figure 3.2: Typical microstructure of dual phase and TRIP steels. Source: www.worldautosteel.org.

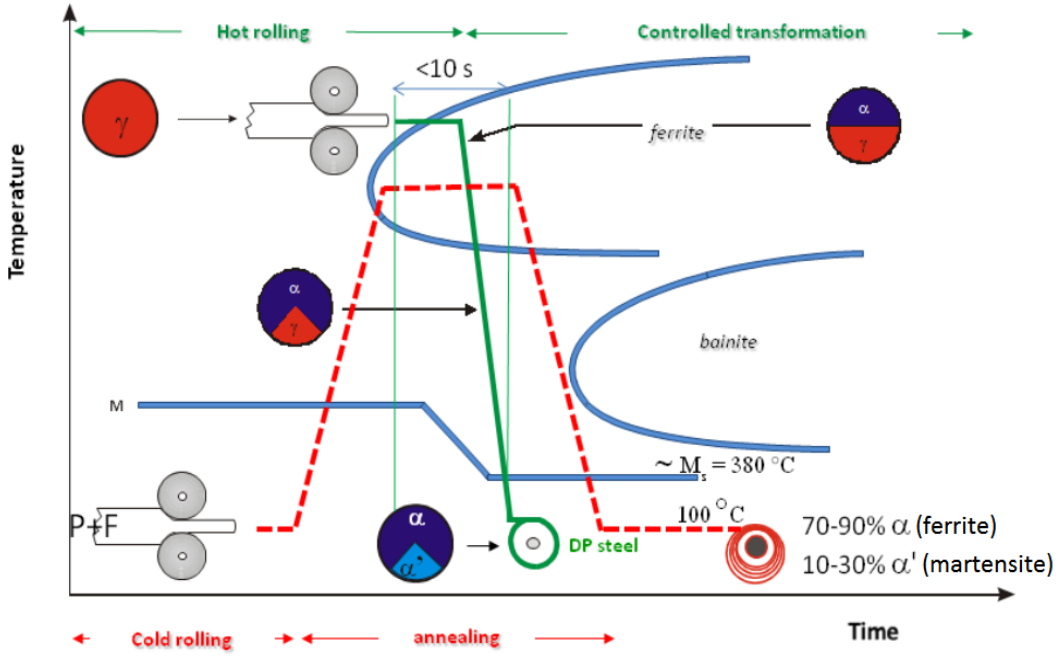

Figure 3.3: The cold rolling and hot rolling processing routes for the production of DP steels. The green solid line shows the hot rolling process and the red dashed line shows the cold rolling process [74].

The microstructure of *Transformation Induced Plasticity, or TRIP steels* consists of ferrite with interdispersed hard phases of martensite and bainite, along with volume fractions of austenite that are greater than 5 %, cf. Figure 3.2. The primary benefit of TRIP steels is their increased formability as compared with dual phase steels of similar strength. This high level of formability is attributed to their extremely high work-hardening rate and the presence of austenite in the matrix that, upon straining, changes into martensite. This takes advantage of the soft ferrite matrix for enhanced formability with a very high strain hardening rate provided by the transformation of austenite to martensite.

TRIP steels are produced in a similar manner to dual phase steels. In comparison to DP steels, TRIP steels require a somewhat slower cooling rate and an isothermal hold at

an intermediate temperature, which produces some bainite. The higher silicon and carbon content of TRIP steels also results in significant volume fractions of retained austenite in the final microstructure.

In this thesis the focus lies on the hot-rolled dual phase steels. The hot rolling process for the production of DP steels will be considered in detail in Chapter 6. In this chapter, we additionally discuss the problem of controlled cooling in the ferrite region to achieve a desired DP microstructure.

3.2 Modelling of phase transformations in hot-rolled dual phase steel

DP steels typically consist of 70 %–90 % ferrite transformed from austenite during isothermal holding at ferrite transformation region temperatures, and 30 %–10 % martensite formed upon rapid quenching. Hence, the main modelling issue is to develop a suitable mathematical austenite-ferrite and austenite-martensite transformation model.

In this work, we will not discuss micro- or mesoscopic models, but concentrate on the development of a macroscopic, phenomenological model for the phase transformations in dual phase steels. Before presenting the model itself, we have to formulate some important assumptions. In the description of the phase transformations, we follow a phase mixture approach and consider steel as a coexisting mixture of phases. We assume that in every point x of our domain and time t the austenite, ferrite and martensite phases are given in phase fractions $a(x,t) \in [0,1]$, $f(x,t) \in [0,1]$ and $m(x,t) \in [0,1]$, respectively. Moreover, we assume that the general balance

$$a(x,t) + f(x,t) + m(x,t) = 1$$

at every time t is fulfilled. As this leads to one dependent variable, e.g., $a = 1 - f - m$, we restrict our consideration to the phase fractions of ferrite and martensite. Indeed, in the case of controlled cooling after hot rolling, only phase transformations from the high-temperature phase austenite to the low-temperature product phases are considered. Starting with full austenization, the austenite fraction at initial time is 1 and the fractions of the product phases are 0. Then, only the explicit description of the fractions of the product phases is required.

The phase evolution occurs at each point independently from the neighbouring points and phase diffusion is omitted (we do not consider spatial derivatives). As (macroscopic spatial) diffusion of the phases is neglected, the spatial variable x only plays the role of a parameter. Therefore, in the subsequent models for the ferrite and martensite growth, it will be often suppressed in notation. An overview of the modelling of phase transformations in steel based on the phase mixture approach can be found in numerous research works, e.g., Hömberg [34], Hömberg and Weiss [37], Wolff, Boettcher, and Böhm [90], and the references therein.

The mathematical model for the phase transformations in Mo-Mn dual phase steel, which is discussed in this section, was developed in close cooperation with engineers from the Department of Ferrous Metallurgy of the RWTH Aachen. The modelling results have already been reported in [76].

3.2.1 Austenite-ferrite phase transformation

The essential and, at the same time, very delicate part of the modelling of phase transformations in dual phase steel is the modelling of the austenite-ferrite phase transformation. Here, the most important phenomena of the hot rolling process that affect the growth of ferrite on the run out table have to be taken into account. During hot rolling, the repeated deformation and recrystallization provides progressively refined austenite grains. It is a well-known fact that the austenite initial grain size plays an important role on the kinetics of transformation, particularly on the nucleation rate of ferrite, cf. [4].

The mathematical models for the kinetics of ferrite transformation including the effect of austenite grain size have been studied in many papers. The macroscopic model, based on the Johnson–Mehl–Avrami–Kolmogorov equation and the additive rule, has been proposed, e.g., in Donnay et al. [17] and Serajzadeh [67]. In the early work of Leblond and Devaux [50], the mathematical model for anisothermal diffusion-controlled phase transformations was studied, which also comprises the influence of the austenite grain size on the phase kinetics.

In this work, we follow the Leblond–Devaux approach in the modelling of the ferrite phase transformation, extended by an additional factor that couples the influence of the austenite grain size and the retained strain before the cooling process on the formation of ferrite.

Effect of the austenite grain size and the retained strain on the ferrite transformation

The first step in the modelling of the austenite-ferrite phase transformation in hot-rolled dual phase steels is to characterize the austenite conditioning, i.e. the austenite grain size, before the phase transformation occurs on the run out table (ROT). There are some phenomena in the hot rolling process that affect the austenite conditioning:

(1) Austenite formation and grain growth during slab reheating.

(2) Dynamic recrystallization, directly during rolling at high temperatures.

(3) Static recovery and recrystallization, between rolling passes at lower temperatures.

(4) Deformation in the non-recrystallization region.

We give here only a short description of the phenomena listed above. For more details, we refer to, e.g., [4, 55, 74]. The austenitizing temperature determines the initial austenite grain size of a slab. Then, the slab is hot worked at the recrystallization region to refine the austenite grains by recrystallization.

Recrystallization can be defined as the process by which deformed grains are replaced by a new set of undeformed grains that nucleate and grow until the original grains have been entirely consumed. The process is divided into nucleation of new grains and growth of the same. A schematic representation of the development of recrystallizing grains is given in Figure 3.4. The recrystallized grain size is reduced when larger deformations are applied. Larger deformations give smaller subgrains and thereby increase the number of nuclei for recrystallization. The recrystallized grain size is also dependent on temperature.

At lower temperatures, finer recrystallized grains are obtained due to the lower mobility of the grain boundaries and consequently slower growth rate of the recrystallizing grains [4].

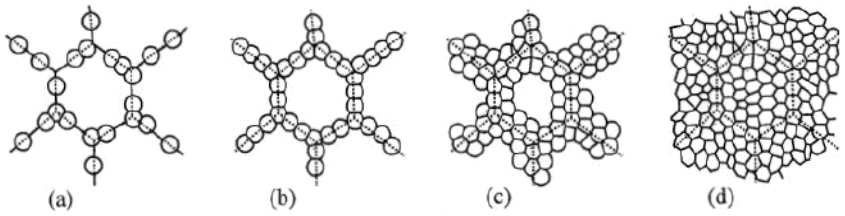

Figure 3.4: A schematic picture of the development of recrystallizing grains, where the initial grain size is large in comparison to the new recrystallized grains. The dotted lines illustrate prior grain boundaries and the continuous lines show new recrystallized grains [4].

In order to predict the recrystallized austenite grain size, different approaches can be used. We will apply the model proposed by Sun et al. [73]:

$$D_\gamma = BD_0^{1/3}\phi^{-0.37}e^{-\frac{28000}{RT}}, \tag{3.1}$$

where D_0 is the austenite grain size before recrystallization and D_γ is the newly recrystallized austenite grain size, which must be recalculated for each deformation step. Here, the degree of deformation is denoted by ϕ.

The effect of *deformation* in the non-recrystallization region can be explained as follows: under deformation, the austenite is flattened, and contains some irregularities at the grain boundaries as well as at the deformation bands inside the grains. This feature accelerates the ferritic phase transformation as the irregularities and deformation bands can act as additional nucleation sites. It results in faster transformation kinetics.

Recrystallization and deformation must be taken into account to estimate the austenite conditioning. In order to describe the state of austenite before phase transformation, we introduce a function S_v. It determines the grain boundary surface area of austenite in a unit volume and therefore has a unit of mm^{-1}. In this work, S_v was taken from the empirical equation of Kvackaj and Mamuzic [48] as shown in (3.2) and illustrated in Figure 3.5

$$S_v = 429\frac{1}{D_\gamma e^\varepsilon} + 1571\frac{e^\varepsilon}{D_\gamma} + [157.2(1-e^{-\varepsilon}) - 59.47]_+, \tag{3.2}$$

where D_γ is the recrystallized austenite grain size. It can be calculated from (3.1), and ε is a retained strain from the last deformation step defined by $\varepsilon = -\ln(1-\phi)$, where ϕ is a deformation degree. The quantity in the bracket comes from the deformation bands, which are taken into account by Kvackaj only when the retained strain ε exceeds 0.475.

It can be observed that S_v increases sharply with small austenite grain size, and increases more slowly with the deformation. In the following, this function will be used for the modelling of the austenite-ferrite transformation.

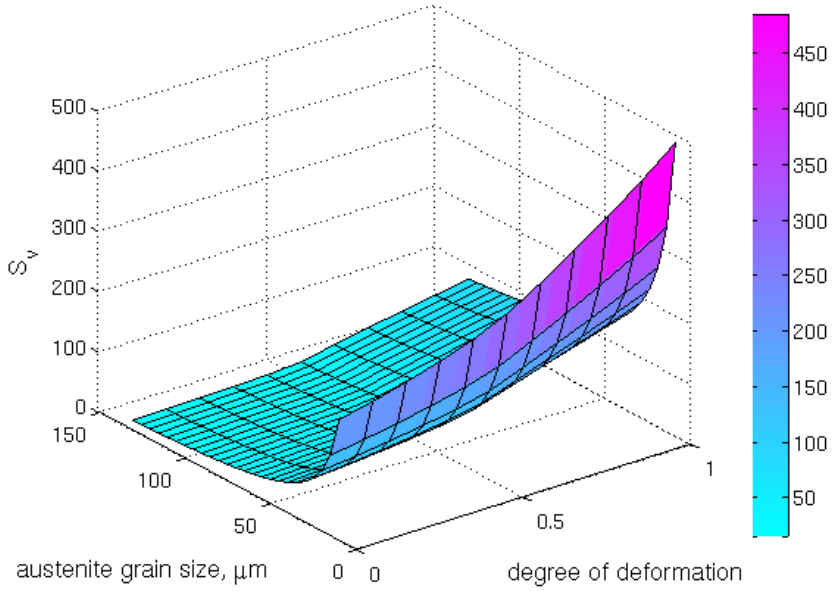

Figure 3.5: The function $S_v(D_\gamma, \varepsilon)$.

A mathematical model

A well-known and widely used approach for the modelling of anisothermal diffusion-controlled as well as martensitic phase transformations is the Leblond–Devaux model first presented in 1984 [50]. To incorporate the effect of austenite grain size and retained strain on the formation of ferrite, the Leblond–Devaux model is modified as follows:

$$\begin{aligned} \dot{f}(t) &= [f_{eq}(\theta) - f(t)]_+ g_1(\theta) g_2(D_\gamma, \varepsilon), \\ f(0) &= 0, \end{aligned} \tag{3.3}$$

where f is the volume fraction of ferrite, and θ the temperature. The term $f_{eq}(\theta)$ describes the asymptotic equilibrium fraction of ferrite as a function of temperature θ after isothermal holding. The function g_1 relates to the isothermal transformation behaviour of ferrite, starting from the homogeneous austenite state. The function g_2 couples the influence of the austenite grain size D_γ and the effect of retained strain ε on the isothermal ferrite transformation kinetics.

The factors g_1 and g_2 in (3.3) have to be identified by experimental data. The temperature dependent function g_1 can be identified from dilatometer experiments, see, e.g., [76]. The equilibrium volume fraction of ferrite f_{eq} can be predicted by the thermodynamic calculation software $ThermoCalc^{TM}$. The functions g_1 and f_{eq} are plotted in Figure 3.6.

The function g_2 in (3.3) describes the influence of austenite grain size and retained strain coupled in the function S_v on the ferrite transformation, cf. (3.2). The simplest choice of the appropriate model for this factor is to assume a linear relationship between g_2 and S_v, i.e.,

$$g_2(D_\gamma, \varepsilon) = \alpha_1 S_v(D_\gamma, \varepsilon) + \alpha_2,$$

where S_v is calculated from (3.2) and the parameters α_1, α_2 have to be fitted to the experimental data.

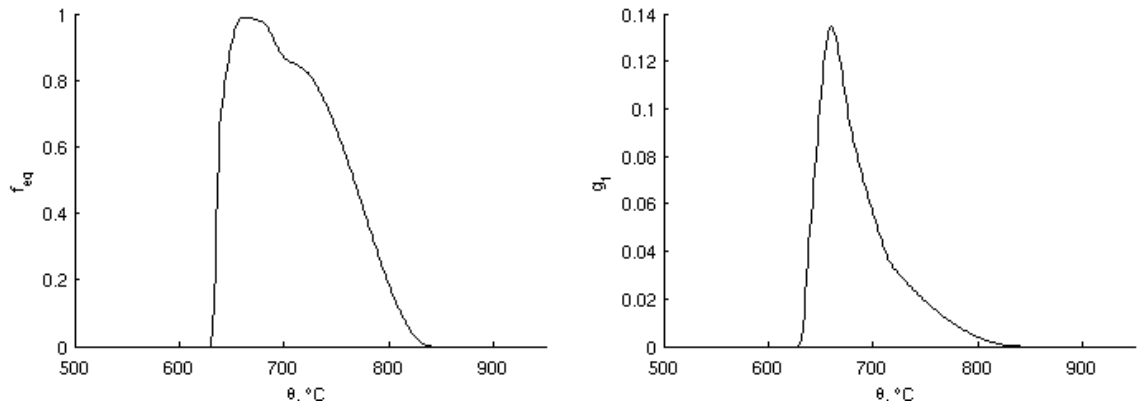

Figure 3.6: The functions f_{eq} (left) and g_1 (right) for the Mo-Mn dual phase steel.

The unknown parameters α_1, α_2 are identified through experiments in the deformation dilatometer that have been performed at the IEHK Aachen. In these experiments, the process simulation of hot rolling for dual phase steel has been carried out. It is documented in [76]. The ferrite fractions were obtained from dilatometer experiments with varying process parameters like the retained strain ε as well as the temperature and the holding time on ROT $(T_{\mathrm{ROT}}, t_{\mathrm{hold}})$. For the identification of the constants α_1, α_2, the least squares approach for the data sets $(\varepsilon_i, T_{\mathrm{ROT}}, t_{\mathrm{hold}}, f_i)$ has been used. The calculated optimal values are $\alpha_1 = 0.2174$ and $\alpha_2 = 3.0436$. It should be noted, that these parameters are fitted using the austenite grain size $D_\gamma = 35\,\mu\mathrm{m}$. It corresponds to the austenite grain size before entering the last deformation step, which is considered to be a non-recrystallization zone. More details on the parameter identification for the austenite-ferrite phase transformation model can be found in [76].

The factors g_1, g_2 are now defined, and the model (3.3) for the ferrite growth can be used for further simulations.

We note that (3.3) can be approximated as

$$\dot{f}(t) = (f_{\mathrm{eq}}(\theta) - f)\mathcal{H}(f_{eq}(\theta) - f)g_1(\theta)g_2(D_\gamma, \varepsilon),$$

where $\mathcal{H}$ is a monotone approximation of the Heaviside function as proposed by Hömberg and Volkwein in [38],

$$\mathcal{H}(x) = \begin{cases} 1, & \text{for } \delta \leq x, \\ 10(\frac{x}{\delta})^6 - 24(\frac{x}{\delta})^5 + 15(\frac{x}{\delta})^4, & \text{for } 0 \leq x < \delta, \\ 0, & \text{for } x < 0. \end{cases}$$

Since $\mathcal{H}$ is a regularized Heaviside function, the term $x\mathcal{H}(x)$ is a regularization of the positive part function $[x]_+$. We will use this form of the model in our numerical calculations for the optimal control. The regularized Heaviside function $\mathcal{H} \in C^{2,1}(\mathbb{R})$, which is an important assumption for the analysis and numerical implementation of the optimal control problem discussed in Chapter 5.

In order to validate our model, we compare the model results with additional experimental data. The isothermal ferrite growth was simulated during the holding time on ROT, $t_{\mathrm{ROT}} = 7\,\mathrm{s}$, with holding temperature $T_{\mathrm{ROT}} = 680\,^{\circ}\mathrm{C}$, and for two different retained

strains, $\varepsilon = 0$ and $\varepsilon = 0.3$. The simulation results and the experimental data are compared in Figure 3.7. It shows a good agreement between calculated and measured ferrite fractions for the degree of deformation $\varepsilon = 0$ (blue line). The prediction of the ferrite transformation in the case of a degree of deformation of 0.3 (green line) shows deviations from the experimental values in the early transformation stages. The reason for the big deviation of the simulation results from the measurement for the end time $t = 7\,\mathrm{s}$ is an inaccuracy in experimental data, which shows a nonphysical decrease of ferrite fraction at this time instant.

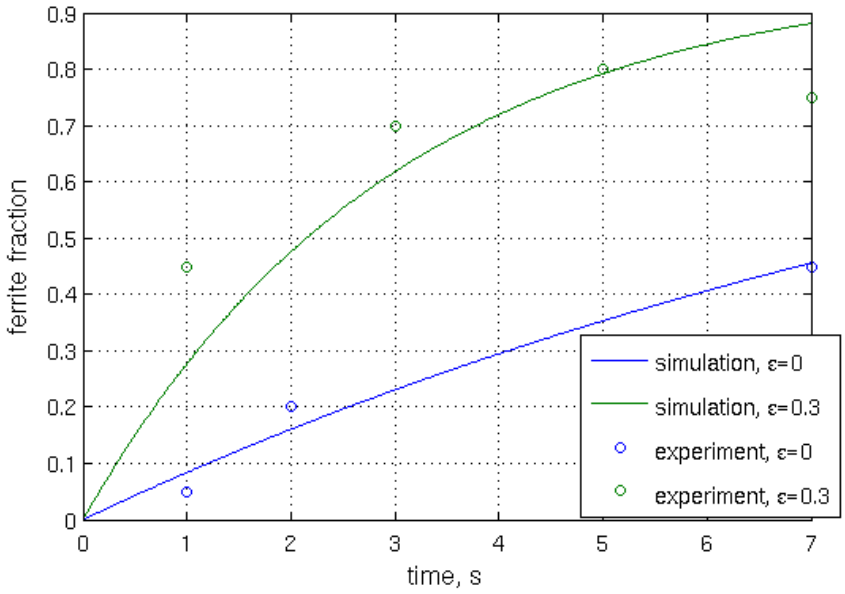

Figure 3.7: Comparison between the simulated and measured ferrite fraction.

With a mathematical model for the ferritic kinetics available, it is also possible to analyze and predict the optimal process window on the run out table. As for the hot rolling process, the final ferrite fraction after coiling is a function of three process parameters: ε (the degree of last deformation), T_{ROT} (the isothermal holding temperature on ROT) and t_{ROT} (the isothermal holding time on ROT). The contour lines of the simulated ferrite fraction are plotted for one fixed parameter and two free parameters on the axes in Figure 3.8 and 3.9. Keeping in mind that a typical dual phase steel consists of approximately 80 % ferrite, those process parameters have to be identified when this fraction can be reached.

Figure 3.8 shows that for the isothermal holding time $t_{\mathrm{hold}} = 7\,\mathrm{s}$, the optimal process window concerning the temperature on the ROT becomes narrow with decreasing deformation. As it can be seen in Figure 3.9, there is a stable process window in terms of a holding time between 660 °C and 680 °C for the retained strain $\varepsilon = 0.3$. We can thus state that the model allows for predicting the preferable degree of retained strain and holding temperature on the run out table for the required ferrite fraction.

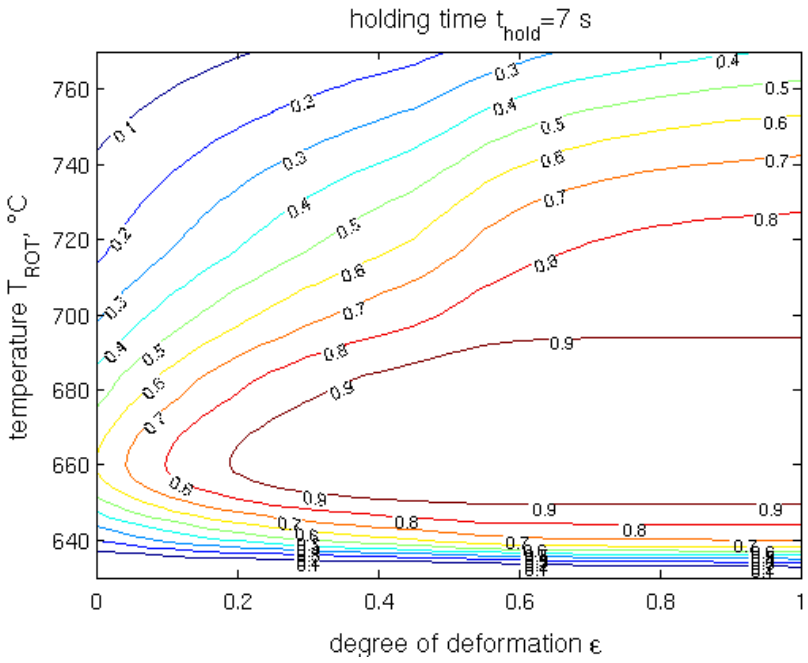

Figure 3.8: Contours of the simulated transformed ferrite fraction represented as a function of different retained strains and holding temperatures on ROT for a holding time of 7 s.

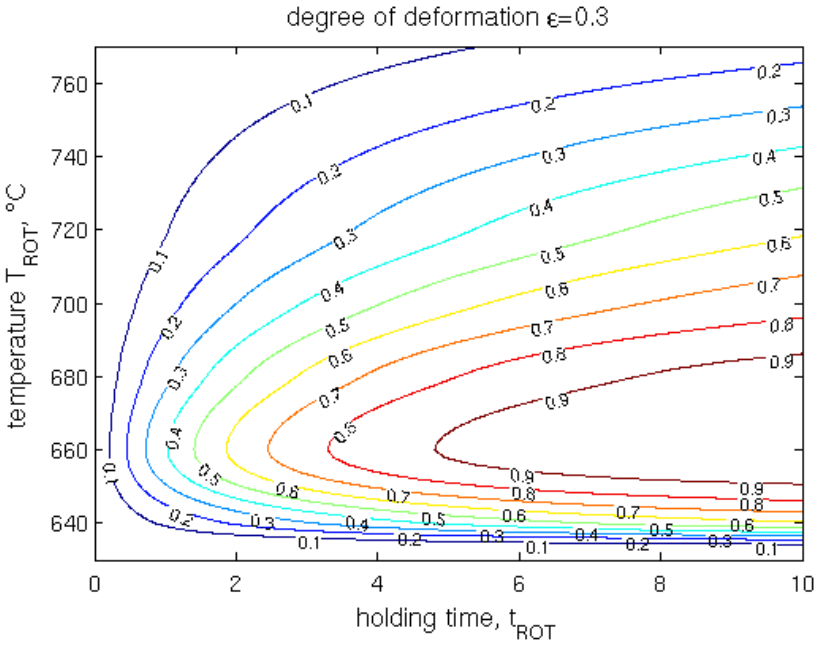

Figure 3.9: Contours of the simulated transformed ferrite fraction represented as a function of different holding times and temperatures on ROT for a retained strain of $\varepsilon = 0.3$.

3.2.2 Austenite-martensite phase transformation

We consider the austenite-martensite phase transformation that occurs during rapid cooling after the isothermal ferritic transformation on the ROT. As it was discussed in Section 2.2, the martensite transformation during continuous cooling is diffusion-less and irreversible. It is temperature dependent in such a way that the fraction of martensite only increases during nonisothermal stages of the cooling process. The formation of martensite during cooling begins at a well-defined temperature M_s and continues whilst the temperature decreases until the martensite finish temperature M_f.

A key point in the modelling of the martensite phase transformation in hot-rolled dual phase steels is that a carbon enrichment of the remaining austenite after the ferrite transformation has to be taken into account. We assume that when ferrite forms, the carbon forced out of ferrite is evenly distributed in the remaining austenite phase. Further, the carbon content in the remaining austenite after the ferrite transformation is denoted by C_γ. An easy way to take care of carbon partitioning between ferrite and austenite is to define C_γ by

$$C_\gamma = \frac{C_{total} - C_f \cdot f}{1 - f},$$

where C_{total} corresponds to the nominal carbon content of the respective steel, and C_f is the total carbon content in ferrite, which decreases with decreasing temperature θ and can be computed from the empirical formula, cf. [8]

$$C_f = 2.55 e^{-\frac{4850}{\theta[\mathrm{K}]}}.$$

Then, M_s as a function of C_γ can be calculated from, e.g., [53]:

$$M_s(C_\gamma)[^\circ\mathrm{C}] = 506.6 - 338.7(\%C_\gamma) - 18.3(\%\mathrm{Mn}) + 1.3(\%\mathrm{Si}) - 14.5(\%\mathrm{Cr}).$$

Usually, exponential growth laws like the Koistinen and Marburger formula [44]

$$m_{\mathrm{KM}}(\theta, C_\gamma) = 1 - e^{-c_{\mathrm{KM}}(M_s(C_\gamma) - \theta)}$$

are used to model the kinetics of the austenite-martensite phase transformation. Here, c_{KM} is a constant that does not depend on the temperature, but only on the alloy composition. As it was reported by Hömberg [34] and Wolff, Frerichs, and Lysenko [91], the drawback of these models is that they do not take the irreversibility of the austenite-martensite phase transformation into account. In numerical simulations based on these models, owing to the release of latent heat, usually a decrease in the martensite fraction is observed. In order to avoid this adverse effect, the rate law model based on the Leblond–Devaux ansatz has been proposed in [34]. It is appropriate to also follow this approach for the modelling of the kinetics of the austenite-martensite phase transformation in dual phase steels. Therefore, we take Leblond–Devaux type differential equation with an initial condition for the volume fraction of martensite m to describe the martensite transformation

$$\begin{aligned} \dot{m}(t) &= \frac{1}{\tau_m}[\bar{m}(\theta, C_\gamma) - m]_+, \\ m(0) &= 0. \end{aligned} \tag{3.4}$$

Here, τ_m is a constant that has to be fitted to the experimental data. The bracket $[\cdot]_+$ denotes the positive part function $[\cdot]_+ = \max\{\cdot, 0\}$, the term $\bar{m}(\theta, C_\gamma)$ represents the maximal fraction that can be transformed to martensite. The function $\bar{m}$ is defined by

$$\bar{m}(\theta, C_\gamma) = \min\{m_{\mathrm{KM}}(\theta, C_\gamma), 1 - f\},$$

where m_{KM} describes the volume fraction of martensite by the Koistinen–Marburger formula, i.e.,

$$m_{\mathrm{KM}}(\theta, C_\gamma) = 1 - e^{-c_{\mathrm{KM}}(M_s(C_\gamma)-\theta)}. \tag{3.5}$$

Using the dilatometer data for the case of fast cooling, where only martensite is produced, one can obtain the following values for the parameters c_{KM} and τ_m in (3.5) and (3.4)

$$c_{\mathrm{KM}} = 0.0214, \quad \tau_m = 0.67.$$

Knowing the mathematical models for the ferrite and martensite phase transformations, one can simulate the phase evolutions in dual phase steel on the run out table.

3.3 Simulation results

Next, we show a numerical result for the simulation of phase transformations in dual phase steel that we compare with experimental data from deformation dilatometer experiments. In these experiments, the process of hot rolling for dual phase steel has been simulated. For a detailed description of the deformation dilatometer experiments we refer to [76].

The phase transformation kinetics of ferrite and martensite are computed from (3.3) and (3.4) with the process parameters in the hot rolling mill, namely, austenite conditioning ($\mathcal{D}_\gamma$), isothermal holding time and temperature (t_{hold}, T_{ROT}) as well as the final quenching at the end of ROT. The numerical computations are carried out using Matlab ODE solvers.

In Figure 3.10, the development of phases is shown along the processing time and temperature curve and compared with those derived at the end of the dilatometer experiment. The dashed line shows the temperature evolution taken from the experiment. The transformation shown here starts after 1 s of the simulated process on ROT, at 690 °C. After 7.85 s, which includes the holding time on ROT $t_{\mathrm{hold}} = 7$ s, the ferrite fraction reaches 0.81. The next cooling region simulates the cooling step to coiling temperature, in this case with the average cooling rate of 61 K/s, measured from 600 °C down to 200 °C. When the temperature reaches the martensite start temperature M_s, which was calculated to be 351.3 °C according to the carbon enrichment from the corresponding simulated ferrite fraction, martensite starts to form and then finishes at 267.7 °C with the phase fraction of 0.19.

The phase fraction analyzed from the dilatometer sample is revealed to be as follows: ferrite 0.78, bainite 0.03 and martensite 0.19. The results of the numerical simulation are in a good agreement with the measured ferrite and martensite fractions. The deviation of the simulated ferrite fraction from the experimental one is less then 4 %.

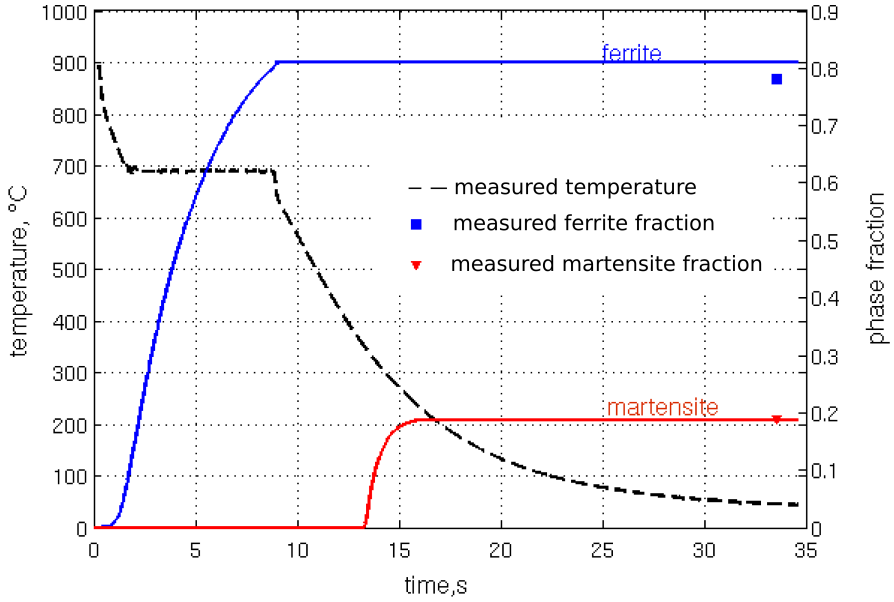

Figure 3.10: Simulated evolution of phase fractions along the processing time and the measured temperature profile, in comparison with the measured phase fraction at the end of the dilatometer experiment. The elapsed time starts from the beginning of ROT. The retained strain is 0.3, the holding temperature 690 °C and the holding time 7 s. The average cooling rate in the following step, measured from 600 °C–200 °C, is 61 K/s.

Chapter 4

Parameter identification for the phase transformations in steel

Phase transformations during heat treatment are an important phenomenon in the material behaviour of steel. Together with the thermal and mechanical behaviour of the steel workpiece, phase transformations cause a change in volume and shape. Dilatometry is a means to measure material properties that are related to a change in volume. A dilatometer is able to measure this volumetric change of the workpiece in one dimension, which is often related to the change in temperature. Even the small length changes that occur during the heating and cooling of steel with respect to the change in its temperature can be registered by a dilatometer and used to study the kinetics of phase transformations. The temperature at which the phase transformation occurs, can be detected precisely by correlating the temperature and the specimen's change of length. While the determination of the start and end of a phase transformation is relatively simple, the determination of the resulting phase fractions requires additional metallographic investigations, in which the samples are ground, polished, etched and observed under a light optical microscope. This procedure has some drawbacks. We discuss them in detail in Section 4.1, which is devoted to the description of dilatometer experiments.

In this chapter, an inverse problem of identifying the phase transformation kinetics by two dilatometer measurements is studied. These measurements are the length change and the temperature evolution of a specimen at a single point of its surface. This problem is considered as a parameter identification problem, i.e., the problem of reconstructing unknown coefficients in partial differential equations from indirect measurements of the solution. In Section 4.2, we give a formulation of the direct and inverse problem and derive a thermo-elasticity system which describes interactions between temperature, mechanical behaviour and phase transformations in steel during the dilatometer experiment.

The analysis of the direct problem is carried out in Section 4.3. The inverse problem is investigated in Section 4.4. Our main result is a global stability estimate for the solution of the inverse problem, which is an important theoretical result for the numerical computations.

Finally, Section 4.5 is devoted to the numerical solution of the inverse problem. The parameter identification problem, which is formulated as an optimal control problem, is treated numerically applying the "first discretize, then optimize" approach. The numerical approach is first tested using the so-called "model data", that is, measurements of

temperature and displacement generated by the solution of the direct problem with the known kinetics of the phase transformations. In Section 4.5.4, the numerical results for the real dilatometer data are presented.

4.1 Dilatometer experiments

A dilatometer is an instrument for magnifying and measuring expansion and contraction of a solid during heating and subsequent cooling. It is often used in the determination of phase transformations occurring with the change of temperature in heat treatment of steels. Figure 4.1 depicts a typical measurement setup of a dilatometer and Figure 4.2 additionally shows the steel sample fixed in the inner part of a dilatometer device. The steel specimen is contained in a heating device, which is usually an induction heating device. Through a rod on its right-hand side, length changes $\lambda(t)$ caused by compression or expansion are measured as a function of time t. In addition, the temperature $\tau(t)$ is measured on the surface of the steel sample.

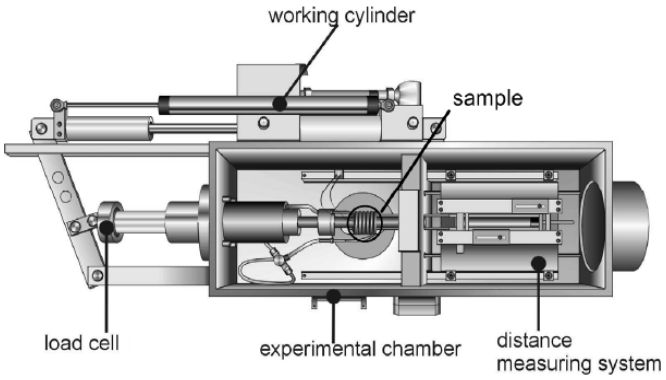

Figure 4.1: Schematic illustration of a dilatometer Bähr DIL-805A/D.

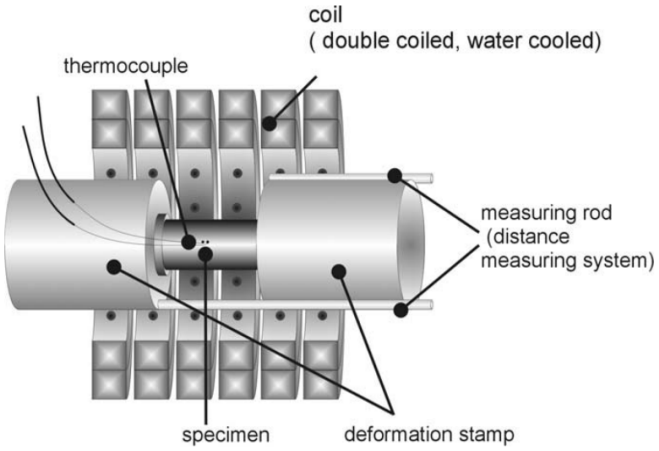

Figure 4.2: Configuration of the driving rod system of the deformation dilatometer type DIL-805A/D produced by the company Bähr Thermoanalyse GmbH. A cylindrical sample is shown in this figure.

Usually, the results are documented in a dilatometer curve, that depicts the length change parameterized by the time t plotted versus the temperature. A typical dilatometer curve for the cooling of a specimen made of eutectoid carbon steel is shown in Figure 4.3. The part of the curve to the right of point A shows the normal contraction of the specimen during slow cooling of steel in the austenitic phase. At point A, a phase transformation (from austenite to pearlite) starts and it ends at point B. Then, again a period with a linear contraction prevails followed by another phase transformation (austenite to martensite) between C and D, and finally another linear contraction period appears. Therefore, the main information drawn from such a dilatometer experiment usually is the start (θ_A, θ_C) and the end (θ_B, θ_D) temperatures of the occurring phase transformations. Moreover, one knows that above θ_A, the microstructure of steel is purely austenitic. Between θ_B and θ_C, there is a constant mixture of austenite and pearlite and below θ_D we have a mixture of the product phases pearlite and martensite. Usually, this data is used to derive Continuous Cooling Transformation diagrams, which illustrate the beginning and the end of a phase transformation during continuous cooling.

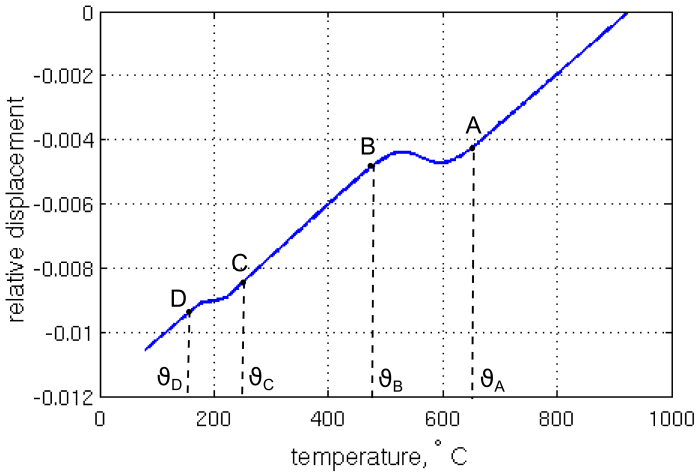

Figure 4.3: Dilatometer curve for steel C1080 exhibiting 2 phase transformations.

This approach has two drawbacks. First of all, depending on the curvature of the respective dilatometer curve, it might become rather difficult and error-prone to identify transformation points $A, \ldots, D$. Secondly, in the case of two phase transformations as illustrated in Figure 4.3, the actual phase fractions of the different product phases cannot be inferred directly from the dilatometer curve. Therefore, usually costly polished micrograph sections have to be made and investigated under the microscope. The fractions of the product phases are determined from the metallographs by a purely visual judgement of the experimenter or with the help of image analysis software, which works under a pixel based principle, i.e., different phases are distinguished according to their colours. The precision of the predicted phase fractions then highly depends on the experience of the respective experimenter. Moreover, the determination of the phase fraction depends also on the homogeneity and the phase distribution in the sample as the metallographically observed areas are not truly representative for the entire specimen.

In the following, it will be shown that one can uniquely identify the evolution of two product phases from the measurements of temperature and length change of a steel

sample. In the next section we formulate this problem as an inverse problem and derive a mathematical model that describes a dilatometer experiment.

4.2 Problem formulation

The problem of identifying the evolution of phase fractions from the measurements of a dilatometer experiment can be formulated as an inverse problem. Generally speaking, to predict the result of a measurement, a model of the system under investigation is required, and a physical theory linking the parameters of the model to the parameters being measured. In the case of known values of the model parameters, the prediction of observations constitutes the *direct problem* or, in terms of inverse problem theory, the forward problem. The *inverse problem* consists in using the results of actual observations to infer the values of the parameters characterizing the system under investigation. In the case of the dilatometric investigations, the scheme presented in Figure 4.4 is valid.

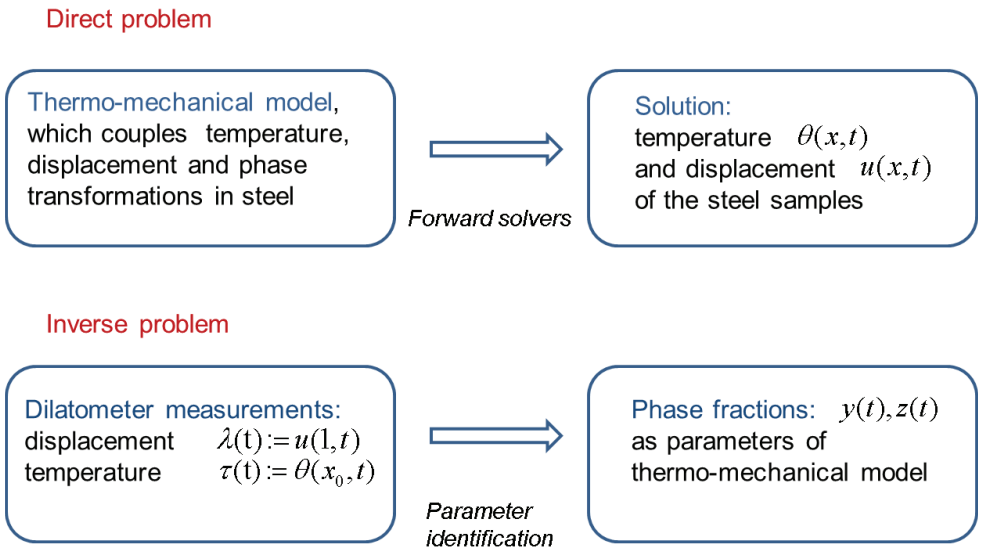

Figure 4.4: Direct and inverse problem for a dilatometer experiment.

The inverse problem can be formulated as follows: Identify two phase fractions $y(t), z(t)$ as the parameters of the thermo-mechanical model from the measurements of the displacement and the temperature in the dilatometer experiment. Hence, the first step is to derive an appropriate mathematical model that describes the interplay between temperature, displacement and phase transformations in steel during the cooling in the dilatometer.

Modelling the relevant interactions between temperature, mechanical behaviour and phase transformations during the cooling of steel leads to a thermo-elasticity system. In general, this is a system of coupled nonlinear partial and ordinary differential equations for the time and space-dependent temperature, displacement and phase fractions. The modelling of the thermo-elastic behaviour of steel under consideration of phase transformations is discussed, e.g., in Chelminski, Hömberg, and Kern [14], Hömberg [32], Kern [42], Wolff and Böhm [89]. A thermo-elasto-plasticity model is considered in Boettcher

[10]. In [10], the mathematical analysis is given for a coupled model for the material behaviour of steel which describes the phase transformations, the transformation-induced and the classical plasticity in addition to the temperature and the deformation.

Here, we only give a brief description of the model which describes the thermo-elastic behaviour of steel in a dilatometer experiment. For more details on the derivation of equations of linearized thermo-elasticity, we refer to the literature cited above.

The standard shape for a dilatometer specimen is a cylinder as depicted in Figure 4.5. In this work, we restrict ourselves to the consideration of a one-dimensional model for the dilatometer experiment. We will neglect radial variations of the physical quantities and just consider variations along the symmetry axis. For convenience, we define the domain

$$\Omega = (0, 1)$$

and assume small deformations which will allow us to write down the equations in the undeformed domain.

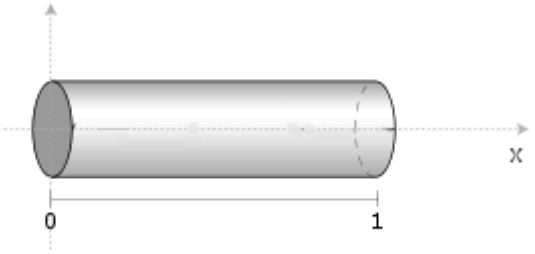

Figure 4.5: The dilatometer specimen.

Here, we are interested in a cooling process in the dilatometer experiment. Therefore, we consider a steel sample of purely austenitic structure which is cooled from a high temperature range of 1000 °C–1200 °C down to a lower temperature of about 100 °C. Henceforth, we denote the initial temperature by θ_0. We assume that at most two phase transformations may occur during the cooling with phase fractions $y(t)$ and $z(t)$, respectively, depending only on time t but not on space. In addition, they satisfy

$$y(0) = z(0) = 0, \quad 0 \leq y(t), \quad 0 \leq z(t), \quad y(t) + z(t) \leq 1, \quad \text{for all } t \in [0, T]. \tag{4.1}$$

The simplest model to describe a thermal expansion as indicated in Figure 4.3 assumes a mixture ansatz for the thermal strain

$$\varepsilon^{th} = y\varepsilon_1^{th} + z\varepsilon_2^{th} + (1 - y - z)\varepsilon_0^{th}, \tag{4.2}$$

where the thermal strain in each phase is given by the linear model

$$\varepsilon_k^{th} = \delta_k(\theta - \theta_{ref}^k), \ k = 0, 1, 2. \tag{4.3}$$

Here, the constants $\delta_k > 0$ are the thermal expansion coefficients and θ_{ref}^k are the reference temperatures. For convenience, we define

$$\alpha_1 = \delta_1 - \delta_0, \quad \alpha_2 = \delta_2 - \delta_0, \quad \beta_1 = \delta_1\theta_{ref}^1 - \delta_0\theta_{ref}^0, \quad \beta_2 = \delta_2\theta_{ref}^2 - \delta_0\theta_{ref}^0.$$

Setting $w = (y, z)$ and

$$\delta(w) = \alpha_1 y + \alpha_2 z + \delta_0, \quad \eta(w) = \beta_1 y + \beta_2 z + \delta_0 \theta^0_{ref}, \tag{4.4}$$

we can write the overall thermal strain as

$$\varepsilon^{th} = \delta(w)\theta - \eta(w).$$

Moreover, by (4.1) we observe that

$$\delta(w(t)) \geq \min\{\delta_0, \delta_1, \delta_2\} > 0.$$

Assuming furthermore an additive partitioning of the total strain into a thermal and an elastic parts, i.e., $\varepsilon = \varepsilon^{el} + \varepsilon^{th}$ we obtain the following quasistatic linearized thermo-elasticity system:

$$\begin{aligned}
&\big(u_x - \delta(w)\theta + \eta(w)\big)_x = 0 && \text{in } \Omega \times (0,T), && \text{(4.5a)}\\
&\rho c_p \theta_t - \kappa\theta_{xx} + \Lambda\delta(w)u_{xt} - \rho L_1 y' - \rho L_2 z' = \gamma(\theta^e - \theta) && \text{in } \Omega \times (0,T), && \text{(4.5b)}\\
&u(0,t) = 0, \quad u_x(1,t) - \delta(w)\theta(1,t) + \eta(w) = 0 && \text{in } (0,T), && \text{(4.5c)}\\
&\theta_x(0,t) = \theta_x(1,t) = 0 && \text{in } (0,T), && \text{(4.5d)}\\
&\theta(x,0) = \theta_0 && \text{in } \Omega. && \text{(4.5e)}
\end{aligned}$$

Here, θ denotes a temperature and u is a displacement. We set $y' = \frac{dy}{dt}$, $z' = \frac{dz}{dt}$. Moreover, ρ refers to the density in the reference configuration, c_p to the heat capacity, κ to the thermal conductivity and L_1 and L_2 to the latent heats of the phase transformations and are constants. The constant Λ is defined by $\Lambda_1 + 2\Lambda_2$ with the Lamé coefficients Λ_1, Λ_2. All other constants have been normalized to one without loss of generality.

Since the cooling occurs all around the specimen, we choose a distributed Newton type cooling law

$$h = \gamma(\theta^e - \theta),$$

where γ is the heat exchange coefficient and θ^e is the temperature of the coolant. In view of Hooke's law, the stress σ is given by

$$\sigma = (\Lambda_1 + 2\Lambda_2)(u_x - \delta(w)\theta + \eta(w)).$$

The first boundary condition for u in (4.5c) indicates the fact that the sample is fixed from the left-hand side in the dilatometer device. The second one just states that the specimen is stress-free at $x = 1$. The heat flux on the boundary, i.e., at $x = 0$ and $x = 1$, is zero. It is reflected in the boundary condition for θ in (4.5d).

The *direct problem* consists in finding the pair of functions (u, θ) that solve the thermo-elasticity system (4.5a)–(4.5e), provided the parameter functions (y, z) are known. The *inverse problem* amounts to finding the unknown functions (y, z) and (u, θ) satisfying the thermo-elasticity system (4.5a)–(4.5e) and the relations

$$\theta(x_0, t) = \lambda(t), \quad u(1,t) = \tau(t),$$

where the functions λ, τ are the measurements from the dilatometer experiment. This problem can be classified as an inverse problem with an evolution overdetermination at a

fixed point in space, i.e., at $x = x_0$ for the temperature and $x = 1$ for the displacement. We refer, for example, to Prilepko, Orlovsky, and Vasin [60] as a source book concerning similar inverse problems. There exists an extensive literature devoted to inverse problems and their applications. A nice survey on inverse and ill-posed problems is given by Kabanikhin [40]. The mathematical theory of inverse problems and the mathematical theory of regularization methods for ill-posed inverse problems are presented in the textbook of Hofmann [31]. Inverse problems involving partial differential equations are discussed, e.g., in Isakov [39], Prilepko, Orlovsky, and Vasin [60].

4.3 Analysis of the direct problem

We are going to analyze the thermo-elasticity system (4.5a)–(4.5e) derived for the dilatometer experiment. At the beginning, we make the following assumptions for the physical parameters and functions $y(t), z(t)$ in the equations (4.5a)–(4.5e).

Assumptions:

(A1) $L_1, L_2, \delta_0, \delta_1, \delta_2, \gamma > 0$,

(A2) $\theta_0, \theta^e \in C[0,1]$ satisfying $\theta_0(x) > \theta^e(x) > 0$ for all $x \in [0,1]$,

(A3) $y, z \in C^2[0,T]$ such that $y', z' \geq 0$ for all $t \in [0,T]$ and there exists a constant $M > 0$ such that $\|y\|_{C^2[0,T]}, \|z\|_{C^2[0,T]} \leq M$, and (4.1) is satisfied,

(A4) $y'(t) = z'(t) = 0$ for all temperatures $\theta \leq \theta^e$.

Assumption (A2) reflects the fact that we consider a cooling experiment, i.e., we start with a hot specimen, while (A4) rephrases that there are no phase transformations below temperature θ^e.

Remark 4.3.1. *As can be seen in Figure 4.3, the phase transformations are finished when the temperature θ_D is reached. Hence, it is natural to assume that $y'(t) = z'(t) = 0$ for $\theta \leq \theta^e$, where $\theta^e < \theta_D$.*

For the direct problem, we have the following result:

Theorem 4.3.1. *Assume (A1)–(A3), then the thermo-elasticity system* (4.5a)–(4.5e) *admits a unique classical solution (u, θ). Moreover, it satisfies $\theta \geq \theta^e$ in $\Omega \times (0,T)$, if also (A4) holds.*

Proof. The existence of a unique weak solution of the thermo-elasticity system can be proven in a similar way as it is done for the more general thermo-elasticity system in the three-dimensional domain in Chelminski, Hömberg, and Kern [14]. With further regularity analysis one can show that in this specially one-dimensional case one obtains a classical solution.

To show the non-negativity of θ, we first note that (4.5a) implies the existence of a function μ depending only on time such that

$$u_x - \delta(w)\theta + \eta(w) = \mu(t) \quad \text{in } \bar{\Omega} \times (0,T).$$

Regarding (4.5c), we see that $\mu \equiv 0$. Hence, we have

$$u_x = \delta(w)\theta - \eta(w) \quad \text{in } \bar{\Omega} \times (0,T). \tag{4.6}$$

Differentiating (4.6) formally with respect to t, we can infer

$$u_{xt} = (\alpha_1 y' + \alpha_2 z')\theta + \delta(w)\theta_t - \beta_1 y' - \beta_2 z'. \tag{4.7}$$

Inserting this into (4.5b), we obtain

$$(1+\nu\delta(w)^2)\theta_t - \hat{\kappa}\theta_{xx} + \nu\delta(w)(\alpha_1 y' + \alpha_2 z')\theta = \hat{L}_1(w)y' + \hat{L}_2(w)z' + \hat{\gamma}(\theta^e - \theta), \tag{4.8}$$

with

$$\hat{L}_1(w) = \frac{L_1}{c} + \nu\delta(w)\beta_1, \quad \hat{L}_2(w) = \frac{L_2}{c} + \nu\delta(w)\beta_2 \tag{4.9}$$

and

$$\hat{\kappa} = \frac{\kappa}{\rho c_p}, \quad \nu = \frac{\Lambda}{\rho c_p}, \quad \hat{\gamma} = \frac{\gamma}{\rho c_p}.$$

To prove the lower bound for θ, we test (4.8) with $\theta_- := \min\{\theta - \theta^e, 0\}$, integrate by parts, and use the identity $\theta = \theta^e + \theta_- + \theta_+$ to obtain

$$\begin{aligned}
&\int_0^t \int_\Omega (1+\nu\delta(w)^2)\frac{1}{2}\frac{\partial}{\partial s}\theta_-^2 dxdt + \hat{\kappa}\int_0^t \int_\Omega \theta_x \theta_{-,x} dxdt + \int_0^t \int_\Omega \nu\delta(w)(\alpha_1 y' + \alpha_2 z')\theta\theta_- dxdt \\
&\qquad = \frac{1}{2}\int_\Omega (1+\nu\delta(w)^2)\theta_-^2(t)dxdt + \hat{\kappa}\int_0^t \int_\Omega \theta_{-,x}^2 dxdt \\
&\qquad = \int_0^t \int_\Omega (\hat{L}_1(w)y' + \hat{L}_2(w)z')\theta_- dxdt + \hat{\gamma}\int_0^t \int_\Omega (\theta^e - \theta)\theta_- dxdt \\
&\qquad \le 0.
\end{aligned}$$

The latter inequality holds in view of (A1)–(A4). From this we can infer $\theta_- = 0$. □

4.4 A global stability estimate for the inverse problem

In this section we study the inverse problem of reconstructing the phase fractions of at most two product phases from measured data $u(1,t)$ and $\theta(x_0,t)$ for $t \in [0,T]$, at some point $x_0 \in (0,1)$ as it was formulated in Section 4.2. We can expect the existence of (y,z) satisfying the thermo-elasticity system (4.5a)–(4.5e) and realizing the given data $u(1,\cdot)$ and $\theta(x_0,\cdot)$, but here we only prove the stability of the solution of the inverse problem, which is an important theoretical issue for numerical computations.

For given $w(t) = (y(t), z(t))$ and $\lambda(t)$, we set

$$\begin{aligned}
\mathcal{L}_1(\lambda(t), w(t)) &= \frac{L_1}{c} + \frac{\lambda(t) + \eta(w(t))}{\delta^2(w(t))}\alpha_1 - \frac{\beta_1}{\delta(w(t))}, \\
\mathcal{L}_2(\lambda(t), w(t)) &= \frac{L_2}{c} + \frac{\lambda(t) + \eta(w(t))}{\delta^2(w(t))}\alpha_2 - \frac{\beta_2}{\delta(w(t))}.
\end{aligned}$$

Recall that the functions $\hat{L}_1(w)$ and $\hat{L}_2(w)$ are defined by (4.9).

For our inverse problem, we have to enforce the additional assumption that will be needed for the derivation of the global stability estimate:

(A5) For any $w(t), \theta, u$ satisfying (4.5a)–(4.5e), there holds

$$\begin{aligned}\mathcal{L}_1(u(1,t),w(t))(\hat{L}_2(w(t)) - \nu\delta(w(t))\alpha_2\theta(x_0,t)) \\ -\mathcal{L}_2(u(1,t),w(t))(\hat{L}_1(w(t)) - \nu\delta(w(t))\alpha_1\theta(x_0,t)) \neq 0, \quad 0 \leq t \leq T.\end{aligned}$$

Remark 4.4.1. *In Section 4.5.2 we will show that Assumption (A5) is indeed satisfied for realistic physical data.*

The main result of this section is the following global stability estimate, which has already been published in [36]:

Theorem 4.4.1. *Let (y_i, z_i), $i = 1, 2$, be two sets of phase fractions such that (A1)–(A5) are satisfied and let (u_i, θ_i), $i = 1, 2$, be the corresponding solutions to* (4.5a)–(4.5e).

Then, there exists a constant $C > 0$ such that

$$\begin{aligned}\|y_1 - y_2\|_{C^1[0,T]} + \|z_1 - z_2\|_{C^1[0,T]} \\ \leq C(\|(u_1 - u_2)(1,\cdot)\|_{C^1[0,T]} + \|(\theta_1 - \theta_2)(x_0,\cdot)\|_{C^1[0,T]}).\end{aligned}$$

Proof. By (4.6), we have

$$\int_0^x \partial_x u_j(\xi,t)d\xi = \int_0^x \delta(w_j(t))\theta_j(\xi,t)d\xi - \int_0^x \eta(w_j(t))d\xi,$$

and by (4.5c), we obtain

$$u_j(x,t) = \delta(w_j(t)) \int_0^x \theta_j(\xi,t)d\xi - x\eta(w_j(t)), \quad t > 0.$$

Defining

$$\lambda_j(t) := u_j(1,t),$$

we obtain

$$\lambda_j(t) = \delta(w_j(t)) \int_0^1 \theta_j(\xi,t)d\xi - \eta(w_j(t)), \quad t > 0. \tag{4.10}$$

Now, we integrate (4.8) over $x \in (0,1)$ and use (4.5d) and (4.10) to obtain

$$\begin{aligned}(1 + \nu\delta(w_j(t))^2) \left(\frac{\lambda_j(t) + \eta(w_j(t))}{\delta(w_j(t))}\right)' + \nu(\lambda_j(t) + \eta(w_j(t)))(\alpha_1 y_j' + \alpha_2 z_j') \\ = \hat{L}_1(w_j)y_j' + \hat{L}_2(w_j)z_j' - \hat{\gamma}\frac{\lambda_j(t) + \eta(w_j(t))}{\delta(w_j(t))} + \hat{\gamma}\theta^e, \quad t > 0.\end{aligned}$$

Rearranging terms yields

$$\begin{aligned}\mathcal{L}_1(\lambda_j(t), w_j(t))y_j'(t) + \mathcal{L}_2(\lambda_j(t), w_j(t))z_j'(t) \\ = \left(1 + \nu\delta^2(w_j(t))\right)\frac{\lambda_j'(t)}{\delta(w_j)} + \hat{\gamma}\frac{\lambda_j(t) + \eta(w_j(t))}{\delta(w_j(t))} - \hat{\gamma}\theta^e, \quad t > 0.\end{aligned} \tag{4.11}$$

Now, we define $\bar{\lambda} = \lambda_1 - \lambda_2$ and analogously $\bar{y}$ and $\bar{z}$, then we take the difference of (4.11) for $j = 1, 2$:

$$\begin{aligned}\mathcal{L}_1(\lambda_1, w_1)\bar{y}'(t) + \mathcal{L}_2(\lambda_1, w_1)\bar{z}'(t) \\ +(\mathcal{L}_1(\lambda_1, w_1) - \mathcal{L}_1(\lambda_2, w_2))y_2' + (\mathcal{L}_2(\lambda_1, w_1) - \mathcal{L}_2(\lambda_2, w_2))z_2' \\ = (1 + \nu\delta(w_1)^2)\tfrac{\lambda_1'}{\delta(w_1)} - (1 + \nu\delta(w_2)^2)\tfrac{\lambda_2'}{\delta(w_2)} \\ +\hat{\gamma}\left(\tfrac{\lambda_1+\eta(w_1)}{\delta(w_1)} - \tfrac{\lambda_2+\eta(w_2)}{\delta(w_2)}\right).\end{aligned}$$

We can rewrite this equation as

$$\mathcal{L}_1(\lambda_1, w_1)\bar{y}'(t) + \mathcal{L}_2(\lambda_1, w_1)\bar{z}'(t) = K_1(\bar{\lambda}, \bar{\lambda}') + K_2(\bar{y}, \bar{z}), \quad 0 < t < T. \tag{4.12}$$

Here and henceforth, K_i, $\widetilde{K_i}$, $K_i^{(1)}$ are linear functions in their arguments whose coefficients are bounded in $C[0, T]$ by M. We set $\bar{\theta} = \theta_1 - \theta_2$. Next, we take the difference of (4.8) for $j = 1, 2$, leading to

$$\begin{aligned}\left(1 + \nu\delta(w_1)^2\right)\bar{\theta}_t - \hat{\kappa}\bar{\theta}_{xx} + \nu(\delta(w_1) + \delta(w_2))\partial_t\bar{\theta}_2(\alpha_1\bar{y} + \alpha_2\bar{z}) + \nu\delta(w_2)(\alpha_1 y_2' + \alpha_2 z_2')\bar{\theta} \\ + \nu\delta(w_1)\theta_1(\alpha_1\bar{y}' + \alpha_2\bar{z}') + \nu(\alpha_1 y_2' + \alpha_2 z_2')\theta_1(\alpha_1\bar{y} + \alpha_2\bar{z}) \\ = \hat{L}_1(w_1)\bar{y}' + \hat{L}_2(w_1)\bar{z}' + \nu(\beta_1 y_2' + \beta_2 z_2')(\alpha_1\bar{y} + \alpha_2\bar{z}) - \hat{\gamma}\bar{\theta}.\end{aligned}$$

We rewrite the latter as

$$\begin{aligned}\left(1 + \nu\delta(w_1)^2\right)\bar{\theta}_t - \hat{\kappa}\bar{\theta}_{xx} + \nu(\delta(w_2)(\alpha_1 y_2' + \alpha_2 z_2') + \hat{\gamma})\bar{\theta} \\ = (\hat{L}_1(w_1) - \nu\delta(w_1)\alpha_1\theta_1)\bar{y}' + (\hat{L}_2(w_1) - \nu\delta(w_1)\alpha_2\theta_1)\bar{z}' \\ +K_3(\bar{y}, \bar{z}), \quad 0 < x < 1,\, t > 0,\end{aligned} \tag{4.13}$$

and

$$\bar{\theta}(x, 0) = 0, \quad \bar{\theta}_x(0, t) = \bar{\theta}_x(1, t) = 0, \quad 0 < x < 1,\, t > 0. \tag{4.14}$$

Henceforth, we define an operator

$$A(x, t) = \frac{-1}{1 + \nu\delta(w_1)^2}(\hat{\kappa}\partial_x^2 - \nu\delta(w_2(t))(\alpha_1 y_2' + \alpha_2 z_2') - \hat{\gamma}) \quad \text{for} \quad x \in (0, 1), t \in [0, T].$$

With the family of operators $A(x, t)$, $t \in [0, T]$, we associate a family of linear operators $A(t)$, $t \in [0, T]$, in $L^2(0, 1)$ such that

$$(A(t)\theta)(x) = A(x, t)\theta(x) \quad \text{for} \quad \theta \in \mathcal{D}(A(t)) = \{\eta \in H^2(0, 1) : \eta_x(0) = \eta_x(1) = 0\}.$$

This allows us to recast (4.13) and (4.14) as an (abstract) initial value problem

$$\begin{aligned}\bar{\theta}'(t) = -A(t)\bar{\theta}(t) + \frac{\hat{L}_1(w_1) - \nu\delta(w_1)\alpha_1\theta_1}{1 + \nu\delta(w_1)^2}\bar{y}' \\ +\frac{\hat{L}_2(w_1) - \nu\delta(w_1)\alpha_2\theta_1}{1 + \nu\delta(w_1)^2}\bar{z}' + \frac{K_3(\bar{y}, \bar{z})(t)}{1 + \nu\delta(w_1)^2}, \quad t > 0\end{aligned}$$

and $\bar{\theta}(0) = 0$. Here, we write $\bar{\theta}(t) = \bar{\theta}(\cdot, t)$.

Due to Assumption (A3), all coefficients of derivatives in operator $A(x,t)$ are Lipschitz continuous. Since the coefficient of the zeroth-order term is positive, i.e.,

$$\nu\delta(w_2(t))(\alpha_1 y_2' + \alpha_2 z_2') + \hat{\gamma} > 0$$

due to (A1) and (A3), the operator $A(0)^{-1}$ exists (see, e.g., Theorem 2.6 in Tröltzsch [79, p. 35]). Therefore, Assumption 5.1.1 and 5.2.1 in Chapter 5 in Tanabe [77] are satisfied (see Example in Section 5.2 in Tanabe [77, p. 129] or Lemma 6.1 in Pazy [58, p. 227]).

We denote by $U(t,s), 0 \le s \le t \le T$, a fundamental solution, associated with the family $A(t), t \in [0,T]$. In particular, $\partial_s U(t,s) = U(t,s)A(s)$. By Theorem 5.2.2 in Tanabe [77] we have

$$\begin{aligned}\bar{\theta}(t) = &\int_0^t U(t,s)\frac{\hat{L}_1(w_1) - \nu\delta(w_1)\alpha_1\theta_1}{1+\nu\delta(w_1)^2}\bar{y}'(s)ds \\ &+ \int_0^t U(t,s)\frac{\hat{L}_2(w_1) - \nu\delta(w_1)\alpha_2\theta_1}{1+\nu\delta(w_1)^2}\bar{z}'(s)ds + \int_0^t U(t,s)\frac{K_3(\bar{y},\bar{z})(s)}{1+\nu\delta(w_1)^2}ds\end{aligned}$$

for $0 < t < T$. Differentiating the both sides implies

$$\begin{aligned}\bar{\theta}'(t) = &\frac{\hat{L}_1(w_1) - \nu\delta(w_1(t))\alpha_1\theta_1(t)}{1+\nu\delta(w_1(t))^2}\bar{y}'(t) + \frac{\hat{L}_2(w_1) - \nu\delta(w_1(t))\alpha_2\theta_1(t)}{1+\nu\delta(w_1(t))^2}\bar{z}'(t) \\ &+ \int_0^t \widetilde{K_4}(\bar{y}',\bar{z}')(s)ds + \widetilde{K_5}(\bar{y},\bar{z})(t) + \int_0^t \widetilde{K_6}(\bar{y},\bar{z})(s)ds.\end{aligned}$$

Defining $\bar{\tau}(t) := \bar{\theta}(x_0,t)$, we obtain

$$\begin{aligned}&\frac{\hat{L}_1(w_1) - \nu\delta(w_1(t))\alpha_1\theta_1(x_0,t)}{1+\nu\delta(w_1(t))^2}\bar{y}'(t) + \frac{\hat{L}_2(w_1) - \nu\delta(w_1(t))\alpha_2\theta_1(x_0,t)}{1+\nu\delta(w_1(t))^2}\bar{z}'(t) \\ &\quad = \bar{\tau}'(t) - \int_0^t K_4(\bar{y}',\bar{z}')(s)ds - K_5(\bar{y},\bar{z})(t) - \int_0^t K_6(\bar{y},\bar{z})(s)ds. \qquad (4.15)\end{aligned}$$

In view of (A5), we can solve (4.12) and (4.15) with respect to $\bar{y}'$ and $\bar{z}'$, which yields

$$\begin{aligned}\bar{y}'(t) = &K_7(\bar{\lambda},\bar{\lambda}',\bar{\tau}') + K_8(\bar{y},\bar{z}) \\ &+ \int_0^t (K_9(\bar{y},\bar{z})(s) + K_{10}(\bar{y}',\bar{z}')(s))ds, \quad 0 \le t \le T.\end{aligned}$$

Noting that $\bar{y}(0) = 0$, we have

$$|K_8(\bar{y},\bar{z})(t)|,\ |K_9(\bar{y},\bar{z})(t)| \le C\int_0^t (|\bar{y}'(s)| + |\bar{z}'(s)|)ds.$$

Mutatis mutandis, the same reasoning holds for $\bar{z}(t)'$. Altogether, we therefore obtain

$$\begin{aligned}&|\bar{y}'(t)| + |\bar{z}'(t)| \\ &\quad \le C(|\bar{\lambda}(t)| + |\bar{\lambda}'(t)| + |\bar{\tau}'(t)|) + C\int_0^t (|\bar{y}'(s)| + |\bar{z}'(s)|)ds, \quad 0 \le t \le T.\end{aligned}$$

The Gronwall inequality finally gives

$$|\bar{y}'(t)| + |\bar{z}'(t)| \leq C(\|\bar{\lambda}\|_{C^1[0,T]} + \|\bar{\tau}\|_{C^1[0,T]}), \quad 0 \leq t \leq T.$$

This completes the proof. □

The implication of this theorem is that the measurement data $\lambda(t), \tau(t)$ are sufficient for the determination of the unknown functions $y(t), y(z)$ if distinct functions $y(t), y(z)$ cannot produce the same response $u(1,t), \theta(x_0,t)$ to identical input data.

Further, we continue with the numerical treatment of the inverse problem.

4.5 Numerical implementation

In this section we present some results for the numerical identification of the phase fractions $y(t), z(t)$ from dilatometer curves, or more precisely, from certain measurements $\hat{\lambda}$ of the overall displacement $\hat{\lambda}(t) = u(1,t)$, as well as measurements $\hat{\tau}(t)$ of the temperature at one point on the surface, $\hat{\tau}(t) = \theta(x_0,t)$. To this end, we formulate the inverse problem as the optimal control problem (P): *minimize*

$$J(u,\theta,y,z) = \omega_1 \int_0^T (u(1,t) - \hat{\lambda}(t))^2 dt + \omega_2 \int_0^T (\theta(x_0,t) - \hat{\tau}(t))^2 dt$$

subject to the state system

$$u_{xx} - \delta(w)\theta_x = 0 \qquad \text{in } \Omega \times (0,T), \tag{4.16a}$$

$$\rho c_p \theta_t - \kappa\theta_{xx} + \Lambda\delta(w)u_{xt} - \rho L_1 y' - \rho L_2 z' = \gamma(\theta^e - \theta) \qquad \text{in } \Omega \times (0,T), \tag{4.16b}$$

$$u(0,t) = 0, \quad u_x(1,t) - \delta(w)\theta(1,t) + \eta(w) = 0 \qquad \text{in } (0,T), \tag{4.16c}$$

$$\theta_x(0,t) = \theta_x(1,t) = 0 \qquad \text{in } (0,T), \tag{4.16d}$$

$$\theta(\cdot,0) = \theta_0 \qquad \text{in } \Omega. \tag{4.16e}$$

and the control constraints $y, z \in U_{ad}$.

The set of admissible controls U_{ad} can be defined as $U_{ad} = \{y, z : 0 \leq y, z \leq 1\}$. It reflects the fact that from the physical point of view, the phase fractions functions y, z should be non-negative and should not exceed 1. To obtain useful results, an equilibrating of the terms in the cost functional is indispensable. To this end, we set

$$\omega_1 = 10^4, \qquad \omega_2 = \frac{1}{(\hat{\tau}(0) - \hat{\tau}(T))^2}$$

in further numerical computations.

To solve the control problem numerically, we apply the "first discretize, then optimize" approach. It transforms the original continuous optimal control problem into a standard finite dimensional optimization problem. For this purpose, the state system and the objective functional are fully discretized. Then, the discretized optimization problem, which is typically large, can be solved by the existing optimization solvers.

4.5.1 The discretized problem

We first discuss the discretization of the state system of the optimal control problem (P). The solution of the state system (4.16b)–(4.16e) will be approximated using the finite-difference technique. We begin with the initial boundary value problem (4.16b), (4.16d)–(4.16e) for the temperature. We first partition the intervals $[0,1]$ and $[0,T]$ into respective finite equidistant grids as follows

$$x_i = i\Delta x, \quad i = 0,1,\dots,M, \quad \text{where} \quad \Delta x = \frac{1}{M}, \tag{4.17}$$

$$t_j = j\Delta t, \quad j = 0,1,\dots,N, \quad \text{where} \quad \Delta t = \frac{T}{N}. \tag{4.18}$$

Let θ_i^j and u_i^j be an approximation of $\theta(x_i,t_j)$ and $u(x_i,t_j)$, respectively, for $0 \le i \le M$, $0 \le j \le N$. We consider a semi-implicit method, in which we treat the coupling terms explicitly and use the Backward in Time Central in Space Scheme (BTCS) for the rest of the terms. In BTCS, the time derivative in (4.16b) is replaced by a backward difference scheme and a space derivative by the central difference scheme. This yields

$$\begin{aligned}\rho c_p \frac{\theta_i^{j+1}-\theta_i^j}{\Delta t} - \kappa \frac{\theta_{i+1}^{j+1}-2\theta_i^{j+1}+\theta_{i-1}^{j+1}}{(\Delta x)^2} + \Lambda\delta(\omega)\frac{u_{i+1}^{j+1}-u_i^{j+1}-u_{i+1}^j+u_i^j}{\Delta x \Delta t} \\ = \rho L_1 y_t + \rho L_2 z_t + \gamma(\theta^e - \theta_i^j).\end{aligned} \tag{4.19}$$

Next, we introduce the vectors $\boldsymbol{\theta}^j, \boldsymbol{u}^j \in \mathbb{R}^{M+1}$, such that $\boldsymbol{\theta}^j = (\theta_0^j, \theta_1^j, \dots, \theta_M^j)^T$ and $\boldsymbol{u}^j = (u_0^j, u_1^j, \dots, u_M^j)^T$. In order to implement the Neumann boundary condition (4.16d) we consider the virtual grid points outside the domain Ω. Then, for the values of temperature $\theta_{-1}, \theta_{M+1}$ at this virtual grid points, it yields $\theta_{-1} = \theta_1$ and $\theta_{M+1} = \theta_{M-1}$. Analogously, the Neumann boundary condition in (4.16c) for u can be treated. In particular, it implies that

$$u_{M+1} = u_{M-1} + 2\Delta x(\delta(w)\theta_M - \eta(w)).$$

Further, we build up the corresponding matrices and rewrite (4.19) in the form

$$C_1\boldsymbol{\theta}^{j+1} = \Big(\frac{\rho c_p}{\Delta t} - \gamma\Big)C_2\boldsymbol{\theta}^j - C_3\boldsymbol{u}^{j+1} + C_3\boldsymbol{u}^j + D_1 \tag{4.20}$$

with matrices $C_1, C_2, C_3 \in \mathbb{R}^{(M+1,M+1)}$ and vector $D_1 \in \mathbb{R}^{M+1}$.

$$C_1 = \begin{pmatrix} \frac{\rho c_p}{\Delta t} + \frac{2\kappa}{(\Delta x)^2} & -\frac{2\kappa}{(\Delta x)^2} & & & \mathbf{0} \\ -\frac{\kappa}{(\Delta x)^2} & \frac{\rho c_p}{\Delta t} + \frac{2\kappa}{(\Delta x)^2} & -\frac{\kappa}{(\Delta x)^2} & & \\ & & \ddots & & \\ & & -\frac{\kappa}{(\Delta x)^2} & \frac{\rho c_p}{\Delta t} + \frac{2\kappa}{(\Delta x)^2} & -\frac{\kappa}{(\Delta x)^2} \\ \mathbf{0} & & & -\frac{2\kappa}{(\Delta x)^2} & \frac{\rho c_p}{\Delta t} + \frac{2\kappa}{(\Delta x)^2} + \frac{\Lambda\delta(w)^2}{\Delta t} \end{pmatrix},$$

$$C_2 = \begin{pmatrix} 1 & & & & \mathbf{0} \\ & 1 & & & \\ & & \ddots & & \\ & & & 1 & \\ \mathbf{0} & & & & 1 + \frac{\Lambda\delta(w)^2/\Delta t}{\frac{\rho c_p}{\Delta t} - \gamma} \end{pmatrix}, \quad C_3 = \frac{\Lambda\delta(w)}{\Delta x \Delta t}\begin{pmatrix} -1 & 1 & & & \mathbf{0} \\ & -1 & 1 & & \\ & & \ddots & & \\ & & & -1 & 1 \\ \mathbf{0} & & & 0 & 0 \end{pmatrix}.$$

$$D_1 = \begin{pmatrix} \rho L_1 y_t + \rho L_2 z_t + \gamma\theta^e \\ \vdots \\ \rho L_1 y_t + \rho L_2 z_t + \gamma\theta^e + \Lambda\delta(w)\eta_t(w) \end{pmatrix}.$$

Analogously, we discretize equation (4.16a) for the displacement u. Using the same notations as before, we obtain

$$\frac{u_{i+1}^j - 2u_i^j + u_{i-1}^j}{(\Delta x)^2} - \delta(w)\frac{\theta_{i+1}^j - \theta_i^j}{\Delta x} = 0.$$

Incorporating the boundary conditions (4.16c), this equation can be written in matrix form as

$$C_4 \boldsymbol{u}^j = \Delta x \delta(w) C_5 \boldsymbol{\theta}^j + D_2, \tag{4.21}$$

where the matrices $C_4, C_5 \in \mathbb{R}^{(M+1,M+1)}$ and vector $D_2 \in \mathbb{R}^{M+1}$ are given by

$$C_4 = \begin{pmatrix} 1 & 0 & & & \mathbf{0} \\ 1 & -2 & 1 & & \\ & & \ddots & & \\ & & 1 & -2 & 1 \\ \mathbf{0} & & & 2 & -2 \end{pmatrix}, \quad C_5 = \begin{pmatrix} 0 & 0 & & & \mathbf{0} \\ & -1 & 1 & & \\ & & \ddots & & \\ & & & -1 & 1 \\ \mathbf{0} & & & & -2 \end{pmatrix},$$

$$D_2 = \begin{pmatrix} 0 \\ \vdots \\ 0 \\ 2\Delta x \eta(w) \end{pmatrix}.$$

Then, in order to find a numerical solution to the state system (4.16b)–(4.16e), provided the phase fraction functions (y, z) are known, in each time step j, $j = 0, 1, \ldots, N$, we first have to solve the linear system (4.21). After the solution $\boldsymbol{u}^j$ is found, the linear system (4.19) can be solved for $\boldsymbol{\theta}^{j+1}$.

Next, we specify the ansatz for the time dependent phase fraction functions (y, z), which serve as the control functions in the control problem (P) formulated above. The phase fraction functions (y, z) to be determined are represented as cubic splines. Enforcing the additional conditions

$$y(0) = z(0) = y'(0) = z'(0) = y'(T) = z'(T) = 0,$$

the remaining spline coefficients can be uniquely represented in terms of the values of (y, z) in the temporal grid points $t_1, \ldots, t_n$. Defining the parameter vector

$$p = (y(t_1), \ldots, y(t_n), z(t_1), \ldots, z(t_n))^T,$$

we consider the nonlinear optimization problem

$$(P_d) \qquad \min_p \left\{ \omega_1 \sum_{i=1}^{n} (u(1, t_i, p) - \hat{\lambda}(t_i))^2 dt + \omega_2 \sum_{i=1}^{n} (\theta(x_0, t_i, p) - \hat{\tau}(t_i))^2 dt \right\}$$

subject to a discretized version of the state system (4.16a)–(4.16e)

and the control constraint $p \in \widetilde{U}_{ad}$.

The admissible control set $\widetilde{U}_{ad}$ is defined as $\widetilde{U}_{ad} = \{p : \mathbf{0} \leq p \leq \mathbf{1}\}$. In the following, we will use the MATLAB routine `lsqnonlin` to solve the discretized optimization problem (P_d). It provides a choice of two optimization methods, the Trust-Region-Reflective algorithm and the Levenberg–Marquardt method. It should be noted that the Levenberg–Marquardt algorithm cannot handle bound constraints. We will apply this method for the parameter identification from the model data, where we consider the optimal control problem without control constraints. This case will be presented later in Section 4.5.3. For the parameter identification from the real dilatometer data in Section 4.5.4, we apply the Trust-Region-Reflective algorithm with respect to the admissible control set $\widetilde{U}_{ad} = \{p : \mathbf{0} \leq p \leq \mathbf{1}\}$.

In the next section, we provide the physical parameters used in the numerical simulations.

4.5.2 Physical parameters

In this thesis, numerical calculations are carried out for high carbon steel C1080 and Mo-Mn dual phase steel. The chemical composition of these steels is shown in Tables 4.1, 4.2.

C	Mn	P	S
0.75–0.88	0.6–0.9	0.04	0.05

Table 4.1: Chemical composition of C1080 steel in mass-%.

C	Mn	Mo	Si	Al
0.08	1.44	0.15	0.03	0.05

Table 4.2: Chemical composition of Mo-Mn dual phase steel in mass-%.

For both steels, the reference density at 20 °C are chosen to be $\rho = 7.85\,\mathrm{g/cm^3}$. The values for the heat conductivity κ and specific heat c_p are set to

$$\kappa = 0.5\,\mathrm{J/(s\,cm\,K)}, \quad c_p = 0.5\,\mathrm{J/(g\,K)}.$$

These values only represent a rough approximation by a constant function for the temperature-dependent factors $\kappa(\theta), c_p(\theta)$. More details on the thermal physical parameters can be found, e.g., in [65, 69]. The latent heats L_1, L_2 of the austenite-pearlite and the austenite-martensite phase transformations, respectively, are specified by the values from [28] as

$$L_1 = 77\,\mathrm{J/g}, \quad L_2 = 84\,\mathrm{J/g}.$$

The latent heat of the austenite-bainite phase transformation is assumed to be equal to the latent heat of the austenite-pearlite phase transformation, i.e., $77\,\mathrm{J/g}$. The Lamé parameters are chosen according to [69] as

$$\Lambda_1 = 1.07 \cdot 10^5\,\mathrm{Pa}, \quad \Lambda_2 = 7 \cdot 10^4\,\mathrm{Pa}.$$

The physical parameters for the thermal strain

Unfortunately, there are some difficulties in obtaining the data of the thermal expansion coefficients and especially of the reference temperatures in the mixing rule of the thermal strain. The data presented in the literature is not very extensive and usually corresponds to steels of a special chemical composition (cf. [69, pp. 104–110]). If several dilatometer curves corresponding to the different cooling rates are available, the thermal expansion coefficients and the reference temperatures can be directly drawn from the dilatation curves.

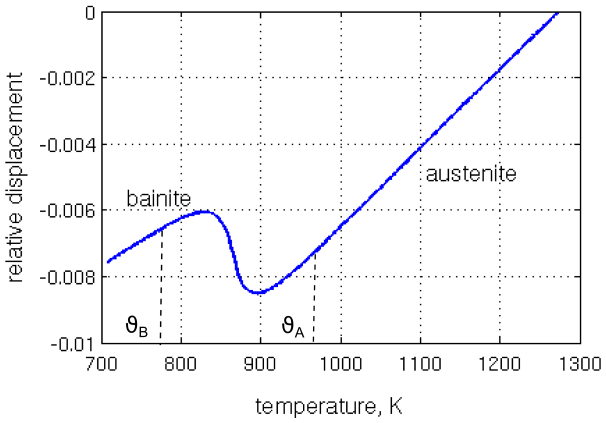

Figure 4.6: Measured dilatometer curve for the Mo-Mn dual phase steel.

As an example, we consider the dilatometer curve observed for the Mo-Mn dual phase steel. It exhibits the austenite-bainite phase transformation in the temperature range between θ_A and θ_B, see Figure 4.6. The resulting phase fraction of bainite is estimated as 100 %. Let $\bar{\lambda}$ denote the relative displacement as a function of the temperature θ as depicted in Figure 4.6. One knows that for any temperature above θ_A, the microstructure of steel is purely austenitic. As a result, the dilatation curve is linear in the high temperature range above θ_A. Hence, the linear thermal expansion coefficient δ_0 and the reference temperature θ^0_{ref} for austenite can be calculated from the ansatz for the thermal strain (4.3) as

$$\delta_0 = \frac{\bar{\lambda}(\theta_2) - \bar{\lambda}(\theta_1)}{\theta_2 - \theta_1}, \quad \theta^0_{ref} = \theta_1 - \frac{\bar{\lambda}(\theta_1)(\theta_2 - \theta_1)}{\bar{\lambda}(\theta_2) - \bar{\lambda}(\theta_1)}.$$

Here, θ_1, θ_2 are two arbitrary temperatures above the temperature θ_A. Analogically, the values of the linear thermal expansion coefficient δ_1 and the reference temperature θ^1_{ref} for bainite can be drawn from the dilatometer curve below the temperature θ_B. In this temperature range, the state is purely bainitic and the dilatation curve has again a linear dependence on the temperature.

In the next step, the data for the martensitic phase transformation can be obtained from the dilatometer curve, which exhibits, for instance, two phase transformations, from austenite to bainite and from austenite to martensite. In this case, the values of the thermal extension coefficient δ_2 and the reference temperature θ^2_{ref} can be calculated from the mixture ansatz for the thermal strain:

$$\bar{\lambda} = \delta_1 y(\theta - \theta^1_{ref}) + \delta_2 z(\theta - \theta^2_{ref}) + \delta_0(1 - y - z)(\theta - \theta^0_{ref}). \tag{4.22}$$

Here, y, z are the resulting phase fractions of bainite and martensite, respectively. Considering the part of the dilatation curve in the low temperature range, where the phase transformations are completed, the values of δ_2 and θ^2_{ref} can be calculated in a similar way as discussed above for austenite and bainite. All data obtained in such a way for Mo-Mn dual phase steel is listed in Table 4.3.

Symbol	Value	Unit	Symbol	Value	Unit
δ_0	$2.5 \cdot 10^{-5}$	1/K	θ^0_{ref}	1272	K
δ_1	$1.59 \cdot 10^{-5}$	1/K	θ^1_{ref}	1181	K
δ_2	$1.34 \cdot 10^{-5}$	1/K	θ^2_{ref}	1300	K

Table 4.3: The values of the thermal expansion and the reference temperatures for Mo-Mn dual phase steel. The constants δ_1 and θ^1_{ref} correspond to the austenite-bainite phase transformation.

The thermal expansion coefficients and reference temperatures used in the numerical computations for C1080 steel are summarized in Table 4.4.

Symbol	Value	Unit	Symbol	Value	Unit
δ_0	$1.55 \cdot 10^{-5}$	1/K	θ^0_{ref}	1473	K
δ_1	$1.7 \cdot 10^{-5}$	1/K	θ^1_{ref}	1234	K
δ_2	$1.16 \cdot 10^{-5}$	1/K	θ^2_{ref}	773	K

Table 4.4: The values of the thermal expansion and the reference temperatures for high carbon steel C1080. The constants δ_1 and θ^1_{ref} correspond to the austenite-pearlite phase transformation.

The heat transfer coefficient

There exist different cooling strategies in the dilatometer experiments. During the quenching, which is characterized by the highest cooling rates, the coolant is blown onto the specimens (forced convection). This is achieved in practice by cooling with helium gas. Normally, the first cooling curves in the Continuous Cooling Transformation (CCT) diagram are produced in this way. The moderate cooling curves are regarded as natural convection. Finally, in order to realize low cooling rates and to decelerate the cooling, the specimens are heated by electromagnetic induction. All these aspects should be taken into account when modelling the heat transfer in the dilatometer experiment. In this thesis, the identification of the phase transformations from the dilatometer experiments with a fast and a moderate cooling is considered. In the case of slow cooling, the effect of electromagnetic induction has to be taken into account by including an additional source term on the right-hand side of the energy balance (4.16b). A precise model of this effect requires further studies but it is out of the scope of this thesis.

According to the experimental setup, the data for the Newton-type cooling model on the right-hand side of heat equation (4.16b) have to be identified. An appropriate measurable coolant temperature θ^e would be the temperature at the inner boundary of the tube surrounding the specimens in the dilatometer (cf. Figures 4.1, 4.2). However,

for preliminary technical reasons, θ^e is assumed to be constant and we set $\theta^e = 20\,^\circ\mathrm{C} = 293.15\,\mathrm{K}$.

For the heat transfer coefficient, or its dimensionless form (the Nusselt number), a lot of expressions exist depending on the exact geometrical configurations, e.g., [63, 83]. However, none of them fits well with the dilatometer being considered. Typically, the Nusselt number is expressed as a product of further dimensionless characteristic numbers with empirical exponents. The general relationship between the heat transfer coefficient α and the Nusselt number Nu is the following

$$\alpha = \frac{\kappa_h \mathrm{Nu}}{L_c}\,\mathrm{W}/(\mathrm{m}^2\,\mathrm{K}) = 10^{-4}\frac{\kappa_h \mathrm{Nu}}{L_c}\,\mathrm{W}/(\mathrm{cm}^2\,\mathrm{K}). \tag{4.23}$$

Here, κ_h refers to the thermal conductivity of the fluid (in our case, helium) and L_c is a characteristic length of the surface. The characteristic length should be selected in the direction of the growth (or the thickness) of the boundary layer. For instance, for the cross-flow over a horizontal cylinder, it is usually a diameter of the cylinder. In our case, due to the restriction of the model to the one-dimensional case, the characteristic length L_c will be chosen to be the length of the cylinder, i.e., $L_c = L$.

The heat transfer coefficient for the *forced convection* is a primary function of the fluid velocity and the fluid properties, and it is a secondary function of the temperature because the fluid properties are temperature-dependent. Considering the forced convection, the average Nusselt number for the cross-flow over a horizontal cylinder can be found from the correlation (cf. [88])

$$\mathrm{Nu} = (0.4\mathrm{Re}^{\frac{1}{2}} + 0.06\mathrm{Re}^{\frac{2}{3}})\mathrm{Pr}^{0.4}\left(\frac{\eta_\infty}{\eta}\right)^{\frac{1}{4}}, \tag{4.24}$$

where Re and Pr denote the Reynolds and the Prandtl number, respectively. The factors η_∞ and η represent the dynamical viscosity of the coolant and are in general temperature-dependent functions. For helium, they can be calculated from the correlation formula (cf. [59])

$$\eta = 3.674 \cdot 10^{-7}\theta^{0.7}\,\mathrm{kg}/(\mathrm{m\,s}), \tag{4.25}$$

$$\eta_\infty = \eta|_{\theta=293.15\,\mathrm{K}} = 1.96 \cdot 10^{-5}\,\mathrm{kg}/(\mathrm{m\,s}), \tag{4.26}$$

with θ in K. We recall that the length of the investigated cylinder is $L = 0.01\,\mathrm{m}$. Hence, the Reynolds number can be computed by

$$\mathrm{Re} = \frac{\rho_h v L}{\eta}, \tag{4.27}$$

where the density of helium ρ_h can be derived from the ideal gas law as

$$\rho_h = \frac{48.78}{\theta}\,\mathrm{kg}/\mathrm{m}^3,$$

with θ in K, and the dynamical viscosity η from (4.25). The velocity of helium v will first be considered as an unknown parameter in the model. The Prandtl number for helium is defined as $\mathrm{Pr} = \frac{2}{3}$. On the other hand, according to the definition, we have

$$\mathrm{Pr} = \frac{\eta c_h}{\kappa_h}, \tag{4.28}$$

where $c_h = 5190\,\mathrm{J/(kg\,K)}$ and κ_h are the specific heat capacity and the thermal conductivity of helium, respectively. Hence, from (4.25) and (4.28), we obtain

$$\kappa_h = \frac{3\eta c_h}{2} = \frac{1.41 \cdot 10^{-4}\theta^{7/6}}{(1 + 0.04 \cdot \theta^2)^{1/4}}\,\mathrm{W/(m\,K)}.$$

In the case of *natural convection*, the heat transfer coefficient is a primary function of the fluid properties and of the temperature difference between the considered solid component and the fluid. The Nusselt number for natural convection for the horizontal cylinder is given in the following form [63]:

$$\mathrm{Nu} = 0.59(\mathrm{Gr} \cdot \mathrm{Pr})^{0.25},$$

where Gr is a Grashof number which characterizes the natural convection effect. It is defined by

$$\mathrm{Gr} = \frac{\beta g \Delta\theta \rho_h^2 L^3}{\eta^2},$$

where

g - the acceleration due to the gravity, $\mathrm{m/s^2}$,
$\Delta\theta = \theta_s - \theta_\infty$ - the temperature difference between the surface and the fluid, K,
β - a coefficient of volumetric expansion, expressed for helium by $\frac{1}{\theta} = \frac{2}{\theta_s + \theta_\infty}\,1/\mathrm{K}$.

The parameters ρ_h, L, η are defined as before. Finally, according to (4.23), the heat transfer coefficient in (4.16b) can be calculated by

$$\gamma = a \cdot 10^{-4}\frac{\kappa_h \cdot\ \mathrm{Nu}}{L} + b\,\mathrm{W/(cm^2\,K)}. \tag{4.29}$$

The constants a, b are the parameters that have to be fitted to the experimental data. In the case of forced convection, where the Nusselt number is given by (4.24), we have an additional unknown parameter v (cf. (4.27)), the velocity of helium.

The first rough approximation for the heat transfer coefficient can be derived from the dilatometer data. We consider the case of forced convection. For a given dilatometer curve, i.e., if the displacement and the temperature data are known, γ, as a function of temperature, can be identified from the heat equation (4.16b), assuming that no phase transformations occur during cooling. Then, the triple of unknown parameters (a, b, v) from the ansatz for the heat transfer coefficient (4.29) can be extracted from these approximate curves for γ. In the case of fast cooling, e.g., as in the first dilatometer curve for Mo-Mn dual phase steel, the parameters in (4.29) are the following:

$$a = 0.097,\ b = 0.01\,\mathrm{W/(cm^2\,K)},\ v = 568\,\mathrm{m/s} = 5.68 \cdot 10^4\,\mathrm{cm/s}.$$

Here, the Nusselt number was computed using (4.24). The heat transfer coefficient is depicted in Figure 4.7. We note that the calculated value of v should not be interpreted as the real velocity of helium in the dilatometer experiment. One possible reason for that is the reduction of the model to the one-dimensional case. Thus, in our model v acts just as the fitting parameter.

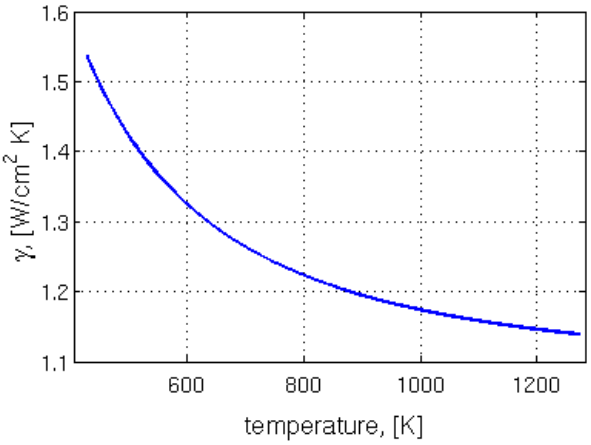

Figure 4.7: The identification of the heat transfer coefficient for the first dilatometer curve for Mo-Mn dual phase steel.

Remark 4.5.1. *We are now able to check the validity of Assumption (A5) for high carbon steel C1080 and Mo-Mn dual phase steel. In view of the data in Tables 4.3 and 4.4, we can conclude that*

$$\delta_2 \leq \delta(w) \leq \delta_1.$$

Since we cool below M_f, we have indeed $y'(t) = z'(t) = 0$ for $\theta < \theta^e$. Hence, it holds

$$\lambda(t) + \eta(w(t)) \geq |\Omega|\theta^e, \quad \delta^2(w(t))\theta(x_0, t) \geq \delta_2^2\theta^e.$$

Inserting the data for $L_{1,2}, \alpha_{1,2}, \beta_{1,2}$, it can be easily seen that the complete expression stays negative. Hence, we can verify that (A5) is satisfied.

4.5.3 Parameter identification from model data

We first validate our approach by using model data for the high carbon steel C1080. To generate the model data, we solve the system of state equations (4.16a)–(4.16e) together with two rate laws for pearlite fraction y and martensite fraction z:

$$y' = (1 - y - z)g(\theta), \tag{4.30}$$
$$z' = 5[\hat{z} - z]_+, \tag{4.31}$$

with

$$\hat{z} = \min\{\bar{m}, 1 - y\}$$

and $\bar{m}(\theta) = 1$ if $\theta < M_f$, $\bar{m}(\theta) = 0$ if $\theta > M_s$. In between, it is defined as the linear interpolation between 0 and 1. Here, M_s, M_f are the starting and finishing temperatures for the martensitic growth. The corresponding values for C1080 steel are $M_s = 227\,°\text{C}$, $M_f = 93\,°\text{C}$. As before, we denote $[\cdot]_+ = \max\{\cdot, 0\}$.

Equations (4.30)–(4.31) represent a simple rate law model. The growth rate y' of pearlite is assumed to be proportional to the remaining fraction of the high temperature phase (austenite) and a function g depending only on the temperature (cf. Figure 4.8),

while the second phase, martensite z, only grows as long as a certain temperature dependent threshold value is not exceeded. The values of M_s, M_f as well as the factor $g(\theta)$ in the model equations were calculated from the isothermal TTT-diagram for C1080 steel taken from [3].

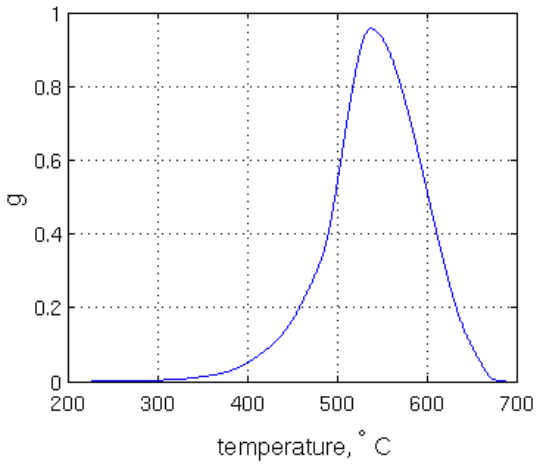

Figure 4.8: The data function $g(\theta)$ in (4.30).

Figure 4.9 and 4.10 show the resulting model dilatometer curves for the case of slow, fast and moderate cooling, respectively. Figure 4.11 shows the results of the parameter identification in the case of fast and slow cooling in comparison with the exact result. We can conclude that indeed the identification was successful.

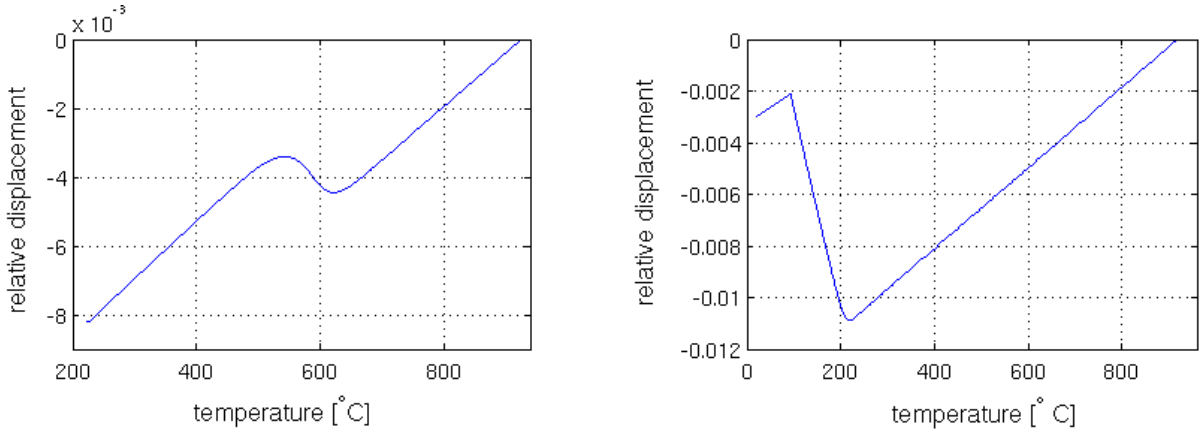

Figure 4.9: Model dilatometer curves for the slow (left) and the fast (right) cooling.

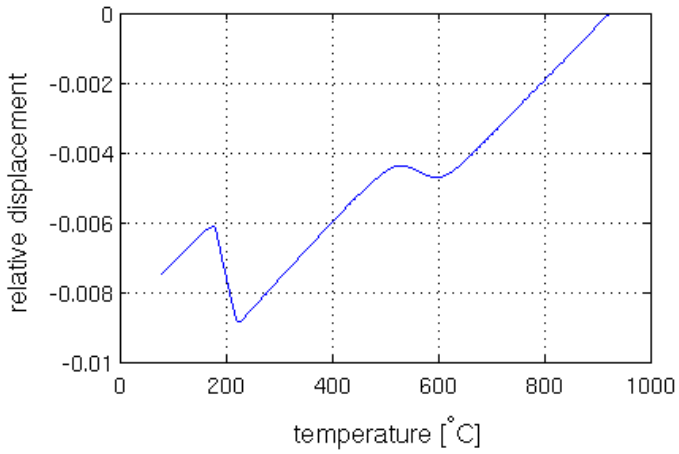

Figure 4.10: Model dilatometer curve for the moderate cooling.

However, the really interesting case is the one with moderate cooling (see Figure 4.10), which exhibits two phase transformations. Figure 4.12 shows three iterations and the final result of the optimization process in this case. Starting from the initial values $y_0 = z_0 \equiv 0$, already after three iterations the correct final phase fraction was reached. This is particularly important since, as it was mentioned before, the standard way of obtaining the resulting phase fraction values in the case of several phase transformations requires expensive and time consuming optical measurements.

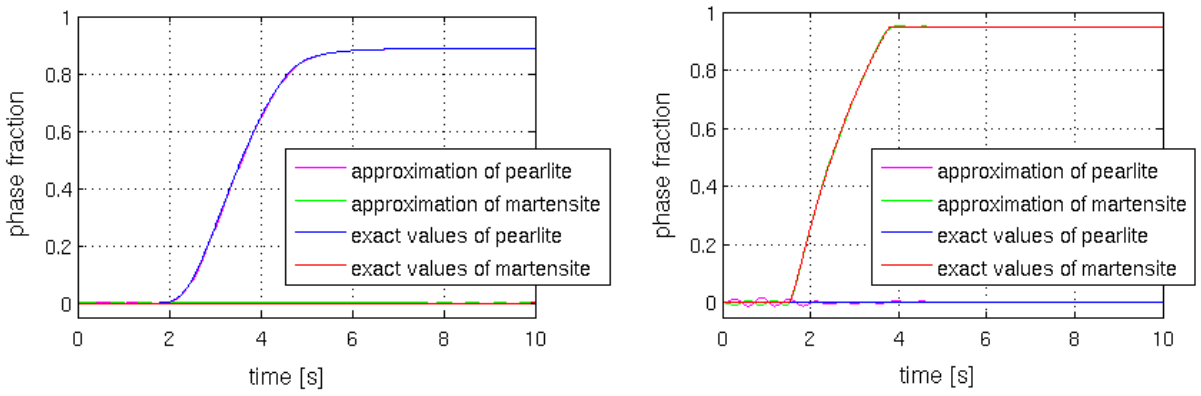

Figure 4.11: Results of the identification process for slow (left) and fast (right) cooling.

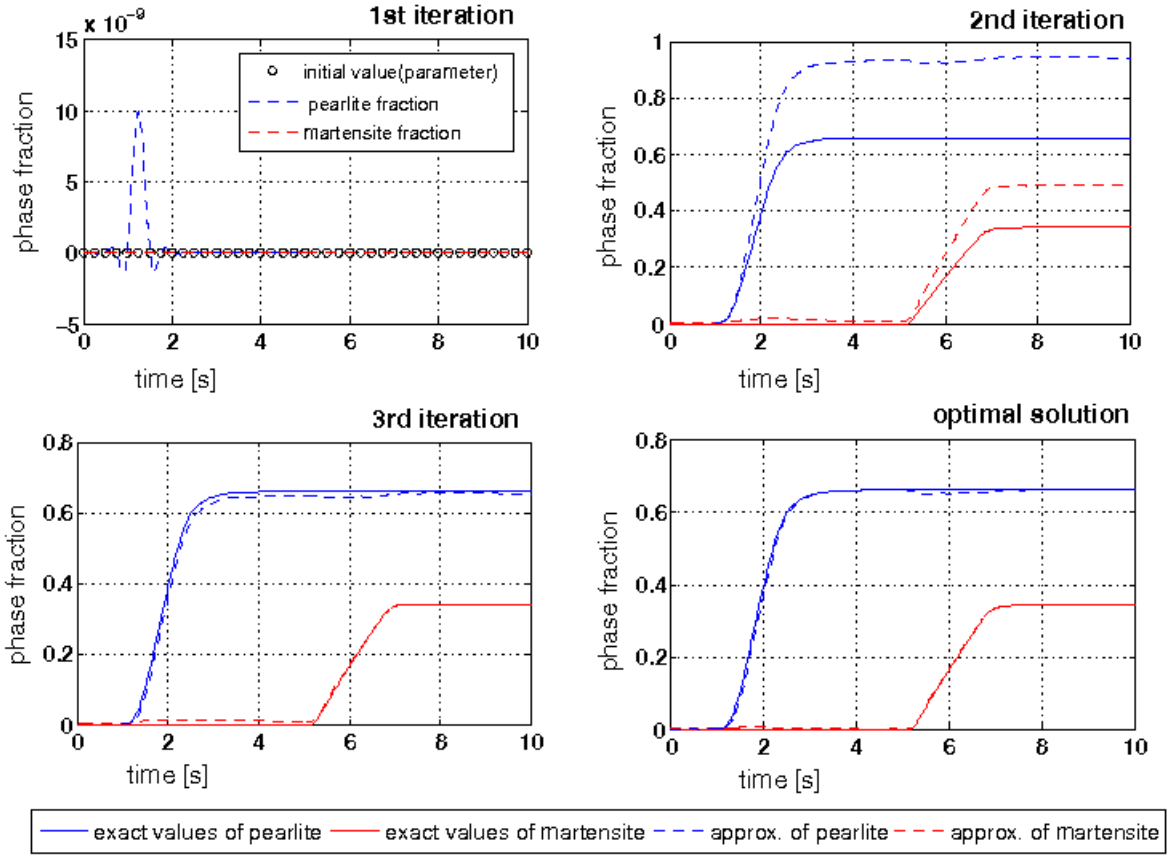

Figure 4.12: Three iterations and the final resulting phase fraction curves in the case of moderate cooling.

In order to confirm the stability estimate derived in Section 4.4, we additionally identify the phase fractions from the noisy model data. We generate the measurements of the displacement $\hat{\lambda}$ and the temperature $\hat{\tau}$ disturbed with a noise level of 5 %, i.e.,

$$\hat{\tau}(t) = \tau(t) + 0.05 \cdot (2 \cdot \mathrm{rand}(t) - 1) \cdot \tau(t),$$
$$\hat{\lambda}(t) = \lambda(t) + 0.05 \cdot (2 \cdot \mathrm{rand}(t) - 1) \cdot \lambda(t).$$

Here, rand denotes the pseudorandom value drawn from the standard uniform distribution on the open interval $(0, 1)$ generated for the time t. The corresponding dilatometer curve is depicted in Figure 4.13. The optimization procedure performed with the same parameter set as in previous calculations provides the phase fractions of pearlite and martensite. The optimal solution is presented in Figure 4.14. The phase fraction functions computed for the dilatometer data without noise are considered as the exact solution. It can be seen from Figure 4.14 that the deviation of the actual results from the exact values of the phase fractions is within acceptable limits. This numerical result confirms our theoretical stability estimate for the solution of the inverse problem.

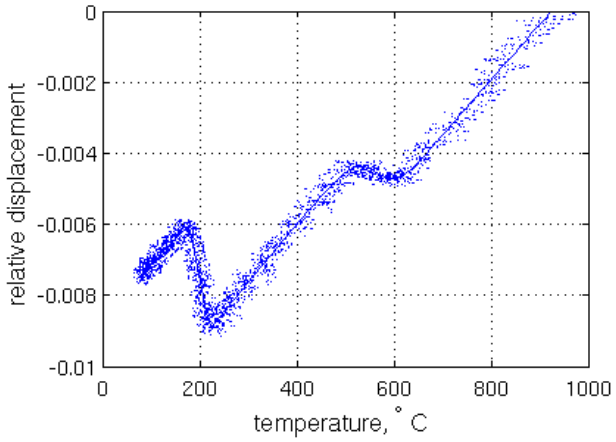

Figure 4.13: Model dilatometer curve for moderate cooling perturbed with a 5 % noise.

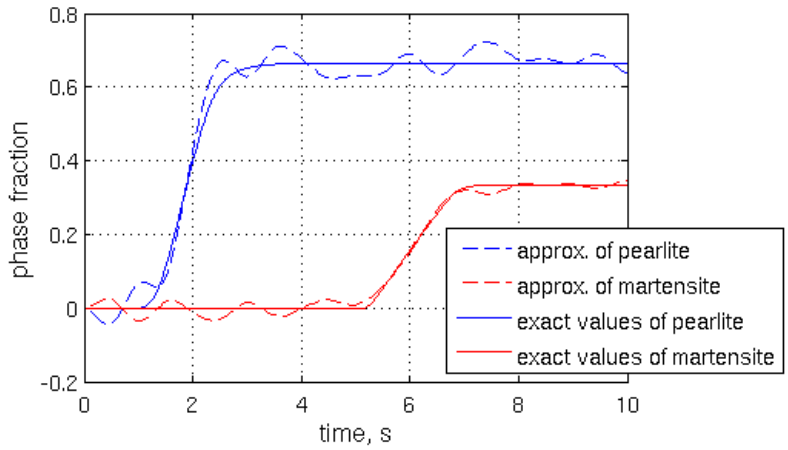

Figure 4.14: Results for the identification process from the noisy dilatometer data in comparison with the exact solution.

4.5.4 Parameter identification from real dilatometer data

To validate our numerical approach in praxis, we performed the parameter identification of the phase transformations from the real dilatometer data. It was observed that the results of the optimization procedure were significantly better when the cost functional in problem (P) additionally included some kind of regularization term, i.e.,

$$J(u,\theta,y,z) = \omega_1 \int_0^T (u(1,t) - \hat{\lambda}(t))^2 dt + \omega_2 \int_0^T (\theta(x_0,t) - \hat{\tau}(t))^2 dt + \omega_3 \int_0^T (y_t(t)^2 + z_t(t)^2) dt.$$

The last term in the cost functional is a so-called "smoothing term" which ensures additional smoothness of the control functions (y, z). For the numerical calculations we set $\omega_3 = 0.01$.

The used dilatometer data came from the dilatometer experiments that were carried out at the IEHK Aachen. For the experiments Mo-Mn dual phase steel with the chemical composition shown in Table 4.2 was chosen. Cylindrical dilatometer samples with a diameter of 5 mm and length of 10 mm were heated up to an austenitizing temperature of 1200 °C at a heating rate of 200 K/min, where the samples were austenitized for 10 minutes and then cooled down to room temperature with different cooling rates. The phase transformation kinetics from the evaluation of the elongation curves, assisted by metallographic results, is presented in the CCT-diagram shown in Figure 4.15. The red points in the diagram correspond to the start and the end time of the phase transformations occurring during cooling. Here, we consider the parameter identification for the first cooling curve highlighted in red in Figure 4.15.

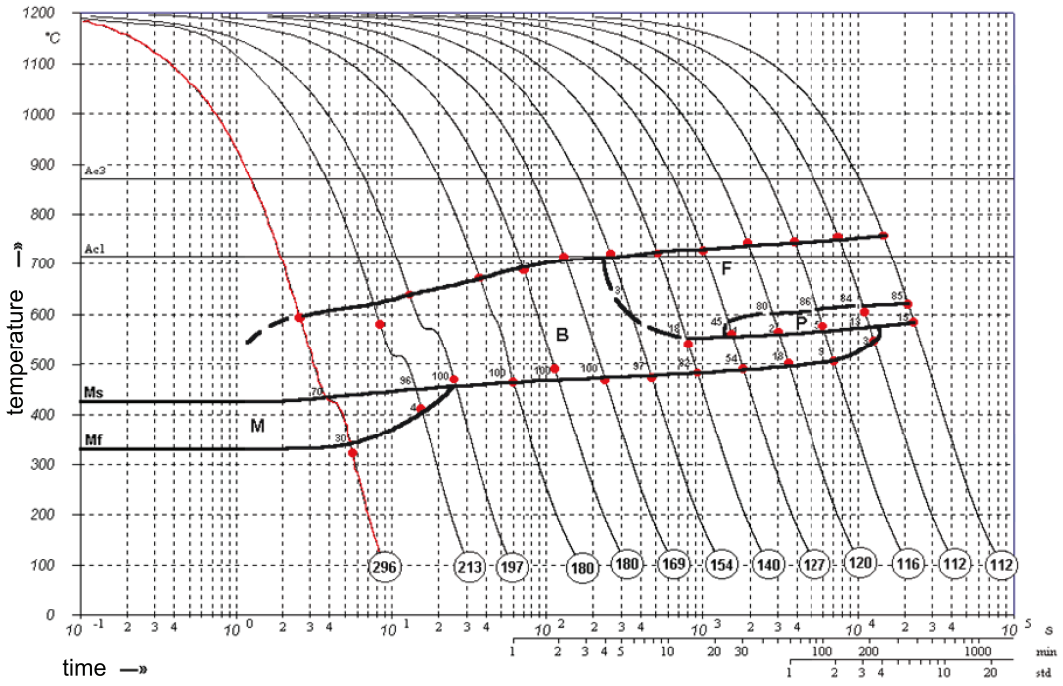

Figure 4.15: Continuous cooling transformation diagram for Mo-Mn dual phase steel (IEHK Aachen).

Figure 4.16 depicts the measurements of the dilatometer experiment, namely the surface temperature at the middle of the sample and the displacement measured on the right-hand side of the specimen. The corresponding dilatometer curve is presented in Figure 4.17. The metallographic investigations in this case estimate 70 % bainite and 30 % martensite. In Figure 4.17 one phase transformation between 600 °C and 400 °C (from austenite to bainite) can easily be seen, another one between 400 °C and 200 °C (from austenite to martensite) is hardly visible. However, our parameter identification procedure is indeed able to detect both phase transformations. Figure 4.18 shows four iterations of the optimization procedure for this case. The final phase fractions obtained by the optimization procedure are 75 % bainite and 25 % martensite. From a physical point of view, one would expect a monotone behaviour of the phase fraction curve which holds only true for one of them. However, the final phase fractions for both phases correspond

to the measured ones with a relative error of less than 8 %. The start and end times of the austenite-bainite phase transformation are 2 s and 4 s, respectively. The austenite-martensite transformation starts after 3.2 s of the cooling process and ends when the cooling time is approximately 6 s. These values have a good agreement with the experimental ones when compared with the data from the CCT diagram.

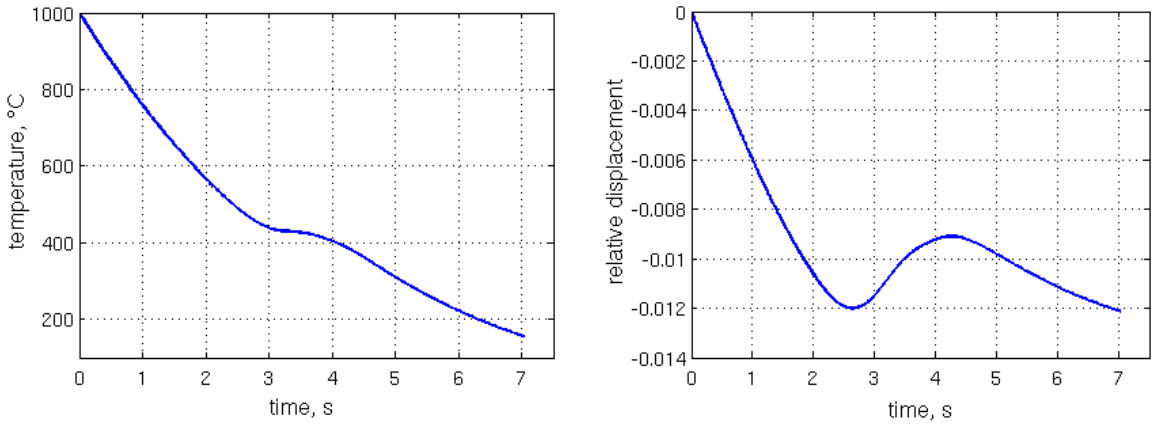

Figure 4.16: The dilatometer measurements of the temperature and the relative displacement for Mo-Mn dual phase steel (IEHK Aachen).

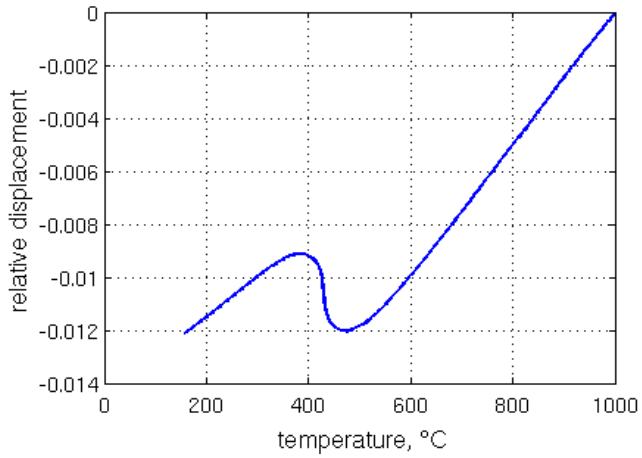

Figure 4.17: Measured dilatometer curve for the Mo-Mn dual phase steel (IEHK Aachen).

Further results for the parameter identification for the phase transformations in steel from the dilatometer measurements can be found in [75]. In this article, the experimental procedure is described in more detail and the numerical results for the medium carbon steel 16MnCr5 are presented.

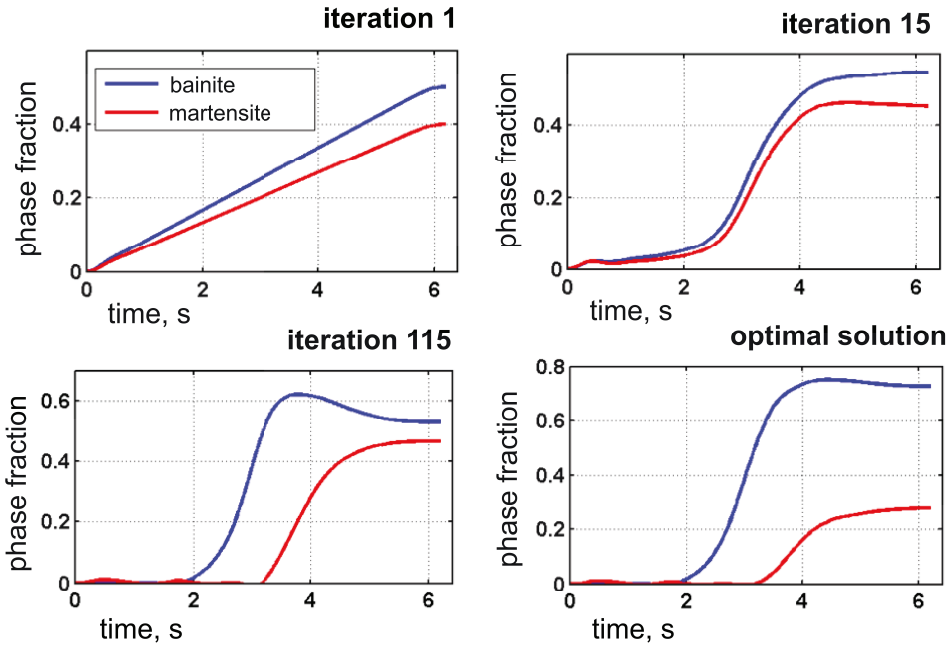

Figure 4.18: Results of the identification of two product phases from dilatometer measurements.

Chapter 5

Optimal control of the heat transfer coefficient for a semilinear parabolic system

The optimal control of heating and cooling processes belongs to the core of optimal control theory of parabolic equations. There are many applications of control theory to the optimal cooling of steel profiles, which have been discussed in a sequence of papers [25, 49, 51, 52, 82]. The control problems arising in these applications are parabolic boundary control problems. The state system consists of the heat equation with a convective boundary condition, in which the heat transfer coefficient serves as a control. The proposed optimal control approaches are solely focused on the evaluation of temperature.

In the current work, an optimal control problem for the cooling line of a hot rolling mill is considered, where the phase transformations in the steel slab are taken into account. It leads to a nonlinear boundary control problem, where the state system consists of a semilinear heat equation and an ordinary differential equation. The latter describes the evolution of the ferrite phase fraction. The time-dependent heat transfer coefficient serves as a control function. Due to the nonlinearity in the coupling term on the right-hand side of the heat equation, the state system requires a detailed analysis, especially concerning the regularity of the solutions, which is of crucial importance for the derivation of second-order sufficient optimality conditions.

In the first section of this chapter, the optimal control problem is introduced and the existence of an optimal solution is investigated. This section also includes the derivation of first-order necessary and second-order sufficient optimality conditions. The essential parts are the second-order optimality conditions, which form the basis for the successful convergence of the second-order optimization algorithms such as the sequential quadratic programming method. Second-order optimality conditions for control problems governed by parabolic equations have been discussed, e.g., in Goldberg and Tröltzsch [21] and Raymond and Tröltzsch [64]. In comparison to the very general and abstract setting of the latter contribution, the focus in this thesis is on the mixed boundary conditions and the control of the parameter function, e.g., the heat transfer coefficient function.

The second part of this chapter is devoted to the numerical implementation of the control problem studied in Section 5.1. In Section 5.2, the reduced sequential quadratic programming (rSQP) method is introduced. This method has proven to be very effective

in many areas of application, such as optimal control. A successful numerical application of the rSQP method to parabolic control problems has been reported by Hintermüller, Volkwein, and Diwoky [29], Kupfer and Sachs [47].

In each iteration of the rSQP method, the quadratic optimal control problem (QP^k) with control constraints has to be solved. To treat the (QP^k) problems, a primal-dual active set strategy is applied as, for instance, proposed by Bergounioux, Ito, and Kunisch [5] for control constrained optimal control problems. It is well-known that SQP methods converge only locally. In order to globalize the convergence behaviour of the rSQP method, first, a few steps of the projected gradient method are performed to find suitable initial values for the rSQP method.

Finally, a numerical test is carried out. This test demonstrates the convergence of the applied rSQP algorithm. The numerical results are presented in the last section of this chapter.

5.1 The optimal control problem

In this section, the optimal control problem is specified and the existence of an optimal solution is proven. Moreover, the first-order necessary and second-order sufficient optimality conditions are studied.

5.1.1 Problem formulation and assumptions

We consider an optimal control problem for the controlled cooling of steel profiles in order to obtain a desired temperature and phase distribution in the steel slab. The cooling process is governed by the coupled system of semilinear heat equation and ordinary differential equation for the phase growth of ferrite. To describe the evolution of ferrite, we take a rate law model based on the Leblond–Devaux ansatz

$$\begin{aligned} f_t &= (f_{eq}(\theta) - f)\mathcal{H}(f_{eq}(\theta) - f)g_1(\theta), \\ f(0) &= 0. \end{aligned}$$

Here, f denotes the volume fraction of ferrite, θ refers to the temperature and $\mathcal{H}$ is a regularized Heaviside function. Thus, the term $x\mathcal{H}(x)$ is a regularization of the positive part function $[x]_+$. The temperature distribution in the steel slab is described by the heat equation

$$\rho c_p \theta_t - \kappa \Delta \theta = \rho L f_t.$$

The density ρ, the heat capacity c_p, the heat conductivity κ and the latent heat L are assumed to be positive constants. The term $\rho L f_t$ describes the release of heat due to the phase transformation of ferrite. The boundary condition for the temperature imposed on the top and the bottom boundary of the domain Ω is given as Newton's law of cooling

$$-\kappa \frac{\partial \theta}{\partial n} = u(t)\beta(x)(\theta - \theta_w), \tag{5.1}$$

where θ_w is the temperature of the coolant. The proportionality factor is the heat transfer coefficient, which is split into two parts, one depending only on time and the other only

on the space variable. The function β can describe, for instance, a profile of cooling medium distribution on the surface of the steel slab, see Figure 5.1. The function u can be expressed through a coolant flow-rate during the cooling and serves as the control variable in our problem.

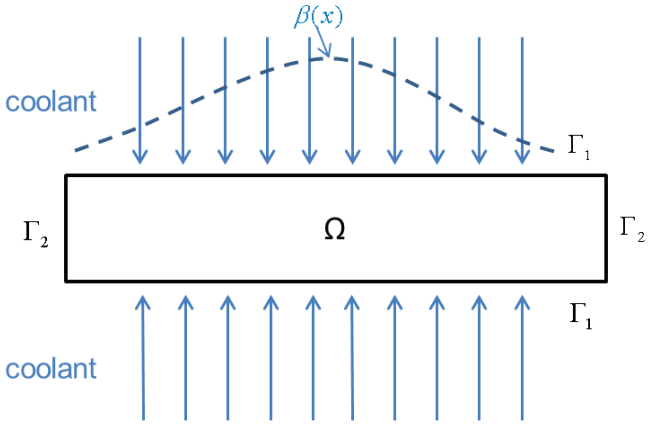

Figure 5.1: The scheme of the cooling of steel profiles.

We seek an optimal cooling strategy $\bar{u} = \bar{u}(t)$ such that a desired final phase distribution $f_d(x)$ is reached. At the same time, we want the temperature $\theta_d(x)$ to be realized at the end time T. Thus, the control problem (P) to obtain an optimal time-dependent heat transfer coefficient $u(t)$ can be formulated as follows: *minimize*

$$J(\theta, f, u) = \frac{\alpha_1}{2} \int_\Omega (f(x,T) - f_d(x))^2 \, dx + \frac{\alpha_2}{2} \int_\Omega (\theta(x,T) - \theta_d(x))^2 \, dx + \frac{\alpha_3}{2} \int_0^T u^2(t) dt$$

subject to

$$\begin{aligned}
f_t &= G(\theta, f) := (f_{eq}(\theta) - f)\mathcal{H}(f_{eq}(\theta) - f) g_1(\theta) && \text{in } Q, && (5.2a)\\
f(0) &= 0 && \text{in } \Omega, && (5.2b)\\
\rho c_p \theta_t - \kappa \Delta \theta &= \rho L f_t && \text{in } Q, && (5.2c)\\
-\kappa \frac{\partial \theta}{\partial n} &= u(t)\beta(x)(\theta - \theta_w) && \text{on } \Sigma_1, && (5.2d)\\
-\kappa \frac{\partial \theta}{\partial n} &= 0 && \text{on } \Sigma_2, && (5.2e)\\
\theta(0) &= \theta_0 && \text{in } \Omega && (5.2f)
\end{aligned}$$

and

$$u \in U_{ad} = \{u \in L^\infty(0,T) : u_a \le u \le u_b, \ u_a, u_b \ge 0\},$$

where $Q = \Omega \times (0,T)$, Γ_1 denotes the top and the bottom boundary of the domain Ω, and $\Sigma_1 = \Gamma_1 \times (0,T)$, $\Sigma_2 = (\partial\Omega \setminus \Gamma_1) \times (0,T)$. The factors α_i, $i = 1, \dots, 3$, are positive

constants. The third term in the cost functional represents a Tikhonov regularization term that can also be interpreted as a measure of the costs of the control. The control is bounded by two positive constants u_a and u_b since we consider only the cooling process and due to the restrictions on the maximal amount of coolant.

Further, we make some assumptions on the quantities of the optimal control problem that we need for the analysis.

Assumptions:

(A1) $\Omega \subset \mathbb{R}^3$ denotes a bounded domain with Lipschitz boundary $\partial\Omega$,

(A2) $f_{eq} \in C^{2,1}(\mathbb{R})$ and $f_{eq}(x) \in [0,1]$ for all $x \in \mathbb{R}$,
$\mathcal{H} \in C^{2,1}(\mathbb{R})$ is a monotone approximation of the Heaviside function satisfying $\mathcal{H}(x) = 0$ for $x \leq 0$,
$g_1 \in C^{2,1}(\mathbb{R})$ is non-negative and bounded,

(A3) $\beta \in L^\infty(\Omega)$ is non-negative, $\theta_w \in L^\infty(\Sigma_1)$, $\theta_0 \in C(\bar{\Omega})$,

(A4) $f_d \in L^\infty(\Omega)$, $0 \leq f_d \leq 1$ a.e. in Ω, $\theta_d \in C(\bar{\Omega})$.

The Assumption (A2) is necessary for the analysis of the state system (5.2) and for the twice Fréchet differentiability of the solution operator.

5.1.2 Analysis of the state system

In this section we will prove existence and uniqueness of a weak solution of the state system (5.2). We divide the proof into two steps. The first part is a preliminary lemma concerning only the ODE system (5.2a)–(5.2b), for θ prescribed. The second step is the coupling of the ODE system with the temperature equation, which gives a solution f, θ of the full state system.

Let us start with the discussion of the initial value problem (5.2a)–(5.2b) in the state system. The following result for the kinetics of the phase transformations in steel has already been discussed, e.g., by Hömberg [34], Hömberg and Volkwein [38], Kern [42] and Panizzi [57].

Lemma 5.1.1. *Suppose that (A2) holds true. Then, we have the following:*

(a) Let $\theta \in L^p(0,T;L^p(\Omega))$, $1 \leq p \leq \infty$, be given. Then (5.2a)–(5.2b) has a unique solution $f \in W^{1,\infty}(0,T;L^\infty(\Omega))$ satisfying

$$\|f\|_{W^{1,\infty}(0,T;L^\infty(\Omega))} \leq M_1$$

with a constant independent of θ. Moreover, $0 \leq f \leq 1$ for a.e. $(x,t) \in Q$.

(b) Let θ_1, $\theta_2 \in L^p(0,T;L^p(\Omega))$, $1 \leq p \leq \infty$, and let f_1, f_2 be the corresponding solutions of (5.2a)–(5.2b). Then, there exists a constant $M_2 > 0$ such that

$$\|f_1 - f_2\|_{W^{1,p}(0,T;L^p(\Omega))} \leq M_2 \|\theta_1 - \theta_2\|_{L^p(0,T;L^p(\Omega))}.$$

Proof. (a) Let $\hat{\theta} \in L^p(0,T;L^p(\Omega))$ be a representative of θ. We consider the ordinary differential equation given by

$$\dot{\zeta}(t) = \hat{G}(t,\zeta), \quad \zeta(0) = 0, \tag{5.3}$$

where $\hat{G}(t,\zeta) = G(\hat{\theta}(x,t),\zeta)$. In view of Assumption (A2), the function $\hat{G}(t,\zeta)$ satisfies the Carathéodory conditions (see B.5 in Appendix):

- $t \mapsto \hat{G}(t,\zeta)$ is measurable for all $\zeta \in \mathbb{R}$,
- $\zeta \mapsto \hat{G}(t,\zeta)$ is continuous for almost all $t \in (0,T)$.

The growth condition is also easily satisfied:

$$|\hat{G}(t,\zeta)| \le |f_{eq}(\hat{\theta}) - \zeta||g_1(\hat{\theta})| \le M + M|\zeta| \qquad \text{for a.e. } t \in (0,T), \tag{5.4}$$

where M is given by the boundedness of g_1 and f_{eq} according to Assumption (A2). Thus, according to Carathéodory Theorem (B.5), system (5.3) has a global solution on the time interval $[0,T]$.

Moreover, the solution is unique. This is deduced from the fact that $\hat{G}(t,\zeta)$ is Lipschitz continuous with respect to $\zeta \in [0,1]$ for almost all $t \in (0,T)$, i.e.,

$$\begin{aligned}
&|\hat{G}(t,\zeta_1) - \hat{G}(t,\zeta_2)| \\
&\qquad \le |(f_{eq}(\hat{\theta}) - \zeta_1)\mathcal{H}(f_{eq}(\hat{\theta}) - \zeta_1)g_1(\hat{\theta}) - (f_{eq}(\hat{\theta}) - \zeta_2)\mathcal{H}(f_{eq}(\hat{\theta}) - \zeta_2)g_1(\hat{\theta})| \\
&\qquad \le c|f_{eq}(\hat{\theta}) - \zeta_1||\mathcal{H}(f_{eq}(\hat{\theta}) - \zeta_1) - \mathcal{H}(f_{eq}(\hat{\theta}) - \zeta_2)| \\
&\qquad\quad + |\zeta_1 - \zeta_2|\mathcal{H}(f_{eq}(\hat{\theta}) - \zeta_2) \\
&\qquad \le c|\zeta_1 - \zeta_2|
\end{aligned}$$

$\forall \zeta_1, \zeta_2 \in [0,1]$. Here, we have used the boundedness of the functions f_{eq}, g_1 and the Lipschitz continuity of $\mathcal{H}$. The constant c is generic. It only remains to show that $\zeta \in [0,1]$ for almost all $t \in (0,T)$. This can be done by means of the classical comparison criterion for ODEs.

Due to the inequality

$$\begin{aligned}
\dot{\zeta}(t) &= (f_{eq}(\hat{\theta}) - \zeta(t))\mathcal{H}(f_{eq}(\hat{\theta}) - \zeta(t))g_1(\hat{\theta}) \\
&\le |f_{eq}(\hat{\theta}) - \zeta(t)|g_1(\hat{\theta})
\end{aligned}$$

we obtain

$$\zeta(t) \le f_{eq}(\hat{\theta})(1 - e^{-g_1(\hat{\theta})t}).$$

We conclude that $\zeta(t) \le f_{eq}(\hat{\theta}) \le 1$ almost everywhere in $(0,T)$. Since $\hat{G}(t,\zeta) \ge 0$ and $\zeta(0) = 0$, we have $\zeta(t) \ge 0$. From $0 \le \zeta(t) \le 1$, we deduce that

$$\|f\|_{W^{1,\infty}(0,T;L^\infty(\Omega))} \le M_1$$

with a constant M_1 independent of θ. Thus, the proof of part (a) is finished.

(b) Let $\theta_i \in L^p(0,T;L^p(\Omega))$, $1 \le p \le \infty$, $i = 1,2$, and define $\theta = \theta_1 - \theta_2$. Then, $f = f_1 - f_2$ solves

$$f_t = G(\theta_1, f_1) - G(\theta_2, f_2). \tag{5.5}$$

The function $G(\theta, f)$ is Lipschitz continuous in both variables. Testing (5.5) with f^{p-1}, $1 \leq p < \infty$, we obtain

$$\int_0^t \int_\Omega f_t(t) f^{p-1}(t) dxds = \int_0^t \int_\Omega (G(\theta_1, f_1) - G(\theta_2, f_2)) f^{p-1}(t) dxds,$$
$$\frac{1}{p} \int_\Omega |f|^p dx \leq c_1 \int_0^t \int_\Omega |\theta||f|^{p-1} dxds + c_2 \int_0^t \int_\Omega |f|^p dxds \tag{5.6}$$

for two constants $c_1, c_2 > 0$. To estimate the first additive term on the right-hand side of (5.6), we apply Young's inequality

$$ab \leq \frac{a^q}{q} + \frac{b^{q'}}{q'}, \text{ where } a, b \geq 0 \text{ and } \frac{1}{q} + \frac{1}{q'} = 1.$$

Choosing $q = p$, we have $q' = p/(p-1)$. Hence, we arrive at

$$\int_0^t \int_\Omega |\theta||f|^{p-1} dxds \leq \frac{1}{p} \int_0^t \int_\Omega |\theta|^p dxds + \frac{p-1}{p} \int_0^t \int_\Omega |f|^p dxds.$$

Inserting this bound into (5.6) gives

$$\int_\Omega |f|^p dx \leq c_1 \int_0^t \int_\Omega |\theta|^p dxds + (c_1(p-1) + c_2 p) \int_0^t \int_\Omega |f|^p dxds.$$

By applying Gronwall's lemma (Lemma B.1 in Appendix), we obtain

$$\int_\Omega |f|^p dx \leq c_1 e^{((c_1+c_2)p - c_1)t} \int_0^t \int_\Omega |\theta|^p dxds.$$

Taking the p-th root,

$$\|f\|_{L^p(\Omega)} \leq c_1^{1/p} e^{c_1+c_2} e^{-c_1 t/p} \|\theta\|_{L^p(0,t;L^p(\Omega))}.$$

Letting $p \to \infty$, we arrive at the estimate for $p = \infty$. Using (5.5) once again, part (b) of the lemma follows.

□

Before considering the heat equation, we recall the following results from the theory of linear parabolic equations. We consider the following linear parabolic problem

$$\rho c_p \theta_t - \kappa \Delta \theta = r \qquad \text{in } Q, \tag{5.7a}$$
$$-\kappa \frac{\partial \theta}{\partial n} = u(t)\beta(x)\theta + g \qquad \text{on } \Sigma_1, \tag{5.7b}$$
$$-\kappa \frac{\partial \theta}{\partial n} = 0 \qquad \text{on } \Sigma_2, \tag{5.7c}$$
$$\theta(0) = \theta_0 \qquad \text{in } \Omega. \tag{5.7d}$$

It is well known that a suitable function space for the solution of linear parabolic partial differential equations is

$$W(0,T) = \{\theta \in L^2(0,T; H^1(\Omega)) : \theta_t \in L^2(0,T; H^1(\Omega)^*)\}.$$

Under additional assumptions on the data r, g, u, θ_0, the following result can be obtained from Theorem 5.5 in Tröltzsch [79]:

Lemma 5.1.2. *Suppose that (A3) holds, and* $r \in L^{s_1}(Q)$, $g \in L^{s_2}(Q)$, $u \in L^\infty(0,T)$, $u \geq 0$. *Let* $s_1 > 5/2$, $s_2 > 4$, *then the initial value problem* (5.7a)–(5.7d) *admits a unique solution* $\theta \in W(0,T) \cap C(\bar{Q})$ *satisfying the a priori estimate with a constant* $C > 0$

$$\|\theta\|_{W(0,T)} + \|\theta\|_{C(\bar{Q})} \leq C(\|r\|_{L^{s_1}(Q)} + \|g\|_{L^{s_2}(\Sigma_1)} + \|\theta_0\|_{C(\bar{Q})}). \tag{5.8}$$

We will use this result in order to show the continuity of the solution of the semilinear heat equation in the state system (5.2). Moreover, this lemma will later be needed to ensure the solvability of a number of linearized systems.

With Lemma 5.1.1 and 5.1.2 at hand, we are now able to prove the existence and uniqueness of the solution of the state system (5.2).

Theorem 5.1.1. *Let (A1)–(A4) be satisfied. Then, the state system* (5.2) *admits for every control* $u \in U_{ad}$ *a unique solution*

$$(\theta,\, f) \in W(0,T) \cap C(\bar{Q}) \times W^{1,\infty}(0,T; L^\infty(\Omega))$$

satisfying

$$\|\theta\|_{W(0,T)} + \|\theta\|_{C(\bar{Q})} + \|f\|_{W^{1,\infty}(0,T;L^\infty(\Omega))} \leq M_3.$$

Proof. To prove the existence of a local unique solution of (5.2c)–(5.2f), we apply Banach's fixed point theorem. For that purpose, we define an operator

$$F : K \subset W(0,T) \to W(0,T)$$

that maps $\hat{\theta} \in W(0,T)$ to the solution θ of

$$\rho c_p \theta_t - \kappa \Delta \theta = \rho L \hat{f}_t \qquad \text{in } Q, \tag{5.9a}$$

$$-\kappa \frac{\partial \theta}{\partial n} = u(t)\beta(x)(\theta - \theta_w) \qquad \text{on } \Sigma_1, \tag{5.9b}$$

$$-\kappa \frac{\partial \theta}{\partial n} = 0 \qquad \text{on } \Sigma_2, \tag{5.9c}$$

$$\theta(0) = \theta_0 \qquad \text{in } \Omega, \tag{5.9d}$$

where $\hat{f}$ solves (5.2a)–(5.2b) with $\hat{\theta}$.

From Lemma 5.1.1 we find that $\hat{f} \in W^{1,\infty}(0,T; L^\infty(\Omega))$ is uniquely determined. Moreover, $\|f\|_{W^{1,\infty}(0,T;L^\infty(\Omega))} \leq M_1$. It follows from the theory of linear parabolic equations that (5.9) possesses a unique solution in $W(0,T)$ (see, e.g. [79, Chap. 3.4.4]). Hence, we can conclude that F is well-defined. Furthermore, the following a priori estimate with a constant $c > 0$ is valid:

$$\|\theta\|_{W(0,T)} \leq c(\|\hat{f}_t\|_{L^2(Q)} + \|u\beta\theta_w\|_{L^2(\Sigma_1)} + \|\theta_0\|_{L^2(\Omega)}). \tag{5.10}$$

We show that F is a self-mapping on some

$$K = \{\eta \in W(0,T) :\ \|\eta\|_{W(0,T)} \leq M\}.$$

Utilizing the Assumptions (A2)–(A3) and the fact that $u \in L^\infty(0,T)$, we obtain from (5.10)

$$\|\theta\|_{W(0,T)} \leq c,$$

where c depends on the constant M_1 from Lemma 5.1.1. Hence, $F(K) \subset K$, provided M has been chosen large enough.

Now, we want to show that F is a contraction. Let $\hat{\theta}_i \in K,\ i = 1, 2,\ \theta_i = F(\hat{\theta}_i)$, and $\hat{\theta} = \hat{\theta}_1 - \hat{\theta}_2$. Then, $\theta = \theta_1 - \theta_2$ solves

$$\begin{aligned} \rho c_p \theta_t - \kappa \Delta \theta &= \rho L(G(\hat{\theta}_1, f_1) - G(\hat{\theta}_2, f_2)) && \text{in } Q, \\ -\kappa \frac{\partial \theta}{\partial n} &= u(t)\beta(x)\theta && \text{on } \Sigma_1, \\ -\kappa \frac{\partial \theta}{\partial n} &= 0 && \text{on } \Sigma_2, \\ \theta(0) &= 0 && \text{in } \Omega. \end{aligned} \tag{5.11}$$

Here again, we use the a priori estimate

$$\|\theta\|_{W(0,T)} \le c\|\rho L(G(\hat{\theta}_1, f_1) - G(\hat{\theta}_2, f_2))\|_{L^2(Q)}. \tag{5.12}$$

Due to the Lipschitz continuity of G in both variables (Assumption (A2)) and Lemma 5.1.1 (b), we obtain

$$\|\theta\|_{W(0,T)} \le c(\|\hat{\theta}\|_{L^2(Q)} + \|f_1 - f_2\|_{L^2(Q)}) \le c\|\hat{\theta}\|_{L^2(Q)}. \tag{5.13}$$

Further, we use the fact that $W(0,T) \hookrightarrow C(0,T;L^2(\Omega))$

$$\|\theta\|_{W(0,T)} \le c\|\hat{\theta}\|_{L^2(Q)} \le cT^{1/2}\|\hat{\theta}\|_{L^\infty(0,T;L^2(\Omega))} \le cT^{1/2}\|\hat{\theta}\|_{W(0,T)}. \tag{5.14}$$

Hence, choosing $T^+ < T$ small enough, we conclude that F is a contraction on $W(0,T^+)$. Since F is also a self-mapping on K, we can apply Banach's fixed point theorem to conclude that F has a unique fixed point θ, which is a local solution to (5.2c)–(5.2f). By a bootstrapping argument, the solution can be extended to the time interval $[0,T]$. The regularity of θ, i.e., $\theta \in C(\bar{Q})$, follows from Lemma 5.1.2, provided we take

$$r := \rho L f_t \in L^\infty(Q),\ g := u(t)\beta(x)\theta_w \in L^\infty(\Sigma_1).$$

□

5.1.3 Existence of an optimal solution

Since the state system is nonlinear, we cannot expect uniqueness of an optimal control and we have to deal with local optimal controls. We have the following result.

Theorem 5.1.2. *Let Assumptions (A1)–(A4) be satisfied. Then, there exists at least one solution of the optimal control problem (P).*

To prove Theorem 5.1.2, we need the following auxiliary result:

Lemma 5.1.3. *Assume that $\{\theta_k\}$ is bounded in $L^2(0,T;H^1(\Omega)) \cap L^\infty(Q)$ and*

$$\theta_k \to \theta \quad \text{strongly in } L^2(0,T;L^2(\Omega)) \tag{5.15}$$

$$\text{and weakly in } L^2(0,T;H^1(\Omega))\,. \tag{5.16}$$

Then, it also holds

$$\theta_k \to \theta \quad \text{strongly in } L^2(0,T;L^2(\partial\Omega))\,.$$

Proof. We define the operator $A : L^2(0,T;H^1(\Omega)) \to L^2(0,T)$ by

$$A\theta = \int_{\partial\Omega} \theta(\sigma,t)d\sigma.$$

A is linear and also continuous, since the application of the trace theorem yields

$$\begin{aligned}\|A\theta\|^2_{L^2(0,T)} &= \int_0^T \left(\int_{\partial\Omega} \theta(\sigma,t)d\sigma\right)^2 dt \\ &\le |\partial\Omega| \int_0^T \int_{\partial\Omega} \theta^2(\sigma,t)d\sigma dt \le c\|\theta\|^2_{L^2(0,T;H^1(\Omega))}\,.\end{aligned}$$

In view of (5.16), we can infer

$$A\theta_k \rightharpoonup A\theta \quad \text{in } L^2(0,T)\,.$$

Utilizing the boundedness of $\{\theta_k\}$ in $L^\infty(Q)\cap L^2(0,T;H^1(\Omega))$, we observe that

$$\|\theta_k^2\|^2_{L^2(0,T;H^1(\Omega))} = \int_0^T \int_\Omega \theta_k^4 dxdt + 2\int_0^T \int_\Omega |\theta_k\nabla\theta_k|^2 dxdt \le c\,. \tag{5.17}$$

Now we take smooth functions $\varphi(x)$ and $\chi(t)$, then

$$\begin{aligned}&\int_0^T \left(\int_\Omega \theta_k^2\varphi dx\right)\chi(t)dt + \int_0^T \left(\int_\Omega \nabla(\theta_k^2)\nabla\varphi dx\right)\chi(t)dt \\ &\quad = \int_0^T \left(\int_\Omega \theta_k^2\varphi dx\right)\chi(t)dt + 2\int_0^T \left(\int_\Omega \theta_k\nabla\theta_k\nabla\varphi dx\right)\chi(t)\,dt\,.\end{aligned}$$

Since φ and χ are smooth, using (5.15) and (5.16) we deduce that

$$\langle\theta_k^2, \varphi\chi\rangle_{L^2(0,T;H^1(\Omega))} \to \langle\theta^2, \varphi\chi\rangle_{L^2(0,T;H^1(\Omega))}\,.$$

Together with (5.17), we have shown that

$$\theta_k^2 \rightharpoonup \theta^2 \quad \text{weakly in } L^2(0,T;H^1(\Omega))\,.$$

Since the limit does not depend on the extracted subsequence the whole sequence converges. From this, we infer

$$A\theta_k^2 \rightharpoonup A\theta^2 \quad \text{which means}$$

$$\|\theta_k\|_{L^2(0,T;L^2(\partial\Omega))} \to \|\theta\|_{L^2(0,T;L^2(\partial\Omega))}$$

and thus $\theta_k \to \theta$ strongly in $L^2(0,T;L^2(\partial\Omega))$. □

With Lemma 5.1.3 at hand, we are now able to prove the existence of an optimal solution of the control problem (P).

Proof of Theorem 5.1.2: Due to Theorem 5.1.1, there exists a unique solution

$$(\theta, f) \in W(0,T)\cap C(\bar{Q}) \times W^{1,\infty}(0,T;L^\infty(\Omega))$$

of the state system (5.2) for every control $u \in U_{ad}$. Since the set of admissible controls is bounded in $L^\infty(0,T)$, the set of respective solutions (θ, f) of the state system is bounded in $W(0,T) \cap C(\bar{Q}) \times W^{1,\infty}(0,T;L^\infty(\Omega))$, see Lemma 5.1.1 and Theorem 5.1.1.

By means of boundedness of the cost functional, there exists a minimizing sequence $\{\theta_k, f_k, u_k\}$ such that

$$j = \lim_{k\to\infty} J(\theta_k, f_k, u_k) = \inf J(\theta, f, u),$$

where $(\theta_k, f_k) = S(u_k)$ is the solution of the state system w.r.t. to the control u_k.

Since U_{ad} is bounded, closed and convex, there exists a subsequence $\{u_{k'}\}$ such that (cf. Mazur's Theorem B.11 in Appendix)

$$u_{k'} \rightharpoonup \bar{u} \quad \text{weakly in } L^2(0,T)\,.$$

In view of Theorem 5.1.1, extracting possibly a further subsequence still indexed by k', we have

$$\theta_{k'} \rightharpoonup \theta \qquad \text{weakly in } W(0,T) \tag{5.18}$$

$$\text{strongly in } L^2(Q)\,. \tag{5.19}$$

Applying Lemma 5.1.1 we obtain

$$f_{k'} \to f \quad \text{strongly in } W^{1,2}(0,T;L^2(\Omega))\,,$$

where f is the solution corresponding to θ. We use test functions $\varphi \in H^1(\Omega)$ and $\chi \in C^1[0,T]$ such that $\chi(T) = 0$ and consider the weak formulation of (5.2c)–(5.2f) for $(\theta_{k'}, f_{k'}, u_{k'})$

$$\begin{aligned}\rho c_p \textstyle\int_0^T \int_\Omega \theta_{k',t}\varphi\chi dxdt + \kappa \int_0^T \int_\Omega \nabla\theta_{k'}\nabla\varphi\chi dxdt + \int_0^T \left(\int_{\Gamma_1} \theta_{k'}\beta(\sigma)\varphi d\sigma\right) u_{k'}(t)\chi dt \\ = \int_0^T \left(\int_{\Gamma_1} \theta_w\beta(\sigma)\varphi d\sigma\right) u_{k'}(t)\chi dt + \rho L \int_0^T \int_\Omega f_{k',t}\varphi\chi dxdt\,.\end{aligned} \tag{5.20}$$

Except of the third term in (5.20), we can pass to the limit by standard arguments. To pass to the limit in the remaining term, we define

$$\xi_k(t) = \left(\int_{\Gamma_1} \theta_k\beta(\sigma)\varphi d\sigma\right)\chi(t)$$

and estimate

$$\int_0^T (\xi_{k'} - \xi)^2 dt = \int_0^T \left(\int_{\Gamma_1} (\theta_{k'} - \theta)\beta(\sigma)\varphi d\sigma\right)^2 \chi^2(t) dt \le c \int_0^T \|\theta_{k'} - \theta\|^2_{L^2(\Gamma_1)} dt\,.$$

Now we apply Lemma 5.1.3 and obtain

$$\xi_{k'} \to \xi \quad \text{strongly in } L^2(\Gamma_1)\,,$$

which enables us to pass to the limit in the remaining term in (5.20). Since the solution to the state equation is unique, we can infer

$$\theta = \theta(\bar{u}) =: \bar{\theta} \quad \text{and} \quad f = f(\bar{\theta}) =: \bar{f}\,.$$

It only remains to show the optimality of $(\bar{\theta}, \bar{f}, \bar{u})$. To this end, we write

$$J(\theta, f, u) = F(\theta, f) + Q(u),$$

where

$$F(\theta, f) = \frac{\alpha_1}{2} \int_\Omega (f(x,T) - f_d(x))^2\, dx + \frac{\alpha_2}{2} \int_\Omega (\theta(x,T) - \theta_d(x,T))^2\, dx,$$
$$Q(u) = \frac{\alpha_3}{2} \int_0^T u^2 dt.$$

Due to $\theta_{k'} \to \bar{\theta},\ f_{k'} \to \bar{f}$ and the continuity of $F(\theta, f)$, we have $F(\theta_{k'}, f_{k'}) \to F(\bar{\theta}, \bar{f})$. The functional Q is continuous and convex, therefore weakly lower semicontinuous (see Theorem B.12 in Appendix), i.e.,

$$u_{k'} \rightharpoonup \bar{u} \quad \Rightarrow \lim_{k' \to \infty} \inf Q(u_{k'}) \geq Q(\bar{u})$$

In conclusion, we have

$$\begin{aligned} j &= \lim_{k' \to \infty} J(\theta_{k'}, f_{k'}, u_{k'}) = \lim_{k' \to \infty} F(\theta_{k'}, f_{k'}) + \lim_{k' \to \infty} Q(u_{k'}) \\ &= F(\bar{\theta}, \bar{f}) + \lim_{k' \to \infty} \inf Q(u_{k'}) \geq F(\bar{\theta}, \bar{f}) + Q(\bar{u}) = J(\bar{\theta}, \bar{f}, \bar{u}). \end{aligned}$$

This means that $(\bar{\theta}, \bar{f}, \bar{u})$ is optimal. □

5.1.4 Differentiability of the solution operator

For the derivation of second-order optimality conditions for the control problem (P), it is necessary to show that the control-to-state mapping is twice continuously Fréchet differentiable. In this subsection we introduce the solution operator and show its Lipschitz continuity. Then, we prove the existence of the first and second Fréchet derivatives of the control-to-state mapping.

In view of the analysis of the state system, we define

$$Y = W(0,T) \cap C(\bar{Q})$$

and introduce the control-to-state mapping

$$S = (S_\theta,\, S_f) : L^\infty(0,T) \to Y \times W^{1,\infty}(0,T; L^\infty(\Omega)), \tag{5.21}$$

which assigns to every control $u(t) \in L^\infty(0,T)$ the solution of the state system (5.2). Moreover, the mapping is Lipschitz continuous.

Theorem 5.1.3. *Suppose that (A1)–(A4) hold and let* (θ_1, f_1), (θ_2, f_2) *be the solutions of* (5.2) *corresponding to* $u_1, u_2 \in L^\infty(0,T)$. *Then, there exists a constant* $C > 0$ *such that*

$$\|\theta_1 - \theta_2\|_{C(\bar{Q})} + \|f_1 - f_2\|_{W^{1,\infty}(0,T;L^\infty(\Omega))} \leq C\|u_1 - u_2\|_{L^\infty(0,T)}.$$

Proof. Defining $\theta = \theta_1 - \theta_2$ and $f = f_1 - f_2$, one finds that (θ, f) solves

$$\begin{aligned}
f_t &= G(\theta_1, f_1) - G(\theta_2, f_2) && \text{in } Q, && \text{(5.22a)}\\
f(0) &= 0 && \text{in } \Omega, && \text{(5.22b)}\\
\rho c_p \theta_t - \kappa\Delta\theta &= \rho L f_t && \text{in } Q, && \text{(5.22c)}\\
-\kappa\frac{\partial\theta}{\partial n} &= u_1(t)\beta(x)\theta + (u_1 - u_2)\beta(x)(\theta_2 - \theta_w) && \text{on } \Sigma_1, && \text{(5.22d)}\\
-\kappa\frac{\partial\theta}{\partial n} &= 0 && \text{on } \Sigma_2, && \text{(5.22e)}\\
\theta(0) &= 0 && \text{in } \Omega. && \text{(5.22f)}
\end{aligned}$$

Further, we prove the Lipschitz continuity regarding the $L^\infty(Q)$-norm. The multiplication of (5.22c) by θ^{2k-1}, for an arbitrary $k \in \mathbb{N}$, and integration over Ω and over $(0,t)$ yields

$$\begin{aligned}
&\frac{\rho c_p}{2k}\int_\Omega \theta^{2k}(t)\,dx + \kappa(2k-1)\int_0^t\int_\Omega \theta^{2k-2}|\nabla\theta|^2\,dxds + \int_0^t\int_{\Sigma_1} u_1(t)\beta(\sigma)\theta^{2k}\,d\sigma ds\\
&\quad = -\int_0^t\int_{\Sigma_1}(u_1 - u_2)\beta(\sigma)(\theta_2 - \theta_w)\theta^{2k-1}\,d\sigma ds + \int_0^t\int_\Omega f_t\theta^{2k-1}\,dxds
\end{aligned} \tag{5.23}$$

Applying Lemma 5.1.1(b) and Hölder's inequality gives

$$\int_0^t\int_\Omega |f_t\theta^{2k-1}|\,dxds \leq C_1\int_0^t\int_\Omega \theta^{2k}\,dxds. \tag{5.24}$$

Using Young's inequality

$$|ab| \leq \frac{\varepsilon^p|a|^p}{p} + \frac{\varepsilon^{-q}|b|^q}{q}, \quad \frac{1}{p} + \frac{1}{q} = 1,$$

with $b = (\theta_2 - \theta_w)(u_1 - u_2)\beta$, $a = \theta^{2k-1}$, $p = \frac{2k}{2k-1}$, $q = 2k$, $\varepsilon > 0$

and applying the trace theorem (see Theorem B.4 in Appendix), we obtain

$$\begin{aligned}
&\int_0^t \int_{\Sigma_1} |(u_1-u_2)\beta(\sigma)(\theta_2-\theta_w)\theta^{2k-1}|\,d\sigma ds \le \frac{\varepsilon^p}{p}\int_0^t\int_{\Sigma_1}\theta^{2k}\,d\sigma ds\\
&+\frac{\varepsilon^{-q}}{q}\int_0^t\int_{\Sigma_1}(u_1-u_2)^{2k}\beta^{2k}(\theta_2-\theta_w)^{2k}\,d\sigma ds\\
&\le C_2\frac{\varepsilon^p}{p}\int_0^t\int_\Omega\theta^{2k}\,dxds + C_2k\frac{\varepsilon^p}{p}\int_0^t\int_\Omega\theta^{2k-2}|\nabla\theta|^2\,dxds\\
&+C_3\frac{\varepsilon^{-q}}{q}\|u_1-u_2\|^{2k}_{L^\infty(0,T)}\|\beta(\theta_2-\theta_w)\|^{2k}_{L^\infty(\Sigma_1)}.
\end{aligned} \tag{5.25}$$

Choosing $\varepsilon = (\frac{p\kappa}{2C_2})^{1/p}$, inequality (5.25) can be refined to

$$\begin{aligned}
&\int_0^t \int_{\Sigma_1} |(u_1-u_2)\beta(\theta_2-\theta_w)\theta^{2k-1}|\,d\sigma ds \le \frac{\kappa}{2}\int_0^t\int_\Omega\theta^{2k}\,dxds\\
&+\frac{\kappa k}{2}\int_0^t\int_\Omega\theta^{2k-2}|\nabla\theta|^2\,dxds + \frac{C_5}{2k}C_4^{2k}\|u_1-u_2\|^{2k}_{L^\infty(0,T)}.
\end{aligned} \tag{5.26}$$

Inserting (5.24) and (5.26) into (5.23), we conclude that

$$\int_\Omega\theta^{2k}(t)\,dx \le C_5C_4^{2k}\|u_1-u_2\|^{2k}_{L^\infty(0,T)} + C_62k\int_0^t\int_\Omega\theta^{2k}\,dxds. \tag{5.27}$$

Gronwall's Lemma yields

$$\|\theta(t)\|^{2k}_{L^{2k}} \le C_5C_4^{2k}\|u_1-u_2\|^{2k}_{L^\infty(0,T)}\exp(C_62kt), \qquad \forall t\in[0,T].$$

Taking the $(2k)$-th root,

$$\sup_{0\le t\le T}\|\theta(t)\|_{L^{2k}} \le C_7\|u_1-u_2\|_{L^\infty(0,T)}.$$

Letting $k\to\infty$, we obtain the Lipschitz continuity of the solution operator in the L^∞-norm. The coincidence of $L^\infty(Q)$- and $C(\bar Q)$-norms implies the Lipschitz stability of the solution operator in the space $C(\bar Q)$. The estimate for $\|f_1-f_2\|_{W^{1,\infty}(0,T;L^\infty(\Omega))}$ is deduced from Lemma 5.1.1 (b). □

Now, let us discuss the differentiability of the solution operator. We have the following result.

Theorem 5.1.4. *Let Assumptions (A1)–(A4) be satisfied. Then, the solution operator S is twice Frechét-differentiable from $L^\infty(0,T)$ to $Y\times W^{1,\infty}(0,T;L^\infty(\Omega))$. The first*

derivative $(\theta_h,\, f_h) = S'(u)h = (S'_\theta(u)h, S'_f(u)h)$ *at a point* $u \in L^\infty(0,T)$ *in a direction* $h \in L^\infty(0,T)$ *is given by the solution of*

$$
\begin{aligned}
(f_h)_t &= G_\theta(\theta,f)\theta_h + G_f(\theta,f)f_h && \text{in } Q, && (5.28a)\\
f_h(0) &= 0 && \text{in } \Omega, && (5.28b)\\
\rho c_p(\theta_h)_t - \kappa\Delta\theta_h &= \rho L(f_h)_t && \text{in } Q, && (5.28c)\\
-\kappa\frac{\partial\theta_h}{\partial n} &= u(t)\beta(x)\theta_h + h(t)\beta(x)(\theta-\theta_w), && \text{on } \Sigma_1, && (5.28d)\\
-\kappa\frac{\partial\theta_h}{\partial n} &= 0 && \text{on } \Sigma_2, && (5.28e)\\
\theta_h(0) &= 0, && \text{in } \Omega && (5.28f)
\end{aligned}
$$

with $(\theta,\, f) = S(u)$*. Furthermore,* $(\theta_{h_1h_2}, f_{h_1h_2}) = S''(u)[h_1,h_2]$ *is the solution of*

$$
\begin{aligned}
(f_{h_1h_2})_t &= G_\theta(\theta,f)\theta_{h_1h_2} + G_f(\theta,f)f_{h_1h_2} && \text{in } Q, && (5.29a)\\
&\quad + G''(\theta,f)[(\theta_{h_1},f_{h_1}),(\theta_{h_2},f_{h_2})] && && \\
f_{h_1h_2}(0) &= 0 && \text{in } \Omega, && (5.29b)\\
\rho c_p(\theta_{h_1h_2})_t - \kappa\Delta\theta_{h_1h_2} &= \rho L(f_{h_1h_2})_t && \text{in } Q, && (5.29c)\\
-\kappa\frac{\partial\theta_{h_1h_2}}{\partial n} &= u(t)\beta(x)\theta_{h_1h_2} + h_1(t)\beta(x)\theta_{h_2} + h_2(t)\beta(x)\theta_{h_1} && \text{on } \Sigma_1, && (5.29d)\\
-\kappa\frac{\partial\theta_{h_1h_2}}{\partial n} &= 0 && \text{on } \Sigma_2, && (5.29e)\\
\theta_{h_1h_2}(0) &= 0 && \text{in } \Omega && (5.29f)
\end{aligned}
$$

with $(\theta_{h_1}, f_{h_1}) = S'(u)h_1$, $(\theta_{h_2}, f_{h_2}) = S'(u)h_2$.

Proof.
1. The first derivative.
The existence of a unique solution (θ_h, f_h) of the linearized state system (5.28) in $W(0,T) \times W^{1,\infty}(0,T;L^{10/3}(\Omega))$ can be shown similarly to the proof of Theorem 5.1.1. Moreover, the terms on the right-hand side of (5.28c), (5.28d) have enough regularity, namely

$$h(t)\beta(x)(\theta-\theta_w) \in L^\infty(\Sigma_1),\ G_f(\theta,f)f_h \in L^\infty(0,T;L^{10/3}(\Omega)),\ G_\theta(\theta,f)\theta_h \in L^{10/3}(Q).$$

The latter is true due to the fact that $G_\theta(\theta,f) \in L^\infty(Q)$, $\theta_h \in W(0,T)$ and therefore $\theta_h \in L^{10/3}(Q)$ (see Lemma 6.7 in [35]). Then, the continuity of θ_h follows from Lemma 5.1.2. It implies that $f_h \in W^{1,\infty}(0,T;L^\infty(\Omega))$, which can be shown along the lines of Lemma 5.1.1.

For a given control $u \in L^\infty(0,T)$ and a given direction $h \in L^\infty(0,T)$, we define $(\theta,f) = S(u)$ and $(\theta^h, f^h) = S(u+h)$, respectively. Furthermore, let (θ_h, f_h) be the unique solution of (5.28). Considering the remainder terms

$$\xi_\theta = \theta^h - \theta - \theta_h, \qquad \xi_f = f^h - f - f_h,$$

it remains to verify that

$$\|\xi_\theta\|_{C(\bar{Q})} + \|\xi_f\|_{W^{1,\infty}(0,T;L^\infty(\Omega))} = o(\|h\|_{L^\infty(0,T)}).$$

Due to Assumption (A2), the Nemytskii operator $G(\theta, f)$ is continuously Frechét differentiable. We perform a Taylor expansion for the nonlinear term $G(\theta, f)$ on the right-hand side of (5.2a):

$$G(\theta^h, f^h) = G(\theta, f) + G_\theta(\theta, f)(\theta^h - \theta) + G_f(\theta, f)(f^h - f) + r_1$$

with a remainder term r_1. It is also known that

$$\frac{\|r_1\|_{L^\infty(Q)}}{\|\theta^h - \theta\|_{C(\bar{Q})}} \to 0 \quad \text{as} \quad \|\theta^h - \theta\|_{C(\bar{Q})} \to 0. \tag{5.30}$$

One can easily verify that (ξ_θ, ξ_f) satisfies

$$\begin{aligned}
\rho c_p(\xi_\theta)_t - \kappa\Delta\xi_\theta &= \rho L(\xi_f)_t && \text{in } Q,\\
-\kappa\frac{\partial\xi_\theta}{\partial n} &= u(t)\beta(x)\xi_\theta + h(t)\beta(x)(\theta^h - \theta) && \text{on } \Sigma_1,\\
-\kappa\frac{\partial\xi_\theta}{\partial n} &= 0 && \text{on } \Sigma_2,\\
\xi_\theta(0) &= 0 && \text{in } \Omega,\\
(\xi_f)_t &= G_\theta(\theta, f)\xi_\theta + G_f(\theta, f)\xi_f + r_1 && \text{in } Q,\\
\xi_f(0) &= 0 && \text{in } \Omega.
\end{aligned}$$

It can be shown similarly to the estimates of Corollary 5.1.3 that

$$\|\xi_\theta\|_{C(\bar{Q})} + \|\xi_f\|_{W^{1,\infty}(0,T;L^\infty(\Omega))} \le C_1(\|r_1\|_{L^\infty(Q)} + \|h\beta(\theta^h - \theta)\|_{L^\infty(\Sigma_1)}).$$

In view of Corollary 5.1.3, the solution operator S is Lipschitz continuous and

$$\|\theta^h - \theta\|_{C(\bar{Q})} \le C_2\|h\|_{L^\infty(0,T)}. \tag{5.32}$$

We consider

$$\frac{\|r_1\|_{L^\infty(Q)}}{\|h\|_{L^\infty(0,T)}} = \frac{\|r_1\|_{L^\infty(Q)}}{\|\theta^h - \theta\|_{C(\bar{Q})}} \cdot \frac{\|\theta^h - \theta\|_{C(\bar{Q})}}{\|h\|_{L^\infty(0,T)}} \le C_2\frac{\|r_1\|_{L^\infty(Q)}}{\|\theta^h - \theta\|_{C(\bar{Q})}}.$$

Due to (5.30), we have $\|r_1\|_{L^\infty(Q)} = o(\|h\|_{L^\infty(0,T)})$. Taking (5.32) into account, we obtain a similar property for ξ_θ and ξ_f:

$$\|\xi_\theta\|_{C(\bar{Q})} + \|\xi_f\|_{W^{1,p}(0,T;L^p(\Omega))} = o(\|h\|_{L^\infty(0,T)}).$$

Now, the differentiability of the solution operator is proven.

Additionally, it can be shown that the first Fréchet derivative of the solution operator S is Lipschitz continuous, i.e., for all u_1, u_2, $h \in L^\infty(0,T)$, there exists a constant $C_3 > 0$ such that

$$\|(S'_\theta(u_1) - S'_\theta(u_2))h\|_{C(\bar{Q})} + \|(S'_f(u_1) - S'_f(u_2))h\|_{W^{1,\infty}(0,T;L^\infty(\Omega))} \le C_3\|u_1 - u_2\|_{L^\infty(0,T)}$$

holds true. One can obtain this estimate following the lines of Corollary 5.1.3.

2. The second derivative.
The existence of a unique solution $(\theta_{h_1h_2}, f_{h_1h_2}) \in C(\bar{Q})\times W^{1,\infty}(0,T;L^\infty(\Omega))$ to the system (5.29) can be shown as before for the first derivative of the solution operator. In a similar way, the second derivative of the solution operator can be derived.

Let a control $u \in L^\infty(0,T)$ and directions $h_1, h_2 \in L^\infty(0,T)$ be given. According to the definition, the solution operator is twice Fréchet differentiable if

$$\begin{aligned} &S'(u+h_1) = S'(u) + S''(u)h_1 + \zeta(u,h_1), \\ &\frac{\|\zeta\|_{\mathcal{L}(L^\infty(0,T),C(\bar{Q}))}}{\|h_1\|_{L^\infty(0,T)}} \to 0,\ \|h_1\|_{L^\infty(0,T)} \to 0. \end{aligned} \tag{5.33}$$

It is valid for the remainder term $\zeta(u,h_1)$

$$\begin{aligned} \|\zeta\|_{\mathcal{L}(L^\infty(0,T),C(\bar{Q}))} &= \|S'(u+h_1) - S'(u) - S''(u)h_1\|_{\mathcal{L}(L^\infty(0,T),C(\bar{Q}))} \\ &= \sup_{\|h_2\|_{L^\infty(0,T)}=1} \|S'(u+h_1)h_2 - S'(u)h_2 - S''(u)[h_1,h_2]\|_{C(\bar{Q})}. \end{aligned} \tag{5.34}$$

We define $(\theta_{h_2}, f_{h_2}) = S'(u)h_2$ and $(\theta^1_{h_2}, f^1_{h_1}) = S'(u+h_1)h_2$. Furthermore, let $(\theta_{h_1h_2}, f_{h_1h_2}) = S''(u)[h_1,h_2]$ be the solution of (5.29). We denote

$$\zeta_\theta = \theta^1_{h_2} - \theta_{h_2} - \theta_{h_1h_2}, \qquad \zeta_f = f^1_{h_2} - f_{h_2} - f_{h_1h_2}. \tag{5.35}$$

It remains to show that

$$\frac{\sup_{\|h_2\|_{L^\infty(0,T)}=1} \|\zeta_\theta\|_{C(\bar{Q})}}{\|h_1\|_{L^\infty(0,T)}} \to 0,\ \frac{\sup_{\|h_2\|_{L^\infty(0,T)}=1} \|\zeta_f\|_{C(\bar{Q})}}{\|h_1\|_{L^\infty(0,T)}} \to 0,\ \|h_1\|_{L^\infty(0,T)} \to 0. \tag{5.36}$$

In view of Assumption (A2), the Nemytskii operator G is twice Fréchet differentiable in $C(\bar{Q})$ (see Theorem B.13 in Appendix) and therefore

$$\begin{aligned} G'(\theta_1,f_1)(\theta_{h_2},f_{h_2}) = G'(\theta,f)(\theta_{h_2},f_{h_2}) + G''(\theta,f)[(\theta_{h_1},f_{h_1}),(\theta_{h_2},f_{h_2})] \\ + r_2^G(\theta,\theta_1-\theta)[(\theta_{h_1},f_{h_1}),(\theta_{h_2},f_{h_2})], \end{aligned} \tag{5.37}$$

where $r_2^G \in \mathcal{L}(L^\infty(0,T),C(\bar{Q}))$ is a remainder term. For simplicity we denote $r_{h_1h_2} := r_2^G(\theta,\theta_1-\theta)[(\theta_{h_1},f_{h_1}),(\theta_{h_2},f_{h_2})]$ with the property

$$\sup_{\theta_{h_2}\in C(\bar{Q}),\theta_{h_2}\neq 0} \frac{\|r_{h_1h_2}\|_{C(\bar{Q})}}{\|\theta_{h_2}\|_{C(\bar{Q})}} = o(\|\theta_1-\theta\|_{C(\bar{Q})}). \tag{5.38}$$

Here $(\theta,f) = S(u)$, $(\theta_1,f_1) = S(u+h_1)$ and $(\theta_{h_1},f_{h_1}) = S'(u)h_1$. We recall that $\theta_1-\theta = \theta_{h_1}+\xi_\theta$ and $f_1 - f = f_{h_1} + \xi_f$ with remainders ξ_θ and ξ_f.

Now, invoking the explicit expressions for the quantities in (5.35) and (5.37), it is easily seen that (ζ_θ,ζ_f) is a solution of the system

$$\begin{aligned} \rho c_p(\zeta_\theta)_t - \kappa\Delta\zeta_\theta &= \rho L(\zeta_f)_t && \text{in } Q, \\ -\kappa\frac{\partial\zeta_\theta}{\partial n} &= u(t)\beta(x)\zeta_\theta + h_1(t)\beta(x)(\theta^1_{h_2}-\theta_{h_2}) && \text{on } \Sigma_1, \\ -\kappa\frac{\partial\zeta_\theta}{\partial n} &= 0 && \text{on } \Sigma_2, \\ \zeta_\theta(0) &= 0 && \text{in } \Omega, \\ (\zeta_f)_t &= G_\theta(\theta,f)\zeta_\theta + G_f(\theta,f)\zeta_f + r_{h_1h_2} && \text{in } Q, \\ \zeta_f(0) &= 0 && \text{in } \Omega. \end{aligned}$$

Applying the technique of the proof of Corollary 5.1.3, one can show that

$$\|\zeta_\theta\|_{L^\infty(Q)} + \|\zeta_f\|_{W^{1,\infty}(0,T;L^\infty(\Omega))} \leq C_4(\|r_{h_1h_2}\|_{L^\infty(Q)} + \|h_1\beta(\theta^1_{h_2} - \theta_{h_2})\|_{L^\infty(\Sigma_1)}).$$

From the Lipschitz continuity of the solution operator and its first Fréchet derivative, we have

$$\begin{aligned} \|\theta^1_{h_2} - \theta_{h_2}\|_{L^\infty(Q)} &\leq C_5\|h_1\|_{L^\infty(0,T)}, \\ \|\theta_1 - \theta\|_{C(\bar{Q})} &\leq C_6\|h_1\|_{L^\infty(0,T)}. \end{aligned} \tag{5.40}$$

Taking (5.38) and (5.40) into account, we obtain

$$\begin{aligned} \|\zeta_\theta\|_{L^\infty(Q)} + \|\zeta_f\|_{W^{1,\infty}(0,T;L^\infty(\Omega))} &\leq C_4(\varepsilon\|\theta_1 - \theta\|_{C(\bar{Q})}\|\theta_{h_2}\|_{C(\bar{Q})} + C_5\|h_1\|^2_{L^\infty(0,T)}\|h_1\|_{L^\infty(\Sigma_1)}) \\ &\leq C_4(C_6\varepsilon\|h_1\|_{L^\infty(0,T)}\|\theta_{h_2}\|_{C(\bar{Q})} + C_5\|h_1\|^2_{L^\infty(0,T)}\|h_1\|_{L^\infty(\Sigma_1)}). \end{aligned}$$

This means that

$$\sup_{\|h_2\|_{L^\infty(0,T)}=1} \|\zeta_\theta\|_{C(\bar{Q})} + \sup_{\|h_2\|_{L^\infty(0,T)}=1} \|\zeta_f\|_{W^{1,\infty}(0,T;L^\infty(\Omega))} = o(\|h_1\|_{L^\infty(0,T)}),$$

which concludes the proof of this theorem. □

5.1.5 Necessary and sufficient optimality conditions

We are now able to derive the optimality conditions for the control problem (P). In the following theorem, first-order necessary optimality conditions are characterized by the respective adjoint equations.

Theorem 5.1.5. *Let $\bar{u} \in U_{ad}$ be an optimal control of problem (P) and $(\bar{\theta}, \bar{f}) = S(\bar{u})$ the associated solution of the state system (5.2). Then, there exists a unique solution $(\bar{p}, \bar{q}) \in Y \times W^{1,\infty}(0,T;L^\infty(\Omega))$ such that*

$$-\bar{q}_t = G_f(\bar{\theta}, \bar{f})(\bar{q} + \rho L\bar{p}) \qquad \text{in } Q, \tag{5.41a}$$
$$\bar{q}(T) = \alpha_1(\bar{f}(T) - f_d) \qquad \text{in } \Omega, \tag{5.41b}$$
$$-\rho c_p\bar{p}_t - \kappa\Delta\bar{p} = G_\theta(\bar{\theta}, \bar{f})(\rho L\bar{p} + \bar{q}) \qquad \text{in } Q, \tag{5.41c}$$
$$-\kappa\frac{\partial\bar{p}}{\partial n} = \bar{u}(t)\beta(x)\bar{p} \qquad \text{on } \Sigma_1, \tag{5.41d}$$
$$-\kappa\frac{\partial\bar{p}}{\partial n} = 0 \qquad \text{on } \Sigma_2, \tag{5.41e}$$
$$\bar{p}(T) = \frac{\alpha_2}{\rho c_p}(\bar{\theta}(T) - \theta_d) \qquad \text{in } \Omega. \tag{5.41f}$$

Moreover, the following variational inequality is valid

$$\iint_{\Sigma_1} \left(-\bar{p}\beta(\bar{\theta} - \theta_w) + \frac{\alpha_3}{|\Gamma_1|}\bar{u}\right)(u - \bar{u})d\sigma dt \geq 0 \quad \forall u \in U_{ad}. \tag{5.42}$$

Proof. First, observe that the system (5.41) is a linear backward-in-time system of the parabolic equation and the ODE. After the time transformation $\tilde{t} \mapsto T - t$, one can proceed as in the proof of Theorem 5.1.4 in order to prove the existence of a unique solution $(\bar{p}, \bar{q}) \in W(0,T) \cap C(\bar{Q}) \times W^{1,\infty}(0,T; L^\infty(\Omega))$ of the system (5.41).

Using the control-to-state mapping defined in (5.21), the reduced cost functional of problem (P) is given by

$$\min_{u \in U_{ad}} j(u) = J(S(u), u) = \frac{\alpha_1}{2} \int_\Omega (S_f(u)(T) - f_d)^2 \, dx + \frac{\alpha_2}{2} \int_\Omega (S_\theta(u)(T) - \theta_d)^2 \, dx + \frac{\alpha_3}{2} \int_0^T u^2 dt.$$

By Theorem 5.1.4, j is differentiable and the set of admissible controls U_{ad} bounded, closed and convex. Hence, the first-order necessary optimality conditions for a (local) optimal solution $\bar{u} \in U_{ad}$ is given by $j'(\bar{u})(u - \bar{u}) \geq 0$, $\forall u \in U_{ad}$. For a given direction $h_1 \in L^\infty(0,T)$, we have

$$\begin{aligned} j'(\bar{u})h_1 = \alpha_1 \int_\Omega (S_f(\bar{u})(T) - f_d) S_f'(\bar{u})h_1 \, dx \\ + \alpha_2 \int_\Omega (S_\theta(\bar{u})(T) - \theta_d) S_\theta'(\bar{u})h_1 \, dx + \alpha_3 \int_0^T \bar{u} h_1 dt. \end{aligned} \tag{5.43}$$

We will rewrite the directional derivative with the help of $(\bar{p}, \bar{q})$ which solves the adjoint system (5.41). For notational simplicity, we introduce $f_{h_1} = S_f'(\bar{u})h_1$ and $\theta_{h_1} = S_\theta'(\bar{u})h_1$ as the solution of the linearized system (5.28). We start by multiplying (5.28a) with $\bar{q}$ and integrating over Q:

$$\begin{aligned} 0 &= \iint_Q ((f_{h_1})_t - G_\theta(\bar{\theta}, \bar{f})\theta_{h_1} - G_f(\bar{\theta}, \bar{f}) f_{h_1}) \bar{q} dx \, dt \\ &= \iint_Q -\bar{q}_t f_{h_1} - \bar{q}(G_\theta(\bar{\theta}, \bar{f})\theta_{h_1} + G_f(\bar{\theta}, \bar{f}) f_{h_1}) dx \, dt + \int_\Omega f_{h_1}(T)\bar{q}(T) dx. \end{aligned} \tag{5.44}$$

Due to the end-time condition for $\bar{q}$, from (5.44) and (5.41a) we conclude that the first term in (5.43) reads

$$\begin{aligned} \alpha_1 \int_\Omega (f_{h_1}(T) - f_d) f_{h_1}(T) \, dx &= \iint_Q \bar{q}_t f_{h_1} + \bar{q}(G_\theta(\bar{\theta}, \bar{f})\theta_{h_1} + G_f(\bar{\theta}, \bar{f}) f_{h_1}) dx \, dt \\ &= \iint_Q -\rho L G_f(\bar{\theta}, \bar{f}) \bar{p} f_{h_1} + \bar{q} G_\theta(\bar{\theta}, \bar{f}) \theta_{h_1}. \end{aligned}$$

Next, we test (5.41c) with θ_{h_1} and integrate over Q. Integrating by parts and involving

$\bar{p}(T) = \frac{\alpha_2}{\rho c_p}(\bar{\theta}(T) - \theta_d)$ we obtain

$$\begin{aligned}
\alpha_2 \iint_Q (\bar{\theta} - \theta_d)\theta_{h_1} dx\, dt &= -\int_0^T \rho c_p \bar{p}_t \theta_{h_1} dt - \kappa \iint_Q \Delta \bar{p} \theta_{h_1} dx\, dt \\
&\quad - \iint_Q G_\theta(\bar{\theta}, \bar{f})(\rho L \bar{p} + \bar{q})\theta_{h_1} dx\, dt \\
&= \int_0^T \rho c_p \bar{p} (\theta_{h_1})_t dt - \kappa \iint_Q \Delta \theta_{h_1} \bar{p} dx\, dt \\
&\quad - \iint_Q G_\theta(\bar{\theta}, \bar{f})(\rho L \bar{p} + \bar{q})\theta_{h_1} dx\, dt - \iint_{\Sigma_1} h_1 \beta(\bar{\theta} - \theta_w)\bar{p} d\sigma dt \\
&= -\iint_{\Sigma_1} h_1 \beta(\bar{\theta} - \theta_w)\bar{p} d\sigma dt - \iint_Q G_\theta(\bar{\theta}, \bar{f})(\rho L \bar{p} + \bar{q})\theta_{h_1} dx\, dt \\
&\quad + \iint_Q \rho L (G_\theta(\bar{\theta}, \bar{f})\theta_{h_1} + G_f(\bar{\theta}, \bar{f}) f_{h_1})\bar{p} dx dt.
\end{aligned}$$

Summarizing, it is possible to replace (5.43) by

$$j'(\bar{u})h_1 = -\iint_{\Sigma_1} h_1 \beta(\bar{\theta} - \theta_w)\bar{p} d\sigma dt + \alpha_3 \int_0^T \bar{u} h_1 dt.$$

Thus, the first-order optimality conditions for a (local) optimal solution $\bar{u}$ are represented by the variational inequality (5.42). □

Since the control problem (P) is non-convex, the first-order necessary optimality conditions formulated above are not sufficient. However, it is of crucial importance, e.g., for the numerical solution of (P), to derive sufficient optimality conditions. We will use two different norms for the derivation of sufficient second-order optimality conditions, namely, the L^∞-norm for the differentiation and the L^2-norm for the positive definiteness of the second derivative of the reduced cost functional. This is motivated by the so-called "two-norm" discrepancy, see e.g. Tröltzsch [79].

Next, we will formulate second-order sufficient optimality conditions regarding the optimal control problem (P). To this end, we provide the second derivative of the reduced cost functional $j(u) = J(S(u), u)$. According to Theorem 5.1.4, the solution operator S is twice continuously Fréchet differentiable. Due to the chain rule, the reduced cost functional j as a composite function is also twice Fréchet differentiable in $L^\infty(0,T)$. We recall that

$$\begin{aligned}
j'(u)h_1 &= \alpha_1 \int_\Omega (S_f(u)(T) - f_d) S_f'(u)h_1\, dx \\
&\quad + \alpha_2 \int_\Omega (S_\theta(u)(T) - \theta_d) S_\theta'(u)h_1\, dx + \alpha_3 \int_0^T u h_1 dt.
\end{aligned} \tag{5.45}$$

Differentiating $\tilde{j}(u) := j'(u)h_1$ in the direction $h_2 \in L^\infty(0,T)$ gives

$$\begin{aligned} j''(u)[h_1,h_2] &= \alpha_1 \int_\Omega S_f'(u)h_2(T)S_f'(u)h_1 + (S_f(u)(T)-f_d)S_f''(u)[h_1,h_2]\,dx \\ &\quad + \alpha_2 \int_\Omega S_\theta'(u)h_2(T)S_\theta'(u)h_1(T) + (S_\theta(u)(T)-\theta_d)S_\theta''(u)[h_1,h_2]\,dx \\ &\quad + \alpha_3 \int_0^T h_1h_2dt \\ &= \alpha_1 \int_\Omega f_{h_1}(T)f_{h_2}(T)dx + \alpha_2 \int_\Omega \theta_{h_1}(T)\theta_{h_2}(T)dx \\ &\quad + \alpha_1 \int_\Omega (f(T)-f_d)f_{h_1h_2}(T)\,dx + \alpha_2 \int_\Omega (\theta(T)-\theta_d)\theta_{h_1h_2}(T)\,dx \\ &\quad + \alpha_3 \int_0^T h_1h_2dt \end{aligned} \tag{5.46}$$

with $(\theta_{h_i}, f_{h_i}) = S'(u)h_i$, $i = 1,2$, and $(\theta_{h_1h_2}, f_{h_1h_2}) = S''(u)[h_1,h_2]$. Further, we express the second derivative in terms of adjoint variables (p,q) that solve the adjoint system (5.41). To this end, we multiply (5.29c), (5.29a) with p and q, respectively. The integration over Q and by parts yields

$$\begin{aligned} &\alpha_1 \int_\Omega (f(T)-f_d)f_{h_1h_2}(T)\,dx + \alpha_2 \int_\Omega (\theta(T)-\theta_d)\theta_{h_1h_2}(T)\,dx = \\ &\iint_Q G''(\theta(u),f(u))[(\theta_{h_1},f_{h_1}),(\theta_{h_2},f_{h_2})](\rho Lp+q)dxdt \\ &- \iint_{\Sigma_1} (\theta_{h_1}h_2+\theta_{h_2}h_1)pd\sigma dt. \end{aligned} \tag{5.47}$$

Hence, we conclude

$$\begin{aligned} j''(u)[h_1,h_2] &= \alpha_1 \int_\Omega f_{h_1}(T)f_{h_2}(T)dx + \alpha_2 \int_\Omega \theta_{h_1}(T)\theta_{h_2}(T)dx \\ &\quad + \alpha_3 \int_0^T h_1h_2dt - \iint_{\Sigma_1} (\theta_{h_1}h_2+\theta_{h_2}h_1)pd\sigma dt \\ &\quad + \iint_Q G''(\theta(u),f(u))[(\theta_{h_1},f_{h_1}),(\theta_{h_2},f_{h_2})](\rho Lp+q)dxdt. \end{aligned} \tag{5.48}$$

In all what follows, we denote by $\bar{u}$ an admissible control of problem (P) with an associated solution $(\bar{\theta},\bar{f}) = S(\bar{u})$ of the state system (5.2). We suppose that the first-order optimality

conditions given in Theorem 5.1.5 are satisfied with respective adjoint states $(\bar{p}, \bar{q})$. Let us define the strongly active set associated to $\bar{u}$. For fixed $\tau > 0$, we set

$$A_\tau(\bar{u}) = \left\{ t \in (0,T) : \left| \int_{\Gamma_1} -\bar{p}(\sigma,t)\beta(\sigma)(\bar{\theta}(\sigma,t) - \theta_w(\sigma,t))d\sigma + \alpha_3 \bar{u}(t) \right| > \tau \right\}.$$

The set $A_\tau(\bar{u})$ is fundamental for the introduction of the τ-critical cone. The τ-critical cone $C_\tau(\bar{u})$ can be defined as the set of all $v \in L^\infty(0,T)$ satisfying

$$v(t) \begin{cases} = 0 & \text{if} \quad t \in A_\tau(\bar{u}), \\ \geq 0 & \text{if} \quad \bar{u} = u_a \text{ and } t \notin A_\tau(\bar{u}), \\ \leq 0 & \text{if} \quad \bar{u} = u_b \text{ and } t \notin A_\tau(\bar{u}). \end{cases}$$

Next, we shall assume a coercivity condition on the second derivative of the cost functional for directions from the τ-critical cone $C_\tau(\bar{u})$, henceforth called second-order sufficient optimality conditions:

$$\left.\begin{array}{l} \text{There exist } \tau > 0 \text{ and } \delta > 0 \text{ such that} \\ \qquad j''(\bar{u})v^2 \geq \delta \|v\|^2_{L^2(0,T)} \\ \text{holds for all } v \in C_\tau(\bar{u}). \end{array}\right\} \tag{SSC}$$

Theorem 5.1.6. *Let $\bar{u}$ be an admissible control of problem (P) with an associated state $(\bar{\theta}, \bar{f}) = S(\bar{u})$ satisfying the first-order necessary optimality conditions given in Theorem 5.1.5 with associated adjoint states $(\bar{p}, \bar{q})$. Further, it is assumed that (SSC) holds for $\bar{u}$. Then, there exist $\tilde{\delta} > 0$ and $\varepsilon > 0$ such that*

$$J(\theta, f, u) \geq J(\bar{\theta}, \bar{f}, \bar{u}) + \tilde{\delta} \|u - \bar{u}\|^2_{L^2(0,T)} \tag{5.49}$$

holds for all $u \in U_{ad}$ with $\|u - \bar{u}\|_{L^\infty(0,T)} \leq \varepsilon$ with associated states $(\theta, f) = S(u)$.
In particular, $\bar{u}$ is locally optimal in the sense of $L^\infty(0,T)$.

Proof. This proof closely resembles that of Theorem 5.17 in Tröltzsch [79, pp. 291–294].

(i) Preliminaries.
The crucial point in this proof is the fact that the quadratic form $j''(u)[h_1, h_2]$ has to depend continuously on h_i, $i = 1, 2$ in the L^2-norm, i.e., we have to ensure the following continuity estimate

$$| \, j''(u)[h_1, h_2] \, | \leq c \|h_1\|_{L^2(0,T)} \|h_2\|_{L^2(0,T)}. \tag{5.50}$$

The first two terms in $j''(u)[h_1, h_2]$ (see (5.48)) can be estimated with respect to the L^2-norm of h_i, $i = 1, 2$, by applying standard a priori estimates and Lemma 5.1.1 (b), e.g.,

$$\begin{aligned} \|\theta_{h_i}\|_{L^\infty(Q)} &\leq c \|\bar{\theta}\|_{C(\bar{Q})} \|h_i\|_{L^2(0,T)}, \\ \|f_{h_i}\|_{L^\infty(Q)} &\leq c \|\bar{\theta}\|_{C(\bar{Q})} \|h_i\|_{L^2(0,T)}. \end{aligned}$$

The other terms are more delicate. Here we take advantage of the regularity of the adjoint state discussed in Theorem 5.1.5. Using the trace theorem, we estimate

$$\begin{aligned} \Big| \iint_{\Sigma_1} \theta_{h_i} h_j p \, d\sigma dt \Big| &\leq c \|p\|_{C(\bar{Q})} \|\theta_{h_i}\|_{L^2(0,T;H^1(\Omega))} \|h_j\|_{L^2(0,T)} \\ &\leq c \|p\|_{C(\bar{Q})} \|\theta_{h_i}\|_{W(0,T)} \|h_j\|_{L^2(0,T)} \leq c \|p\|_{C(\bar{Q})} \|h_i\|_{L^2(0,T)} \|h_j\|_{L^2(0,T)} \end{aligned}$$

for $i, j = 1, 2$, $i \neq j$. For the last term in (5.48) we need to estimate the second derivative of $G(\theta, f)$

$$\begin{aligned}|G''(\theta, f)[(\theta_{h_1}, f_{h_1}), (\theta_{h_2}, f_{h_2})]| = \\ &|G_{\theta\theta}[\theta_{h_1}, \theta_{h_2}] + G_{\theta f}[\theta_{h_1}, f_{h_2}] + G_{f\theta}[f_{h_1}, \theta_{h_2}] + G_{ff}[f_{h_1}, f_{h_2}]| \\ &\leq c(\|\theta_{h_1}\|_{C(\bar{Q})}\|\theta_{h_2}\|_{C(\bar{Q})} + \|\theta_{h_1}\|_{C(\bar{Q})}\|f_{h_2}\|_{C(\bar{Q})} \\ &+ \|f_{h_1}\|_{C(\bar{Q})}\|\theta_{h_2}\|_{C(\bar{Q})} + \|f_{h_1}\|_{C(\bar{Q})}\|f_{h_2}\|_{C(\bar{Q})}).\end{aligned}$$

The last step of the estimation is valid due to the uniform boundedness of the partial derivatives of $G(\theta, f)$ up to order 2 on bounded sets (it follows from Assumption (A2)).

Note also that $f'(\bar{u})$ can be expressed with

$$g(t) := \int_{\Gamma_1} -\bar{p}(\sigma, t)\beta(\sigma)(\bar{\theta}(\sigma, t) - \theta_w(\sigma, t))d\sigma + \alpha_3\bar{u}(t)$$

in the form

$$f'(\bar{u})h = \int_0^T g(t)h(t)dt.$$

(ii) Taylor expansion.
Let $u \in U_{ad}$ with $\|u - \bar{u}\|_{L^\infty(0,T)} \leq \varepsilon$ be arbitrary. For almost every $t \in [0, T]$, we have the pointwise variational inequality

$$g(t)(u(t) - \bar{u}(t)) \geq 0 \quad \forall u \in [u_a, u_b]. \tag{5.51}$$

We denote $h := u - \bar{u}$. It follows from Taylor's theorem with integral remainder (see, e.g. Theorem 8.14.3 in [16, p. 186]) that

$$j(u) = j(\bar{u}) + j'(\bar{u})h + \frac{1}{2}j''(\bar{u})h^2 + r_2^j(\bar{u}, h)$$

with the remainder

$$r_2^j(\bar{u}, h) = \int_0^1 (1 - s)(j''(\bar{u} + sh) - j''(\bar{u}))h^2 ds.$$

In view of (5.51),

$$\begin{aligned}j(u) - j(\bar{u}) &= j'(\bar{u})h + \frac{1}{2}j''(\bar{u})h^2 + r_2^j(\bar{u}, h) \\ &\geq \int_{A_\tau(\bar{u})} g(t)h(t)dt + \frac{1}{2}j''(\bar{u})h^2 + r_2^j(\bar{u}, h) \\ &\geq \tau \int_{A_\tau(\bar{u})} |h(t)|dt + \frac{1}{2}j''(\bar{u})h^2 + r_2^j(\bar{u}, h).\end{aligned}$$

We now make the decomposition $h := h_0 + h_1$, where

$$h_0(t) := \begin{cases} h(t) & \text{if} \quad t \notin A_\tau, \\ 0 & \text{if} \quad t \in A_\tau. \end{cases}$$

By construction, we have $h_0 \in C_\tau(\bar{u})$, since h_0 satisfies the sign conditions of the critical cone. With these functions, it follows that

$$j(u) - j(\bar{u}) \geq \tau \int\limits_{A_\tau(\bar{u})} |h(t)|dt + \frac{1}{2} j''(\bar{u})(h_0 + h_1)^2 + r_2^j(\bar{u}, h) \tag{5.52}$$

(iii) Estimation of $j''(\bar{u})(h_0 + h_1)^2$.
Invoking (SSC) and $h_0 \in C_\tau(\bar{u})$, we readily see that

$$\frac{1}{2} j''(\bar{u}) h_0^2 \geq \frac{\delta}{2} \|h_0\|^2_{L^2(0,T)}.$$

Using Young's inequality, we conclude from (5.50) that, with a generic constant $c > 0$,

$$\begin{aligned} | \, j''(\bar{u})[h_0, h_1] \, | &\leq c\|h_0\|_{L^2(0,T)} \|h_1\|_{L^2(0,T)} \leq \frac{\delta}{4} \|h_0\|_{L^2(0,T)} + c\|h_1\|_{L^2(0,T)} \\ &\leq \frac{\delta}{4} \|h_0\|_{L^2(0,T)} + c\|h_1\|_{L^1(0,T)} \|h_1\|_{L^\infty(0,T)} \\ &\leq \frac{\delta}{4} \|h_0\|_{L^2(0,T)} + c_1 \varepsilon \|h_1\|_{L^1(0,T)}, \end{aligned}$$

because $\|h\|_{L^\infty(0,T)} \leq \varepsilon$. By the same token,

$$| \, j''(\bar{u}) h_1^2 \, | \leq c\|h_1\|^2_{L^2(0,T)} \leq c_2 \varepsilon \|h_1\|_{L^1(0,T)}.$$

Summarizing, we obtain after combining the above inequalities that

$$\begin{aligned} \frac{1}{2} j''(\bar{u})(h_0 + h_1)^2 &\geq \frac{\delta}{2} \|h_0\|_{L^2(0,T)} - \Big[\frac{\delta}{4} \|h_0\|_{L^2(0,T)} + (c_1 + c_2)\varepsilon \|h_1\|_{L^1(0,T)} \Big] \\ &\geq \frac{\delta}{4} \|h_0\|_{L^2(0,T)} - (c_1 + c_2)\varepsilon \|h_1\|_{L^1(0,T)}. \end{aligned}$$

Now we choose $\varepsilon > 0$ so small that $\varepsilon(c_1 + c_2) \leq \tau/2$. Since $h_1 = 0$ on $\Omega \backslash A_\tau$ we can infer that

$$\|h_1\|_{L^1(0,T)} = \int\limits_{A_\tau(\bar{u})} |h|dt.$$

Substituting the above estimates into (5.52) then yields

$$\begin{aligned} j(u) - j(\bar{u}) &\geq \tau \int\limits_{A_\tau(\bar{u})} |h(t)|dt - \frac{\tau}{2} \int\limits_{A_\tau(\bar{u})} |h(t)|dt + \frac{\delta}{4} \|h_0\|_{L^2(0,T)} + r_2^j(\bar{u}, h) \\ &\geq \frac{\tau}{2} \int\limits_{A_\tau(\bar{u})} |h(t)|dt + \frac{\delta}{4} \|h_0\|_{L^2(0,T)} + r_2^j(\bar{u}, h). \end{aligned}$$

Now we choose $\varepsilon \leq 1$, which can be done without loss of generality. Then, by the definition of h, we have $|h(t)| \geq h^2(t)$. Since

$$\|h_0\|^2_{L^2(0,T)} = \int\limits_{[0,T]\setminus A_\tau(\bar{u})} h^2 dt,$$

we finally obtain that

$$\begin{aligned} j(u) - j(\bar{u}) &\geq \frac{\tau}{2} \int\limits_{A_\tau(\bar{u})} h^2 dt + \frac{\delta}{4}\|h\|_{L^2([0,T]\setminus A_\tau)} + r_2^j(\bar{u}, h) \\ &\geq \min\Big\{\frac{\tau}{2}, \frac{\delta}{4}\Big\}\|h\|_{L^2(0,T)} + r_2^j(\bar{u}, h). \end{aligned}$$

(iv) Estimation of the remainder term $r_2^j(\bar{u}, h)$.
Let $(\bar{\theta}, \bar{f}) = S(\bar{u})$, $(\theta, f) = S(\bar{u} + sh)$ and $(\bar{\theta}_h, \bar{f}_h) = S'(\bar{u})h$, $(\theta_h, f_h) = S'(\bar{u} + sh)h$. Further, we consider

$$\begin{aligned} (j''(\bar{u} + sh) - j''(\bar{u}))h^2 &= \alpha_1 \int\limits_\Omega f_h^2(T) - \bar{f}_h^2(T) dx + \alpha_2 \int\limits_\Omega \theta_h^2(T) - \bar{\theta}_h^2(T) dx \\ &- 2 \iint\limits_{\Sigma_1} (\theta_h p - \bar{\theta}_h \bar{p}) h d\sigma dt + \iint\limits_Q G''(\theta, f)(\theta_h, f_h)^2(\rho L p + q) \\ &- G''(\bar{\theta}, \bar{f})(\bar{\theta}_h, \bar{f}_h)^2(\rho L \bar{p} + \bar{q}) dx dt. \end{aligned} \tag{5.53}$$

In order to estimate the terms in (5.53), we need the following estimates

$$\begin{aligned} &\|f_h - \bar{f}_h\|_{W^{1,p}(0,T;L^p(\Omega))} + \|\theta_h - \bar{\theta}_h\|_{C(\bar{Q})} \leq cs\|h\|_{L^\infty(0,T)}\|h\|_{L^2(0,T)}, \\ &\|q - \bar{q}\|_{W^{1,p}(0,T;L^p(\Omega))} + \|p - \bar{p}\|_{C(\bar{Q})} \leq cs\|h\|_{L^\infty(0,T)}, \end{aligned} \tag{5.54}$$

which can be obtained by standard a priori estimates and the Lipschitz continuity of the solution operator. Using (5.54) and the Lipschitz continuity of $G''(\theta, f)$, we can estimate the remainder term r_2^j as follows:

$$|r_2^j(\bar{u}, h)| \leq c \int_0^1 (1 - s)s\|h\|_{L^\infty(0,T)}\|h\|^2_{L^2(0,T)} ds \leq c\|h\|_{L^\infty(0,T)}\|h\|^2_{L^2(0,T)}.$$

Hence, for sufficiently small $\varepsilon > 0$ we have the estimate

$$j(u) - j(\bar{u}) \geq \min\Big\{\frac{\tau}{2}, \frac{\delta}{4}\Big\}\|h\|_{L^2(0,T)} = \tilde{\delta}\|h\|_{L^2(0,T)},$$

which is the asserted quadratic growth of the cost functional. □

Such kind of sufficient optimality conditions is an indispensable tool basis for carrying out numerical analysis of optimal control problems, e.g., convergence analysis of the sequential quadratic programming method in order to solve optimal control problems numerically.

5.2 Numerical implementation

In this section, we introduce a numerical algorithm for the solution of the optimal control problem (P) analyzed in the previous section. Basically, there are two major approaches to implement optimal control problems numerically, "first discretize then optimize" and "first optimize then discretize".

In the *"first discretize then optimize"* strategy, the state equation is first discretized and then, using the discrete Lagrangian, a finite-dimensional optimality system is derived, which can be solved by existing optimization solvers. There exist a variety of numerical methods to solve the finite-dimensional optimization problems. These are well studied in the literature, e.g., Alt [1], Nocedal and Wright [56], Spellucci [68]. Thus, this approach can be successfully applied to the wide range of PDE constrained optimal control problems with different inequality bounds and constraints. Unfortunately, discrete equations derived from (coupled, instationary) partial differential equations usually have an immense number of variables to approximate the continuous equations well enough. This requires a big data storage and may lead to a large computational effort.

In the *"first optimize then discretize"* approach, one first finds the continuous necessary optimality conditions analytically and then applies discretization techniques. The state and adjoint system can be treated numerically separately. The need for working memory does not increase too much even if one uses a simple algorithmic approach. The description and comparison of both approaches can be found, e.g., in Hinze et al. [30].

In this thesis, the "first optimize then discretize" strategy is applied in the numerical implementation of control problem (P). We focus on the infinite-dimensional version of the reduced SQP (rSQP) method, which has proven to be very effective in many areas of application, such as optimal control. In this method, the reduction to the control space takes place when solving linear quadratic subproblems, arising in each iteration of the usual SQP method. An overview on reduced-Hessian SQP methods in finite-dimensional spaces is presented, e.g., in Nocedal and Wright [56]. A prospective look at SQP methods, in particular the rSQP for semilinear parabolic control problems is given by Kupfer and Sachs [46]. A numerical application of the reduced SQP method to parabolic control problems was considered by Hintermüller, Volkwein, and Diwoky [29], Kupfer and Sachs [47]. To treat the control constraints, a primal-dual active set strategy will be applied, which has proven to be an efficient numerical tool in the context of optimization problems including inequality constraints, e.g., Bergounioux, Ito, and Kunisch [5]. For a globalization of the rSQP method, we use a projected gradient algorithm (see, e.g., Kelley [41]) with a line search according to the Armijo rule to find suitable initial values for the rSQP method.

In Subsection 5.2.1, we will briefly describe the gradient projection method for the optimal control problem (P). The reduced SQP method and the primal-dual active set strategy are introduced in Subsections 5.2.2 and 5.2.3, respectively. Subsection 5.2.4 includes a description of the CG method, used for the solution of the reduced Hessian system. Some details on the discretization of the optimal control problem can be found in Subsection 5.2.5. Finally, Subsection 5.2.6 is devoted to the illustration of the numerical results.

5.2.1 Gradient projection method

We begin with the gradient projection method. For convenience, we recall the control problem (P) introduced in Section 5.1: *minimize*

$$J(\theta, f, u) = \frac{\alpha_1}{2} \int_\Omega (f(x,T) - f_d(x))^2 \, dx + \frac{\alpha_2}{2} \int_\Omega (\theta(x,T) - \theta_d(x))^2 \, dx + \frac{\alpha_3}{2} \int_0^T u^2(t) dt$$

subject to

$$\begin{aligned}
f_t &= G(\theta, f) := (f_{eq}(\theta) - f)\mathcal{H}(f_{eq}(\theta) - f) g_1(\theta) g_2 && \text{in } Q, && (5.55a)\\
f(0) &= 0 && \text{in } \Omega, && (5.55b)\\
\rho c_p \theta_t - \kappa \Delta \theta &= \rho L f_t && \text{in } Q, && (5.55c)\\
-\kappa \frac{\partial \theta}{\partial n} &= u(t)\beta(x)(\theta - \theta_w) && \text{on } \Sigma_1, && (5.55d)\\
-\kappa \frac{\partial \theta}{\partial n} &= 0 && \text{on } \Sigma_2, && (5.55e)\\
\theta(0) &= \theta_0 && \text{in } \Omega && (5.55f)
\end{aligned}$$

and

$$u \in U_{ad} = \{u \in L^\infty(0,T) : u_a \le u \le u_b, \ u_a, u_b \ge 0\}.$$

In the following, we will also use the adjoint system of the control problem (P) derived in Section 5.1.5:

$$\begin{aligned}
-\bar{q}_t &= G_f(\bar{\theta}, \bar{f})(\bar{q} + \rho L \bar{p}) && \text{in } Q, && (5.56a)\\
\bar{q}(T) &= \alpha_1(\bar{f}(T) - f_d) && \text{in } \Omega, && (5.56b)\\
-\rho c_p \bar{p}_t - \kappa \Delta \bar{p} &= G_\theta(\bar{\theta}, \bar{f})(\rho L \bar{p} + \bar{q}) && \text{in } Q, && (5.56c)\\
-\kappa \frac{\partial \bar{p}}{\partial n} &= \bar{u}(t)\beta(x)\bar{p} && \text{on } \Sigma_1, && (5.56d)\\
-\kappa \frac{\partial \bar{p}}{\partial n} &= 0 && \text{on } \Sigma_2, && (5.56e)\\
\bar{p}(T) &= \frac{\alpha_2}{\rho c_p}(\bar{\theta}(T) - \theta_d) && \text{in } \Omega. && (5.56f)
\end{aligned}$$

Using the control-to-state mapping

$$S = (S_\theta, \, S_f) : L^\infty(0,T) \to Y \times W^{1,p}(0,T; L^p(\Omega)), \quad 1 \le p \le \infty,$$

the reduced cost functional of problem (P) is given by

$$j(u) = J(S(u), u) = \frac{\alpha_1}{2} \int_\Omega (S_f(u)(T) - f_d)^2 \, dx + \frac{\alpha_2}{2} \int_\Omega (S_\theta(u)(T) - \theta_d)^2 \, dx + \frac{\alpha_3}{2} \int_0^T u^2 dt.$$

The directional derivative of j at the point u^n in the direction $h \in L^\infty(0,T)$ is

$$j'(u^n)h = -\iint\limits_{\Sigma_1} h\beta(\theta_n - \theta_w)p_n d\sigma dt + \alpha_3 \int\limits_0^T u^n h dt,$$

where p_n solves an adjoint system to (P). Thus, the gradient of the functional j can be identified by the Riesz representation theorem as

$$j'(u^n) = -\int_{\Gamma_1} p_n\beta(\theta_n - \theta_w)d\sigma + \alpha_3 u^n.$$

According to the gradient projection algorithm (see, e.g., [41, pp. 91–96]) the actual iterate for the control is

$$u^n(s) = \mathcal{P}_{U_{ad}}\big(u^n + sv_n\big) \quad \text{for } s \geq 0,$$

with gradient descent $v_n = -j'(u^n)$ and a steplength parameter s given by the Armijo rule or some other line search scheme. $\mathcal{P}_{U_{ad}}$ is the projection on the set of admissible controls, i.e.,

$$\mathcal{P}_{U_{ad}}(u) = \begin{cases} u_a & \text{if } u \leq u_a, \\ u & \text{if } u_a < u \leq u_b, \\ u_b & \text{if } u > u_b. \end{cases}$$

The general algorithmic description follows in Algorithm 1.

Algorithm 1 *Gradient projection method.*

1: Choose an initial iteration for the control $u^0 \in U_{ad}$
2: Set $n := 0$
3: **while** $n < n_{\max}$ **do**
4: Solve the state system for (θ^n, f^n)
5: Evaluate (p^n, q^n) as the solution of the adjoint system of (P)
6: Calculate the gradient

$$j'(u^n) = -\int_{\Gamma_1} p_n\beta(\theta_n - \theta_w)d\sigma + \alpha_3 u^n$$

and set $v_n = -j'(u^n)$
7: Identify the steplength s_n

$$s_n = \arg\min_{s>0} j(\mathcal{P}_{U_{ad}}(u^n + sv_n))$$

8: Update the control

$$u^n(s) = \mathcal{P}_{U_{ad}}\big(u^n + sv_n\big)$$

9: $n := n + 1$
10: **end while**

Remark 5.2.1. *(i) The precise computation of the steplength in step 7 is not possible in general. One of the possible ways to identify the parameter s approximately is a backtracking line search based on the sufficient decrease condition [41]*

$$j(u^n(s)) - j(u^n) \leq -cs \ \|u^n(s) - u^n\|^2_{L^2(0,T)}, \tag{5.57}$$

with parameter c, which is typically set as 10^{-4}.
The strategy is as follows: choose the initial step size $s^0 = 1$ *and then iterate* $s^i = s^{i-1}/2$ *for* $i \geq 1$ *until the condition (5.57) is fulfilled.*
(ii) For each new step size, the evaluation of the cost functional requires the solution of a partial differential equation, which is costly. Therefore, one sometimes chooses to work with a fixed, sufficiently small step size as long as a sufficiently large descent can be maintained.

The projected gradient method exhibits fast converge at the beginning, but it then becomes slow, which is a characteristic behaviour of gradient methods. The convergence of this method in finite-dimensional spaces has been studied, e.g., by Gruver and Sachs [26], Kelley [41], Nocedal and Wright [56]. The Hilbert space case is treated in, e.g., Hinze et al. [30].

5.2.2 The reduced SQP method (outer loop)

Sequential quadratic programming methods have turned out to be one of the most successful methods in nonlinear optimization [1, 56]. The principal idea is to linearize the nonlinear equality constraints and to replace the cost functional by a quadratic approximation of the Lagrangian. The main idea of reduced SQP methods in contrast to usual SQP methods is to use only an approximation of the projected Hessian of the Lagrangian onto the kernel of the linearized constraint, instead of an approximation of the full Hessian of the Lagrangian.

We introduce the Lagrange functional

$$\mathcal{L}(\theta, f, u, p, q) : Y \times W^{1,\infty}(0,T; L^\infty(\Omega)) \times L^\infty(0,T) \times Y \times W^{1,\infty}(0,T; L^\infty(\Omega)) \to \mathbb{R}$$

with $Y := W(0,T) \cap C(\bar{Q})$ and

$$\mathcal{L}(\theta, f, u, p, q) = J(\theta, f, u) - \Bigg(\int_0^T \rho c_p \langle \theta_t, p \rangle_{H^1(\Omega)^*, H^1(\Omega)} dt + a(u)[\theta, p] - (u(t)\beta(x)\theta_w, p)_{\Sigma_1}$$
$$- (\rho L G(\theta, f), p)_Q + (f_t - G(\theta, f), q)_Q \Bigg),$$

with a bilinear form

$$a(u)[\theta, v] := \iint_Q \kappa \nabla\theta \cdot \nabla v dx dt + \iint_{\Sigma_1} u\beta\theta v d\sigma dt.$$

Further, we denote $x := (\theta, f, u)$. At each iteration of the SQP method, the following quadratic approximation of the Lagrangian is minimized under linearized constraints,

where it is assumed that the current iterate $x^k = (\theta^k, f^k, u^k)$ is sufficiently close to a local optimal solution $(\bar{\theta}, \bar{f}, \bar{u})$:

$$
\begin{aligned}
\min \quad & \frac{1}{2}\mathcal{L}''(x^k, p^k, q^k)[\delta x, \delta x] + J'(x^k)\delta x \\
\text{s.t.} \quad & \\
\delta f_t &= G_f(\theta^k, f^k)\delta f + G_\theta(\theta^k, f^k)\delta\theta \\
&\quad - f_t^k + G(\theta^k, f^k) && \text{in } Q, \\
\delta f(0) &= -f^k(0) && \text{in } \Omega, \\
\rho c_p \delta\theta_t - \kappa\Delta\delta\theta &= \rho L \delta f_t - (\rho c_p \theta_t^k - \kappa\Delta\theta^k - \rho L f_t^k) && \text{in } Q, \\
-\kappa\frac{\partial\delta\theta}{\partial n} - u^k(t)\beta(x)\delta\theta &= \delta u(t)\beta(x)(\theta^k - \theta_w) + \kappa\frac{\partial\theta^k}{\partial n} \\
&\quad + u^k(t)\beta(x)(\theta^k - \theta_w) && \text{on } \Sigma_1, \\
-\kappa\frac{\partial\delta\theta}{\partial n} &= \kappa\frac{\partial\theta^k}{\partial n} && \text{on } \Sigma_2, \\
\delta\theta(0) &= \theta_0 - \theta^k(0) && \text{in } \Omega, \\
u_a \leq & \delta u + u^k \leq u_b && \text{in } (0,T).
\end{aligned}
\tag{QP^k}
$$

Note that

$$
J'(x^k)\delta x = \alpha_1(f^k(T) - f_d, \delta f)_\Omega + \alpha_2(\theta^k(T) - \theta_d, \delta\theta)_\Omega + \alpha_3(u^k, \delta u)_{(0,T)}
$$

and

$$
\begin{aligned}
\mathcal{L}''(x^k, p^k, q^k)[\delta x, \delta x] = {} & \alpha_1(\delta f, \delta f)_\Omega + \alpha_2(\delta\theta, \delta\theta)_Q + \alpha_3(\delta u, \delta u)_{(0,T)} \\
& - 2(\beta\delta u\delta\theta, p^k)_{\Sigma_1} + (G''(\theta^k, f^k)[\delta\theta, \delta f]^2, \rho L p^k + q^k)_Q
\end{aligned}
\tag{5.58}
$$

In order to prescribe the resulting optimality system in a preferably compact way, we will introduce an abstract description of the state equation and its linearization. The state system can be written as a mapping

$$
\begin{aligned}
& e : W(0,T) \times W^{1,\infty}(0,T; L^\infty(\Omega)) \times L^\infty(0,T) \to L^2(0,T; H^1(\Omega)^*) \times L^r(Q), \\
& e(\theta, f, u) = \begin{pmatrix} e_1(\theta, f, u) \\ e_2(\theta, f, u) \end{pmatrix}
\end{aligned}
$$

and

$$
e(\theta, f, u) = 0.
$$

This mapping is defined by using test functions $p \in L^2(0,T; H^1(\Omega))$ and $q \in L^s(Q)$:

$$
\begin{aligned}
e_1(\theta, f, u)(p) := {} & \int_0^T \rho c_p \langle\theta_t, p\rangle_{H^1(\Omega)^*, H^1(\Omega)} dt + a(u)[\theta, p] - (\rho L G(\theta, f), p)_Q \\
& - (u(t)\beta(x)\theta_w, p)_{\Sigma_1}, && (5.59) \\
e_2(\theta, f, u)(q) := {} & \iint_Q f_t q - G(\theta, f) q dx dt. && (5.60)
\end{aligned}
$$

Using this notation and that $\delta x = (\delta\theta, \delta f, \delta u)$, the linearized state system in problem (QP^k) is given by

$$e_x(x^k)\delta x = \begin{pmatrix} e_{1,\theta}(x^k)\delta\theta + e_{1,f}(x^k)\delta f + e_{1,u}(x^k)\delta u \\ e_{2,\theta}(x^k)\delta\theta + e_{2,f}(x^k)\delta f \end{pmatrix} = -e(x^k).$$

Note that $e_{2,u}(x^k)$ is zero. The partial derivatives are defined as follows:

$$\begin{aligned} (e_{1,\theta}(x^k)\delta\theta)(p) &= \int_0^T \rho c_p \langle \delta\theta_t, p\rangle_{H^1(\Omega)^*, H^1(\Omega)} dt + a(u^k)[\delta\theta, p] \\ &\quad - (\rho L G_\theta(\theta^k, f^k)\delta\theta, p)_Q, \\ (e_{1,f}(x^k)\delta f)(p) &= -(\rho L G_f(\theta^k, f^k)\delta f, p)_Q, \\ (e_{1,u}(x^k)\delta u)(p) &= (\delta u(t)\beta(x)(\theta^k - \theta_w), p)_{\Sigma_1}, \\ (e_{2,\theta}(x^k)\delta\theta)(q) &= (-G_\theta(\theta^k, f^k)\delta\theta, q)_Q, \\ (e_{2,f}(x^k)\delta f)(q) &= (\delta f_t - G_f(\theta^k, f^k)\delta f, q)_Q. \end{aligned} \tag{5.61}$$

Hence, problem (QP^k) can be written as

$$\begin{aligned} \min \quad & \frac{1}{2}\mathcal{L}''(x^k, p^k, q^k)[\delta x, \delta x] + J'(x^k)\delta x \\ \text{s.t.} \quad & e_x(x^k)\delta x = -e(x^k) \\ & \delta u \in U_{ad} - \{u^k\}. \end{aligned} \tag{QP^k}$$

Introducing adjoint variables with respect to the linearized state system and neglecting the inequality constraints for a moment, the optimality system, also called Karush-Kuhn-Tucker (KKT) system, is given in the following compact form

$$\begin{pmatrix} \mathcal{L}''_{\theta\theta} & \mathcal{L}''_{\theta f} & \mathcal{L}''_{\theta u} & e^*_{1,\theta} & e^*_{2,\theta} \\ \mathcal{L}''_{f\theta} & \mathcal{L}''_{ff} & \mathcal{L}''_{fu} & e^*_{1,f} & e^*_{2,f} \\ \mathcal{L}''_{u\theta} & \mathcal{L}''_{uf} & \mathcal{L}''_{uu} & e^*_{1,u} & 0 \\ e_{1,\theta} & e_{1,f} & e_{1,u} & 0 & 0 \\ e_{2,\theta} & e_{2,f} & 0 & 0 & 0 \end{pmatrix} \begin{pmatrix} \delta\theta \\ \delta f \\ \delta u \\ p \\ q \end{pmatrix} = \begin{pmatrix} -J_\theta \\ -J_f \\ -J_u \\ -e \end{pmatrix}. \tag{5.62}$$

For simplicity, function arguments are now omitted. Unless otherwise stated, all functions are to be evaluated at the k^{th} iterate. Introducing the notation $\mathcal{L}''_{(\theta,f)}$, the second derivative of the Lagrangian $\mathcal{L}$ with respect to the state pair variable (θ, f), we can rewrite the KKT matrix as 3×3 block matrix. Since the linearized state system is uniquely solvable for every right hand side (this can be shown along the lines of Theorem 5.1.1), we can derive the following decomposition of the full KKT matrix in (5.62) by Gaussian block elimination

$$\begin{pmatrix} \mathcal{L}''_{(\theta,f)} & \mathcal{L}''_{(\theta,f)u} & e^*_{(\theta,f)} \\ \mathcal{L}''_{u(\theta,f)} & \mathcal{L}''_{uu} & e^*_u \\ e_{(\theta,f)} & e_u & 0 \end{pmatrix} = \begin{pmatrix} \mathcal{L}''_{(\theta,f)} e^{-1}_{(\theta,f)} & 0 & I \\ \mathcal{L}''_{u(\theta,f)} e^{-1}_{(\theta,f)} & I & e^*_u e^{-*}_{(\theta,f)} \\ I & 0 & 0 \end{pmatrix} \begin{pmatrix} e_{(\theta,f)} & e_u & 0 \\ 0 & H & 0 \\ 0 & W & e^*_{(\theta,f)} \end{pmatrix}. \tag{5.63}$$

The so-called reduced Hessian H is defined by

$$\begin{aligned} H &= (-e^*_u e^{-*}_{(\theta,f)} \; I) \begin{pmatrix} \mathcal{L}''_{(\theta,f)} & \mathcal{L}''_{(\theta,f)u} \\ \mathcal{L}''_{u(\theta,f)} & \mathcal{L}''_{uu} \end{pmatrix} \begin{pmatrix} -e^{-1}_{(\theta,f)} e_u \\ I \end{pmatrix} \\ &= \mathcal{L}''_{uu} + e^*_u e^{-*}_{(\theta,f)} (\mathcal{L}''_{(\theta,f)} e^{-1}_{(\theta,f)} e_u - \mathcal{L}''_{(\theta,f)u}) - \mathcal{L}''_{u(\theta,f)} e^{-1}_{(\theta,f)} e_u. \end{aligned} \tag{5.64}$$

Moreover, we have

$$\begin{aligned} W &= (I \quad 0) \begin{pmatrix} \mathcal{L}''_{(\theta,f)} & \mathcal{L}''_{(\theta,f)u} \\ \mathcal{L}''_{u(\theta,f)} & \mathcal{L}''_{uu} \end{pmatrix} \begin{pmatrix} -e^{-1}_{(\theta,f)} e_u \\ I \end{pmatrix} \\ &= -\mathcal{L}''_{(\theta,f)} e^{-1}_{(\theta,f)} e_u + \mathcal{L}''_{(\theta,f)u}. \end{aligned}$$

Remark 5.2.2. *The reduced Hessian approach is a null space approach to solve the saddle point problem* (5.62)*, see Nocedal and Wright [56], Ch. 16.2, Ch. 18.3. Here the advantage is the splitting of variables into state variables* (θ, f) *and control variable* u *in optimal control, which gives us the representation of the kernel of* $e_x = (e_{(\theta,f)}, e_u)$*. The elements in the kernel of* e_x *are of the form*

$$\begin{pmatrix} -e^{-1}_{(\theta,f)} e_u \\ I \end{pmatrix} \delta u$$

with some $\delta u \in U_{ad}$*.*

Using the decomposition (5.63), (5.62) can be treated by:

(i) Solve the reduced Hessian system:

$$H\delta u = \underbrace{-J_u + e^*_u e^{-*}_{(\theta,f)} (J_{(\theta,f)} - L''_{(\theta,f)} e^{-1}_{(\theta,f)} e) + L''_{u(\theta,f)} e^{-1}_{(\theta,f)} e}_{=:r}. \tag{5.65}$$

(ii) Solve the linearized state system, i.e.,

$$e_{(\theta,f)} \begin{pmatrix} \delta\theta \\ \delta f \end{pmatrix} = -e_u \delta u - e.$$

(iii) Solve the adjoint state system, i.e.,

$$e^*_{(\theta,f)} \begin{pmatrix} p \\ q \end{pmatrix} = -J_{(\theta,f)} - \mathcal{L}''_{(\theta,f)} \begin{pmatrix} \delta\theta \\ \delta f \end{pmatrix} - \mathcal{L}''_{(\theta,f)u} \delta u.$$

Based on these arguments and taking the control constraints into account, the reduced optimality conditions of the linear quadratic problem (QP^k) are given by

$$(H(x^k, p^k, q^k)\delta u - r(x^k, p^k, q^k), \delta v - \delta u)_{(0,T)} \geq 0 \qquad \forall \delta v \in U_{ad} - \{u^k\}, \tag{5.66}$$

where H is defined as in (5.64) and the residuum r in (5.65) has to be evaluated by

$$r := -J_u + e^*_u e^{-*}_{(\theta,f)} (J_{(\theta,f)} - L''_{(\theta,f)} e^{-1}_{(\theta,f)} e) + L''_{u(\theta,f)} e^{-1}_{(\theta,f)} e.$$

The reduced SQP algorithm for solving problem (P) is summarized in Algorithm 2.

It is well known that SQP methods exhibit local quadratic convergence in finite-dimensional spaces. The convergence analysis for nonlinear parabolic boundary control problems in the infinite-dimensional case was presented in the works of Goldberg and Tröltzsch [22], Tröltzsch [80]. It was shown that the SQP method converges locally quadratically to the local minimizer in the sense of the L^∞-norms of control, state and adjoint variables, provided the second-order sufficient optimality conditions are fulfilled. The convergence behaviour of the reduced SQP method in Hilbert spaces is studied, e.g., in Kupfer [45].

In a next step, we have to specify how to solve the linear quadratic optimal control problems arising in the iterations of the above rSQP method. In the next section, we introduce an active set strategy.

Algorithm 2 *Reduced SQP method (outer loop).*

1: Choose initial variables $x^0 = (\theta^0, f^0, u^0)$ sufficiently close to $(\bar{\theta}, \bar{f}, \bar{u})$ and set $k := 0$
2: Evaluate (p^k, q^k) as the solution of the adjoint system (5.56)
3: **repeat**
4: *Primal-dual active set strategy (inner loop)*
Solve (QP^k), i.e., determine δu such that

$$(H(x^k, p^k, q^k)\delta u - r(x^k, p^k, q^k), \delta v - \delta u)_{(0,T)} \geq 0 \qquad \forall \delta v \in U_{ad} - \{u^k\}$$

is satisfied
5: Solve the linearized state system

$$e_{(\theta,f)}(x^k) \begin{pmatrix} \delta\theta \\ \delta f \end{pmatrix} = -e_u(x^k)\delta u - e(x^k)$$

6: Solve the adjoint state system of (QP^k), i.e.,

$$e^*_{(\theta,f)}(x^k) \begin{pmatrix} p \\ q \end{pmatrix} = -J_{(\theta,f)}(x^k) - \mathcal{L}''_{(\theta,f)}(x^k, p^k, q^k) \begin{pmatrix} \delta\theta \\ \delta f \end{pmatrix} - \mathcal{L}''_{(\theta,f)u}(x^k, p^k, q^k)\delta u$$

7: Update iterates

$$u^{k+1} := u^k + \delta u, \quad \theta^{k+1} := \theta^k + \delta\theta, \quad f^{k+1} := f^k + \delta f, \quad p^{k+1} := p, \quad q^{k+1} := q$$

8: Set $k := k + 1$
9: **until**

$$\tau_{rel} = \frac{1}{5}\Big(\frac{\| u^{k+1} - u^k \|_{L^2(0,T)}}{\| u^k \|_{L^2(0,T)}} + \frac{\| \theta^{k+1} - \theta^k \|_{L^2(Q)}}{\| \theta^k \|_{L^2(Q)}} + \frac{\| f^{k+1} - f^k \|_{L^2(Q)}}{\| f^k \|_{L^2(Q)}} + \frac{\| p^{k+1} - p^k \|_{L^2(Q)}}{\| p^k \|_{L^2(Q)}} + \frac{\| q^{k+1} - q^k \|_{L^2(Q)}}{\| q^k \|_{L^2(Q)}} \Big) < tol$$

5.2.3 The primal-dual active set strategy (inner loop)

The primal-dual active set (PDAS) method has proven to be an efficient numerical tool in the context of optimization problems including inequality constraints [5]. PDAS consists in the application of both, primal and dual variables to obtain the solution of the inequality constrained optimization problem. The idea of the active set strategy is to "iterate" with respect to the active sets in which the control function takes either upper or lower boundary values. If the active sets are known, the problem (QP^k) (on p. 86) reduces to a control problem that only has equality constraints. Thus, in each step of the iteration method, a set of active constraints is defined, the associated parts of the control are kept fixed, and its remaining parts are obtained by the solution of the respective free optimal control problem. For control-constrained problems, the practical behaviour of PDAS strategy is characterized by infeasible iterations. Often only the last iteration is feasible. The algorithm stops at a feasible and optimal point. It is proven that the PDAS

method has found the optimal solution whenever two subsequent active sets coincide, see [5].

Now, we consider the application of the PDAS method to our control problem (QP^k). Let us assume that the active sets of the optimal solution of problem (QP^k) are known, i.e., we can define

$$\begin{aligned} A^- &= \{t \in (0,T) \,|\, \delta u = u_a - u^k\}, \\ A^+ &= \{t \in (0,T) \,|\, \delta u = u_b - u^k\}, \\ I &= (0,T) \setminus (A^- \cup A^+). \end{aligned}$$

Furthermore, let us decompose the control $\delta u = \delta u_I + \delta u_A$ in an active part δu_A and inactive part δu_I according to the previous sets:

$$\delta u_A = \begin{cases} u_a - u^k, & t \in A^-, \\ u_b - u^k, & t \in A^+, \\ 0, & \text{else} \end{cases} \quad \text{and} \quad \delta u_I = \begin{cases} 0, & t \in A^-, \\ 0, & t \in A^+, \\ \text{unknown}, & t \in I. \end{cases}$$

The problem (QP^k) can be interpreted as a free optimal control problem, where δu_I serves as a control variable. For a given active part δu_A, the variational inequality (5.66) then simplifies to

$$H(x^k, p^k, q^k)\delta u_I = r(x^k, p^k, q^k) - H(x^k, p^k, q^k)\delta u_A.$$

Now, the idea of the active set strategy is to iterate with respect to the active sets based on initial sets A_0^-, A_0^+ and I_0. Suppose that for given active sets A_l^- and A_l^+, the solution of the respective free optimal control problem is denoted by δu_I^l and we set $\delta u^l = \delta u_I^l + \delta u_A^l$. Based on the variational inequality, an update of the active sets for a fixed constant $c > 0$ can be defined as follows:

$$\begin{aligned} A_{l+1}^- &:= \{t \in (0,T) | c(\delta u_I^l - u_a + u^k) - H(x^k, p^k, q^k)\delta u_I^l + r(x^k, p^k, q^k) < 0\}, \\ A_{l+1}^+ &:= \{t \in (0,T) | c(\delta u_I^l - u_b + u^k) - H(x^k, p^k, q^k)\delta u_I^l + r(x^k, p^k, q^k) > 0\}, \\ I_{l+1} &= (0,T) \setminus (A_{l+1}^- \cup A_{l+1}^+). \end{aligned}$$

A usual stopping criterion of the PDAS algorithm is the coincidence of subsequent active sets $A_{l+1}^- = A_l^-$ and $A_{l+1}^+ = A_l^+$. One can easily check that if the previous condition is satisfied, the optimal active sets are determined such that the variational inequality (5.66) is fulfilled and problem (QP^k) is solved. Summarizing, the active set strategy for solving the linear quadratic subproblems (QP^k) of the rSQP method is presented in Algorithm 3.

In the following, we will explain steps 4–7 of Algorithm 3 in detail. Suppose that $(\theta^k, f^k, u^k, p^k, q^k)$ denotes the current iterate of the SQP-loop. The linear system in step 4 will be treated by an iterative solver in particular the CG method, which is introduced in the next section. According to (5.59), (5.61), in step 5, the following variational problem has to be solved for given control δu_l and for all $v \in L^2(0,T;H^1(\Omega))$, $w \in L^s(Q)$:

$$\begin{aligned} \int_0^T \rho c_p \langle (\delta\theta_l)_t, v\rangle_{H^1(\Omega)^*, H^1(\Omega)} dt + a(u^k)[\delta\theta_l, v] - (\rho L(\delta f_l)_t, v)_Q \\ = (\delta u_l(t)\beta(x)(\theta_w - \theta^k), v)_{\Sigma_1} - e_1(\theta^k, f^k, u^k)(v), \qquad (5.67) \\ ((\delta f_l)_t - G_f(\theta^k, f^k)\delta f_l - G_\theta(\theta^k, f^k)\delta\theta_l, w)_Q = -e_2(\theta, f, u)(w). \qquad (5.68) \end{aligned}$$

Algorithm 3 *Primal-dual active set strategy for solving* (QP^k) *(inner loop).*

1: Choose initial active sets according to the current iterate of the rSQP method, i.e.,

$$A_0^- = \{t \,|\, u^k(t) = u_a\},\ A_0^+ = \{t \,|\, u^k(t) = u_b\},\ I_0 = (0,T) \setminus (A_0^- \cup A_0^+)$$

2: Set $l := 0$ and

$$\delta u_{0,A} = \begin{cases} u_a - u^k, & t \in A_0^-, \\ u_b - u^k, & t \in A_0^+, \\ 0, & \text{else} \end{cases}$$

3: Define operators $E_{I_l} : L^\infty(0,T) \to L^\infty(0,T), u \mapsto \chi_{I_l} u$ and $E_{A_l} := I - E_{I_l}$, where χ_{I_l} is the characteristic function w.r.t. I_l

4: Determine $\delta u_{l,I}$ by solving

$$(E_{I_l} H(x^k,p^k,q^k) E_{I_l} + E_{A_l}) \delta u_{l,I} = E_{I_l}(r(x^k,p^k,q^k) - H(x^k,p^k,q^k)\delta u_{l,A})$$

and set $\delta u_l = \delta u_{l,I} + \delta u_{l,A}$

5: Determine the state variables $(\delta\theta_l, \delta f_l)$ by

$$e_{(\theta,f)}(x^k,p^k,q^k) \begin{pmatrix} \delta\theta_l \\ \delta f_l \end{pmatrix} = -e_u(x^k,p^k,q^k)\delta u_l - e(x^k,p^k,q^k)$$

6: Evaluate the adjoint variables (p_l, q_l) by

$$\begin{aligned} e^*_{(\theta,f)}(x^k,p^k,q^k) \begin{pmatrix} p_l \\ q_l \end{pmatrix} = & -J_{(\theta,f)}(x^k,p^k,q^k) - \mathcal{L}''_{(\theta,f)}(x^k,p^k,q^k) \begin{pmatrix} \delta\theta_l \\ \delta f_l \end{pmatrix} \\ & - \mathcal{L}''_{(\theta,f)u}(x^k,p^k,q^k)\delta u_l \end{aligned}$$

7: Determine

$$\begin{aligned} \lambda^- &:= \delta u_l - u_a + u^k - \left(\mathcal{L}''_u \delta u_l + e^*_{1,u} p_l + \mathcal{L}''_{u(\theta,f)} \begin{pmatrix} \delta\theta_l \\ \delta f_l \end{pmatrix} + J_u \right) \\ \lambda^+ &:= \delta u_l - u_b + u^k - \left(\mathcal{L}''_u \delta u_l + e^*_{1,u} p_l + \mathcal{L}''_{u(\theta,f)} \begin{pmatrix} \delta\theta_l \\ \delta f_l \end{pmatrix} + J_u \right) \end{aligned}$$

and update the active sets

$$A_{l+1}^- = \{t \,|\, \lambda^-(t) < 0\},\ A_{l+1}^+ = \{t \,|\, \lambda^+(t) > 0\},\ I_{l+1} = (0,T) \setminus (A_0^- \cup A_0^+)$$

8: **if** $A_{l+1}^- = A_l^-$ and $A_{l+1}^+ = A_l^+$ **then**

9: STOP

10: **else**

11:

$$\delta u_{(l+1),A} = \begin{cases} u_a - u^k, & t \in A_{l+1}^-, \\ u_b - u^k, & t \in A_{l+1}^+, \\ 0, & \text{else} \end{cases}$$

set $l := l + 1$ and GOTO 3

12: **end if**

Introducing formal adjoint operators to e_x via the definitions in (5.61), step 6 is equivalent to solving the variational problem

$$
\begin{aligned}
-\int_0^T \rho c_p \langle (p_l)_t, v\rangle_{H^1(\Omega)^*,H^1(\Omega)} dt + a(u^k)[p_l, v] - (G_\theta(\rho L p_l + q_l), v)_Q &= -(\delta u_l(t)\beta(x)p^k, v)_{\Sigma_1} \\
&\quad + ((G_{\theta\theta}\delta\theta_l + G_{\theta f}\delta f_l)(\rho L p^k + q^k), v)_Q \\
(p_l(T), v(T))_\Omega &= (\frac{\alpha_2}{\rho c_p}\delta\theta_l(T) + \frac{\alpha_2}{\rho c_p}(\theta^k(T) - \theta_d), v(T))_\Omega \\
(-(q_l)_t - G_f(q_l + \rho L p_l), w)_Q &= ((G_{f\theta}\delta\theta_l + G_{ff}\delta f_l)(\rho L p^k + q^k), w)_Q \\
(q_l(T), w(T))_\Omega &= (\alpha_1\delta f_l(T) + \alpha_1(f^k(T) - f_d), w(T))_\Omega
\end{aligned}
$$

for all $v \in L^2(0,T;H^1(\Omega))$ and $w \in L^p(Q)$ with $w(0) = 0$. According to definition (5.58) of the second derivative, we find the respective terms in step 7:

$$
\mathcal{L}''_u(\theta^k, f^k)\delta u_l + \mathcal{L}''_{u(\theta,f)}(\theta^k, f^k)\begin{pmatrix}\delta\theta_l \\ \delta f_l\end{pmatrix} = \alpha_3\delta u_l - \int_{\Gamma_1}\beta(\sigma)p^k(\sigma,t)\delta\theta_l(\sigma,t)d\sigma.
$$

Moreover, the formal adjoint $e^*_{1,u}$ of the operator $e_{1,u}$ is characterized as follows:

$$
e^*_{1,u}(\theta^k, f^k)p_l = \int_{\Gamma_1}\beta p_l(\theta^k - \theta_w)d\sigma.
$$

Summarizing, λ^- is determined by

$$
\lambda^- = \delta u_l + u^k - u_a - (\alpha_3(\delta u_l + u^k) - \int_{\Gamma_1}\beta p^k\delta\theta_l d\sigma + \int_{\Gamma_1}\beta p_l(\theta^k - \theta_w)d\sigma).
$$

In a last step, we have to provide a method for solving the linear system of equations in step 4 of the primal dual active set strategy. Due to the definition of the reduced Hessian in (5.64), the system matrix H is not explicitly given after choosing a discretization strategy for the underlying partial differential equations. Hence, an iterative solver has to be established for treating the reduced Hessian system, e.g., the generalized minimal residual (GMRES) method or the conjugate gradient (CG) method. The latter is discussed in the next section.

5.2.4 CG method

The reduced Hessian system

$$
\tilde{H}\delta u_l = (E_{I_l}HE_{I_l} + E_{A_l})\delta u_{l,I} = E_{I_l}(r - H\delta u_{l,A}) =: b \tag{5.69}
$$

can be solved iteratively using the CG method since the Hessian is symmetric and positive definite (near a solution that satisfies second order sufficient conditions). The CG method is one of the most useful techniques for solving large linear systems of equations with symmetric and positive definite matrix. This method can be also interpreted as a technique for the minimization of convex quadratic functions. For more details on the CG

method, we refer to, e.g., Nocedal and Wright [56] Chapter 5. The CG method applied to (5.69) is presented in Algorithm 4.

Algorithm 4 *CG algorithm for solving step 4 in the PDAS algorithm.*

1: Choose $\delta u^0 \in L^2(0,T)$, $tol > 0$ and set $r^0 = \tilde{H}\delta u^0 - b$, $d^0 = -r_0$, $n := 0$
2: **while** $\|r^n\| \geq tol$ **do**
3: Determine $g^n = \tilde{H}d^n$, i.e.:
Solve the state system forward in time

$$h_1 = e^{-1}_{(\theta,f)} e_u(E_I d^n)$$

Solve the adjoint system backward in time

$$h_2 = e^{-*}_{(\theta,f)}(\mathcal{L}''_{(\theta,f)}h_1 - \mathcal{L}''_{(\theta,f)u}(E_I d^n))$$

Evaluate

$$g^n = E_I(\mathcal{L}''_u E_I d^n + e^*_u h_2 - \mathcal{L}''_{u(\theta,f)}h_1) + E_A d^n$$

4: Compute

$$t^n = \frac{(r^n, r^n)_{L^2(0,T)}}{(d^n, g^n)_{L^2(0,T)}}$$
$$\delta u^{n+1} = \delta u^n + t^n d^n, \qquad r^{n+1} = r^n + t^n g^n$$

5: Evaluate

$$\beta^n = \frac{(r^{n+1}, r^{n+1})_{L^2(0,T)}}{(r^n, r^n)_{L^2(0,T)}}$$
$$d^{n+1} = -r^{n+1} + \beta^{n+1} d^n$$

6: Set $n := n + 1$
7: **end while**

In the sequel, we neglect the indices k and l regarding the outer SQP-loop and the inner PDAS-loop. Let us explain step 3 of the CG algorithm in detail, which is equivalent to a matrix-vector multiplication. For given $d^n \in L^2(0,T)$ and operators E_I and E_A (compare Algorithm 3, step 3), $h_1 = (h_{1,\theta}, h_{1,f})^T = e^{-1}_{(\theta,f)} e_u(E_I d^n)$ is equivalent to solving the following variational problem

$$\int_0^T \rho c_p \langle (h_{1,\theta})_t, v\rangle_{H^1(\Omega)^*, H^1(\Omega)} dt + a(u^k)[h_{1,\theta}, v] - (\rho L (h_{1,f})_t, v)_Q$$
$$= (\chi_I d^n(t)\beta(x)(\theta^k - \theta_w), v)_{\Sigma_1},$$
$$((h_{1,f})_t - G_f(\theta^k, f^k)h_{1,f} - G_\theta(\theta^k, f^k)h_{1,\theta}, w)_Q = 0.$$

Afterwards the adjoint problem $h_2 = (h_{2,p}, h_{2,q})^T = e^{-*}_{(\theta,f)}(\mathcal{L}''_{(\theta,f)}h_1 - \mathcal{L}''_{(\theta,f)u}(E_I d^n))$ has to

be solved, in particular

$$
\begin{aligned}
-\int_0^T \rho c_p \langle (h_{2,p})_t, v\rangle_{H^1(\Omega)^*,H^1(\Omega)} dt + a(u^k)[h_{2,p}, v] - (G_\theta(\rho L h_{2,p} + h_{2,q}), v)_Q \\
= (\chi_I d^n p^k \beta(x), v)_{\Sigma_1} + ((G_{\theta\theta}\delta\theta_l + G_{\theta f}\delta f_l)(\rho L p^k + q^k), v)_Q, \\
(h_{2,p}(T), v(T))_\Omega = \frac{\alpha_2}{\rho c_p}(h_{1,\theta}(T), v(T))_\Omega, \\
(-(h_{2,q})_t - G_f(h_{2,q} + \rho L h_{2,p}), w)_Q = ((G_{f\theta}h_{1,\theta} + G_{ff}h_{1,f})(\rho L p^k + q^k), w)_Q, \\
(h_{2,f}(T), w(T))_\Omega = \alpha_1 (h_{1,f}(T), w(T))_\Omega.
\end{aligned}
$$

Concluding, we have to evaluate $g^n = E_I(\mathcal{L}''_u E_I d^n + e_u^* h_2 - \mathcal{L}''_{u(\theta,f)} h_1) + E_A d^n$, i.e.:

$$
\begin{aligned}
g^n(t) = \chi_I \left(\alpha_3 d^n(t) + \int_{\Gamma_1} \beta(\sigma) h_{2,p}(\sigma,t)(\theta^k - \theta_w)(\sigma,t) d\sigma + \int_{\Gamma_1} \beta(\sigma) p^k(\sigma,t) h_{1,\theta}(\sigma,t) d\sigma \right) \\
+ \chi_A d^n(t).
\end{aligned}
$$

By now, we introduced the infinite-dimensional optimization algorithms, namely, the gradient projection method and the rSQP method with a primal-dual active set strategy, to solve our control problem numerically. Next, we discuss the discretization techniques used for the numerical implementation of these algorithms.

5.2.5 Discretization

Both optimization algorithms, the gradient projection method and the reduced SQP method, require to solve the state and the adjoint equations several times. These are partial and ordinary differential equations. Below, we describe the discretization schemes used for the numerical treatment of these equations.

The control function u depends only on time and is chosen as a piecewise constant function on the time grid.

The gradient projection method introduced in Section 5.2.1 requires to solve the state system (5.55) and the corresponding adjoint system (5.56) at each iteration (steps 4, 5 in Algorithm 1). The coupled system of nonlinear partial and ordinary differential equations (5.55) is treated by alternately solving the single state equations in which the state values of the other equations act as data.

For the numerical treatment of parabolic differential equations, we apply a semi-discretization approach, namely the horizontal method of lines (Rothe's method), see, e.g., Knabner and Angermann [43]. Let us recall the weak formulation of the heat equation (5.55c): $\forall \varphi \in H^1(\Omega)$, for almost every $t \in [0,T]$

$$
\begin{aligned}
\int_\Omega \rho c_p \dot{\theta}\varphi ds + \int_\Omega \kappa \nabla\theta\nabla\varphi dx + \int_{\Gamma_1} u\beta\theta\varphi ds = \int_\Omega \rho L \dot{f}\varphi dx + \int_{\Gamma_1} u\beta\theta_w\varphi ds, \\
\theta(0) = \theta_0.
\end{aligned}
$$

This equation is first discretized with respect to time. To this end, the time interval $[0,T]$ is divided equidistantly by discretization points

$$
t_0, t_1, \ldots, t_{N_T} \quad \text{with } t_k = k h_T,\ h_T = \frac{T}{N_T},\ k = 0, \ldots, N_T.
$$

Using an implicit time stepping scheme, we obtain

$$\int_\Omega \rho c_p \frac{\theta_{k+1}-\theta_k}{h_T}\varphi dx + \int_\Omega \kappa \nabla\theta_{k+1}\nabla\varphi dx + \int_{\Gamma_1} u(t_{k+1})\beta\theta_{k+1}\varphi ds = \int_\Omega \rho L\dot{f}(t_{k+1})\varphi dx + \int_{\Gamma_1} u(t_{k+1})\beta\theta_w\varphi ds. \tag{5.70}$$

For the spatial discretization, we apply the finite element method. We want to compute an approximate solution $\theta_k \in V_h$ to the exact solution $\theta(t_k) \in V$, where $V_h \subset V := H^1(\Omega)$ is a finite element space. Here, V_h is given as $\mathrm{span}(\varphi_1, \ldots, \varphi_N)$, where φ_i is the basis function, e.g., the "hat function" belonging to mesh node i.

We set

$$\theta_k = \sum_{i=1}^{N} \theta_k^i \varphi_i.$$

Then, the aim is to calculate the coefficient vector $(\vec{\theta_k})_i = \theta_k^i$. Choosing $\varphi_i,\ i = 1, \ldots, N$, as test functions in (5.70), we obtain the fully discretized heat equation. In this way, we arrive at the following system of linear equations of dimension $N \times N$

$$(M + K + Ru(\,t_{k+1}))\vec{\theta}_{k+1} = M\vec{\theta}_k + F$$

with

$$M_{ij} = \frac{\rho c_p}{h_T}\int_\Omega \varphi_i\varphi_j dx, \quad K_{ij} = \kappa\int_\Omega \nabla\varphi_i\nabla\varphi_j dx, \quad R_{ij} = \int_{\Gamma_1}\beta\varphi_i\varphi_j ds,$$

$$F_j = \rho L\int_\Omega \dot{f}(t_k)\varphi_j dx + u(t_{k+1})\int_{\Gamma_1}\beta\theta_w\varphi_j ds,$$

$$i, j = 1, \ldots, N.$$

The solution of the system $\vec{\theta}_{k+1}$ gives us the approximation of $\theta(t_{k+1})$.

For the discretization of the phase equation (5.55a), we use an explicit Euler method. The ferrite fraction f can be updated explicitly by

$$f_{k+1} = f_k + h_T G(\theta_k, f_k), \tag{5.71}$$

where f_{k+1} is an approximation of $f(t_{k+1})$. Alternatively, an implicit scheme can be applied. In this case, the implicit nonlinear equation for f_{k+1} has to be solved by a Newton method or a successive approximation method. Both methods require more computational effort.

The adjoint system (5.56) is solved backwards in time. The substitution of a new time variable $\tilde{t} := T - t$ transforms the partial and ordinary differential equations into a system of the same type as the state system (5.55) and can be treated numerically as described above.

At each iteration of the *reduced SQP method*, the linear quadratic optimal control problem has to be solved (see step 4 of Algorithm 2). This will be done with the primal-dual active set strategy described in Algorithm 3. In this method, as well as in steps 5,

6 of the rSQP algorithm, we are dealing with the linearized state system of the optimal control problem (P) and the corresponding adjoint equations. We will not explain in detail how to solve the linear PDEs and ODEs arising in the rSQP algorithm. For the solution of these equations, the discretization scheme described above is applied.

For more details on the numerical treatment of ordinary differential equations, we refer, e.g., to Quarteroni, Sacco, and Saleri [62], Strehmel, Weiner, and Podhaisky [70]. A general overview on the numerical methods for partial differential equations, including variant approaches besides the finite element method, namely, finite difference and finite volume methods, can be found in Knabner and Angermann [43]. An extensive introduction to the finite element method is also given in Braess [11].

The numerical calculations in this thesis are done with the finite element/finite volume toolbox WIAS-pdelib developed at WIAS (see [20]). This software package is used to set up and solve a numerical scheme based on linear finite elements.

5.2.6 A numerical test

In this subsection, we discuss the application of the optimization algorithms introduced in the previous section to the semilinear parabolic boundary control problem. In order to check the convergence of the reduced SQP method with a primal-dual active set strategy, we construct a test control problem where the analytical optimal solution is known. For this purpose, we use the following approach from Tröltzsch [79]: The optimal quantities $\bar{u}$ and $\bar{\theta}$ and the associated adjoint state $\bar{p}$ are chosen a priori; Then certain parts of the cost functional and terms in the initial-boundary value problem are fitted in such a way that both the optimality system and the second-order optimality condition are satisfied.

Let $\Omega = (0,1) \times (0,1)$, Γ denotes the boundary of Ω and $T > 0$. We consider the semilinear parabolic boundary control problem: *minimize*

$$J(\theta, u) = \frac{1}{2}\int_0^T \int_\Omega (\theta - \theta_{d,\Omega})^2 dxdt + \frac{1}{2}\int_0^T \int_\Gamma (\theta - \theta_{d,\Gamma})^2 dsdt + \frac{1}{2}\int_0^T (u - u_d)^2 dt$$

subject to

$$\begin{aligned}
&\theta_t - \Delta\theta = -\theta^5 + f(x,t) && \text{in } \Omega \times (0,T),\\
&\frac{\partial\theta}{\partial\nu} + \theta = (\tilde{u}(t) - u(t))g(x) && \text{on } \Gamma \times (0,T),\\
&\theta(x,0) = \theta_0(x) && \text{in } \Omega,
\end{aligned}$$

and $u_a \le u(t) \le u_b \quad \text{a.e. in} \quad [0,T]$,
where

$$\begin{aligned}
f(x,t) &= e^{-5t}\cos^5 \pi x_1 \cdot \cos^5 \pi x_2 + e^{-t}(2\pi^2 - 1)\cos \pi x_1 \cdot \cos \pi x_2,\\
\tilde{u}(t) &= \bar{u} + e^{-t},\\
g(x) &= \cos \pi x_1 \cdot \cos \pi x_2,
\end{aligned}$$

$$\theta_{d,\Omega} = -5e^{-4t}(t-T)\cos^5 \pi x_1 \cdot \cos^5 \pi x_2 - (2\pi^2(t-T) - e^{-t} - 1)\cos \pi x_1 \cdot \cos \pi x_2,$$
$$\theta_{d,\Gamma} = (e^{-t} - t + T)\cos \pi x_1 \cdot \cos \pi x_2,$$
$$u_d = -e^{-t} - 2(t-T),$$
$$\theta_0 = \cos \pi x_1 \cdot \cos \pi x_2,$$
$$T = 1,\ u_a = -0.85,\ u_b = -0.4.$$

The optimal solution $\bar{u}$ of this problem with corresponding state and adjoint variables $\bar{\theta}, \bar{p}$ is given by

$$\bar{u} = \Pi_{[u_a,u_b]}(-e^{-t}),$$
$$\bar{\theta} = e^{-t}\cos \pi x_1 \cdot \cos \pi x_2,$$
$$\bar{p} = (t-T)\cos \pi x_1 \cdot \cos \pi x_2.$$

The triple of functions $(\bar{u}, \bar{\theta}, \bar{p})$ is chosen a priori, such that the first-order necessary optimality conditions are fulfilled.

To prove local optimality, we show that the second-order sufficient optimality conditions are satisfied. The formal Lagrange function is given by

$$\mathcal{L}(\theta, u, p) = J(\theta, u) - \int_0^T \int_\Omega (\theta_t - \Delta\theta + \theta^5 - f(x,t))p dx dt$$
$$- \int_0^T \int_\Gamma (\frac{\partial \theta}{\partial \nu} + \theta - (\tilde{u} - u)g)p d\sigma dt - \int_\Omega (\theta(x,0) - \theta_0)p dx$$

with

$$\mathcal{L}''(\bar{\theta}, \bar{u}, \bar{p})(\theta, u) = \int_0^T \int_\Omega \theta^2 dx dt + \int_0^T \int_\Gamma \theta^2 d\sigma dt + \int_0^T u^2 dt - 20 \int_0^T \int_\Omega \bar{\theta}^3 \theta^2 \bar{p} dx dt. \quad (5.73)$$

The last term in (5.73) is non-negative due to $\bar{\theta}^3\bar{p} = (t-T)\cos^4 \pi x_1 \cos^4 \pi x_2 \leq 0$ for all $t \in [0,T]$. Hence,

$$\mathcal{L}''(\bar{\theta}, \bar{u}, \bar{p})(\theta, u) \geq \|u\|^2_{L^2(0,T)}.$$

The sufficient optimality condition holds even in the entire control-state space, i.e., it is satisfied in a strong form. The local optimality of $\bar{u}$ in the sense of $L^\infty(0,T)$ is deduced from Theorem 5.18 in Tröltzsch [79, p. 300].

We choose the following initial point for the rSQP method:

$$u^0(t) \equiv -0.8,\ \theta^0(x,t) \equiv 1,\ p^0(x,t) \equiv 1.$$

The numerical solution of the parabolic problem is performed by the horizontal method of lines (Rothe's method), where the elliptic system in each time increment is solved by the Finite Element Method (FEM). The controls are chosen as piecewise constant functions on the time grid. The spatial domain is discretized with triangular finite elements with a maximal edge length of $h = 0.0125$. The time interval is discretized uniformly with stepsize $\Delta t = 0.001$ in the time interval $[0,1]$.

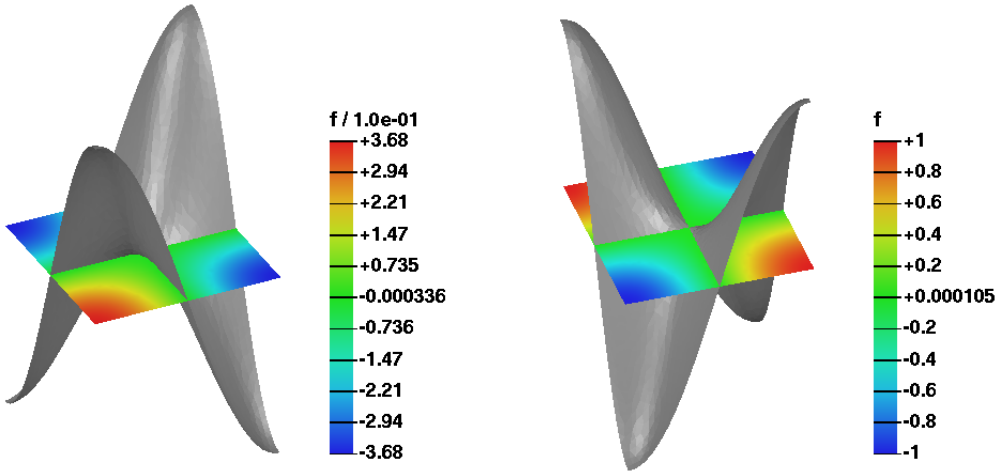

Figure 5.2: State variable $\bar{\theta}$ (left) and adjoint variable $\bar{p}$ (right) at the end time $T = 1$.

The obtained solution is displayed in Figure 5.2. The sequence of controls u^k produced by the rSQP algorithm is depicted in Figure 5.3.

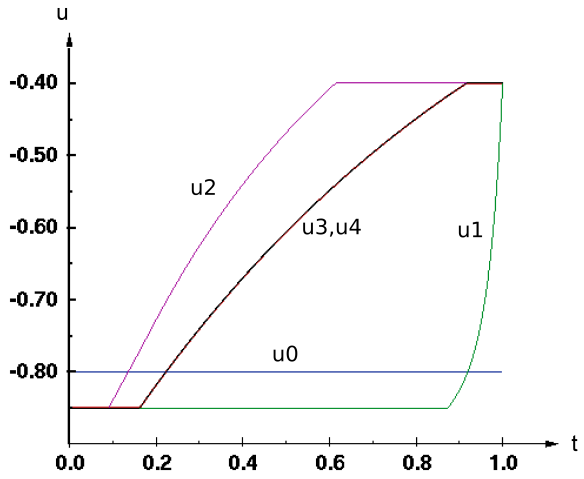

Figure 5.3: Controls $u^k(t)$.

Table 5.1 illustrates the convergence behaviour of the rSQP method. It contains the value of the objective function J_k, the rate of convergence e_k and the error τ_k that was used for the termination criterion,

$$e_k = \frac{\|u^k - \bar{u}\|_{L^2(0,T)} + \|\theta^k - \bar{\theta}\|_{L^2(Q)} + \|p^k - \bar{p}\|_{L^2(Q)}}{\|u^{k-1} - \bar{u}\|^2_{L^2(0,T)} + \|\theta^{k-1} - \bar{\theta}\|^2_{L^2(Q)} + \|p^{k-1} - \bar{p}\|^2_{L^2(Q)}},$$
$$\tau_k = \|u^k - u^{k-1}\|_{L^2(0,T)}$$

and the number of PDAS-Loops in k-th iteration of the rSQP method. The rSQP method shows a good convergence to the exact optimal solution $\bar{u}$. Four iterations were needed to get this result.

Iter	J_k	e_k	τ_k	#PDAS-Loops
1	21.8504	0.94	0.22	3
2	20.3691	0.45	0.33	4
3	20.3517	0.0085	0.0938	3
4	20.3515	140.7	$5 \cdot 10^{-4}$	1

Table 5.1: Iteration history of the rSQP method with the primal-dual active set strategy.

As reported in [22, 23], the quadratic convergence of the SQP method is assured, if the quadratic subproblems (QP^k) are solved with a quite high precision. The mesh size h has to be proportional to the current accuracy of the SQP step. In our test example, we observe that the speed of convergence of the rSQP method is limited after the third iteration by the discretization error of FEM.

Chapter 6

Optimal control of a cooling line for production of multiphase steels

The essential industrial process route for the production of multiphase steels, e.g., dual phase (DP) steel and transformation induced plasticity (TRIP) steel, is by hot rolling and subsequent controlled cooling in the cooling line located between the finishing mill and the coiler of a hot strip mill. The controlled cooling of the strip after rolling is an essential prerequisite for achieving the desired mechanical/technological properties like tensile strength, yield strength, elongation to fracture, ductility etc. These properties should be as uniform as possible over the total width and length of the strip. During the cooling process, the product undergoes various phase transformations, and the microstructure of the resulting product is a function of the amount of various phases present in the product which, in turn, depends on the temperature-time history of cooling.

Cooling systems usually employ multiple stages of either one or a combination of jet impingement systems, such as, high-pressure spray nozzle arrays, laminar flow nozzle arrays and planar water jets [7]. By regulating the water flow, it is possible to regulate the temperature-time history of the strip during cooling and produce steel products with desired mechanical and metallurgical properties.

The problem of controlled cooling of hot-rolled strip was a subject of research in many papers [7, 27, 49, 52, 71, 87, 92]. There are variety of methods used for the control approaches. A method of model predictive control for the temperature of the strip has been proposed by Hashimoto, Yoshioka, and Ohtsuka [27]. Wang et al. [87] presented the method to calculate convective heat transfer coefficient in the control system of finish cooling temperature combining traditional mathematical model with a Backpropagation neural network. Lezius and Tröltzsch [52] formulated the problem of the controlled cooling of steel profiles in cooling sections of hot rolling mill as a nonlinear optimal control problem. The numerical implementation for the simplified linear control problem was given there. An algorithm for the computation of optimal strategies for the cooling of steel strips in hot strip mills was also proposed by Landl et al. [49]. The authors considered the problem of determination of suitable cooling strategy as a discrete optimization problem and demonstrated the numerical results for the real hot rolling mill.

Most of the investigations of the controlled cooling in the hot strip mills are solely focused on the evaluation of the temperature. The direct control of the phase transformation on the run out table (ROT) presented in the literature is not very extensive. Neverthe-

less, the mathematical models that couple the thermal and metallurgical behaviour of the strip on the run out table, are widely presented in the engineering literature. The model which couples the temperature evolution and the phase transformations in steel occurring on the run out table, has been investigated, e.g., by Chen, Zou, and Fu [15], Serajzadeh [67], Sun et al. [72]. In the Nippon Steel technical report [71], the authors discussed the model for the phase transformations in high-carbon steel and its application to the online control on the hot strip mill.

In this chapter, the focus is on the optimal control of a cooling line for production of dual phase steel in a hot rolling process. The aim is to compute the optimal cooling strategy such that the desired dual phase microstructure is achieved most accurately. This problem will be formulated as an optimal control problem and solved numerically applying the optimization algorithms discussed in the previous chapter. The hot rolling process for the production of dual phase steel is introduced in Section 6.1. The modelling of the heat transfer in cooling line are considered in Section 6.2. Finally, Sections 6.3 and 6.4 are devoted to the set-up of the optimal control problem and its numerical realization.

6.1 Hot rolling of dual phase steels

Dual phase steel is one of the most important multiphase steels. It consists of a ferritic matrix containing a hard martensitic second phase in the form of islands (see Chapter 3). The soft phase of ferrite contributes to the good formability and the hard martensite to the strength of material. The hot-rolled DP steels are produced by controlled cooling from the austenite phase to transform some austenite to ferrite before a rapid cooling transforms the remaining austenite to martensite. It provides good microstructure homogeneity with an acceptable surface quality for many applications. The hot rolling process route for the production of DP steel is illustrated in Figure 6.1. It consists of 4 steps as shown in Figure 6.1:

(1) Rolling in roughing and finishing stands, which results in the refinement of austenite grain size due to the repeated static recrystallization.

(2) Laminar cooling into two phase region.

(3) Isothermal holding at ferrite transformation region temperatures, where the temperatures remain relatively constant.

(4) Finally, fast continuous cooling to the required coiling temperature, during which martensite transformation takes place and bainite transformation can be avoided.

The controlled cooling of stages (2)-(4) happens on the run out table. The biggest challenge in producing DP steel in this way is that the process window is very tight as only very short time of less than 10 s is allowed on the run out table according to its limited length. Hence, there is a strong demand for the online control of the process parameters such as the flow-rate of water in the cooling line (step 2 in Figure 6.1), the time and temperature on ROT (step 3) as well as the cooling rate during cooling down to coiling temperature (step 4).

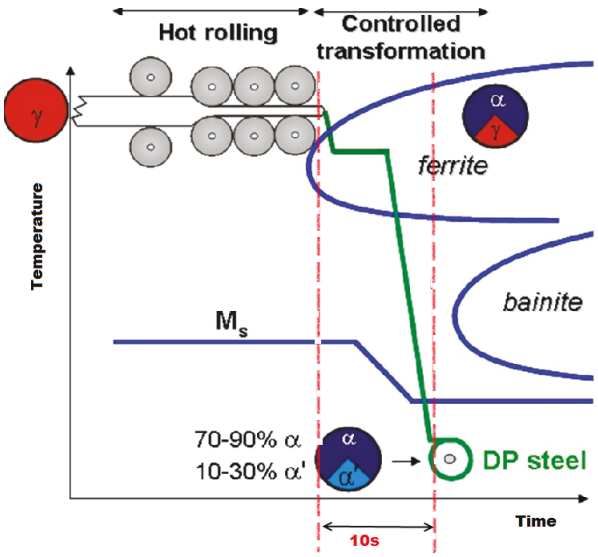

Figure 6.1: A sketch of the processing scheme for hot-rolled dual phase steel.

To simulate a real run out table, we consider the pilot hot rolling mill at the Institute of Metal Forming (IMF) at the TU Bergakademie Freiberg. A rough sketch of the rolling mill is presented in Figure 6.2.

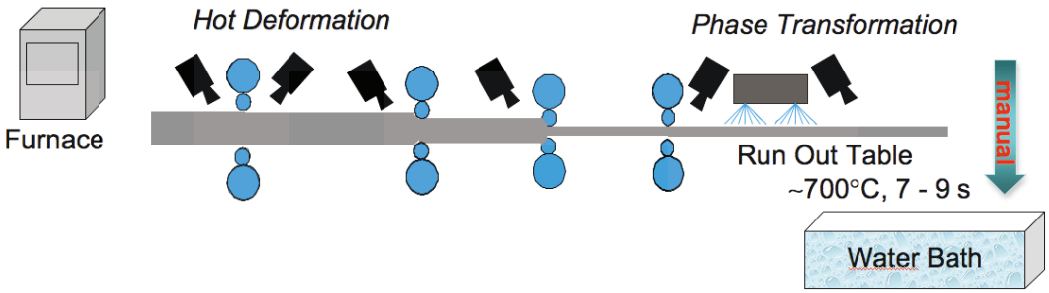

Figure 6.2: Pilot hot rolling mill at the IMF of the TU Bergakademie Freiberg, Germany.

A standard hot rolling experiment performed at the pilot rolling mill at the IMF started with an inductive heating of steel bars to the austenitization temperature, followed by the rolling in the roughing mill and three stand finishing line, where the thickness of the slab is reduced to the desired dimension. Then, the rolled strips are transported through the cooling line which consists of the four sections. Each section has a length of 160 cm. The cooling water only in the first cooling section is turned on. Therefore, the first section will be mentioned as cooling line, while the other three sections correspond to the ROT. After passing the ROT, the specimen is quenched by manually throwing it into a water bath, where the austenite-martensite transformation occurs.

In a joint project with mechanical engineers from the IMF at the TU Bergakademie Freiberg and the Department of Ferrous Metallurgy (abbreviated as IEHK) of the RWTH Aachen University, we have identified the process parameter for the pilot hot rolling mill at the IMF. Here, our focus is on the cooling line and ROT in order to control the phase transformation, i.e., the growth of ferrite and the temperature evolution in the steel slab.

6.2 Modelling of heat transfer in a cooling line

In this section, we discuss the modelling of heat transfer in the cooling line of the pilot hot rolling mill at the IMF of the TU Bergakademie Freiberg. In the hot rolling process, after the last deformation step the steel slabs are transported to the cooling segment, where the laminar water spray cooling takes place on the top and bottom of the slab. Figure 6.3 shows the cooling line of the pilot plant at the IMF with a schematic representation of water jets in the cooling segment. The cooling segment has a length of 160 cm and is equipped with 12 flat jet water nozzles produced by the company *Lechler*.

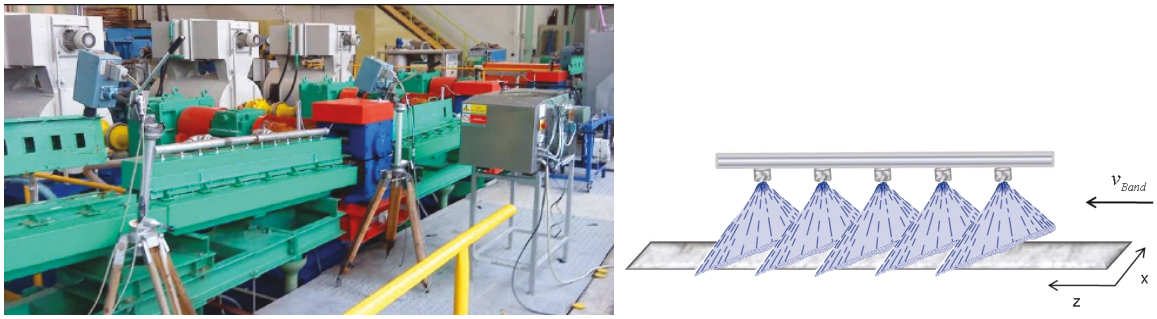

Figure 6.3: Furnace and cooling segment, rolling direction form right to left (left) and schematic representation of the cooling segment with flat jet nozzles (right) at the IMF of the TU Bergakademie Freiberg.

In order to arrive at a reasonably simple mathematical model for the heat transfer in the cooling line, we neglect heat conduction in the feeding direction of the specimen. This reduces the spatial dimension of the model and thus the computational complexity. We consider a cross section of a steel slab moving with the predefined strip speed v through the cooling segment as it presented in Figure 6.4.

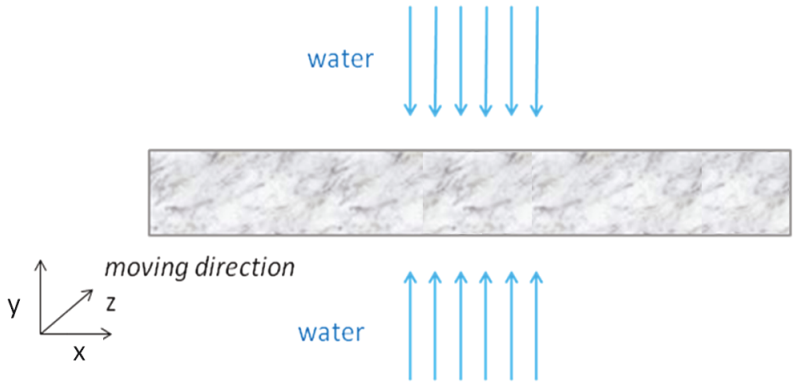

Figure 6.4: Schematic representation of the cross section of the steel slab during the water spray cooling.

Here, x and y define space coordinates in the direction of the width and thickness of the strip, respectively. The space coordinate in direction of the length of the cooling line is denoted by z. The velocity of the strip remains constant throughout the duration of

the process. The governing equation for the temperature distribution $\theta(x, y, t)$ in the 2D cross section of the steel slab during cooling is given by

$$\rho c_p \theta_t - \kappa \Delta\theta = \rho L f_t \qquad \text{in } Q = \Omega \times (0, T), \tag{6.1a}$$

$$-\kappa \frac{\partial \theta}{\partial n} = u(t)\beta(x)(\theta - \theta_w) \qquad \text{on } \Sigma_1 = \Gamma_1 \times (0, T), \tag{6.1b}$$

$$-\kappa \frac{\partial \theta}{\partial n} = 0 \qquad \text{on } \Sigma_2 = (\partial\Omega \setminus \Gamma_1) \times (0, T), \tag{6.1c}$$

$$\theta(0) = \theta_0 \qquad \text{in } \Omega. \tag{6.1d}$$

Here, Ω denotes the rectangular cross section of the steel slab, and Γ_1 corresponds to the upper and lower boundaries of the domain Ω. The end-time T is calculated as a sum of the time in cooling segment and holding time on ROT after the cooling. The term on the right-hand side of (6.1a) represents the latent heat of the austenite-ferrite phase transformation, described by initial value problem (3.3) in Chapter 3. The density ρ, the heat capacity c_p, the heat conductivity κ and the latent heat L from the austenite-ferrite phase transformation are given as

$$\rho = 7.85\,\mathrm{g/cm^3},\ \kappa = 0.5\,\mathrm{J/(s\,cm\,K)},\ c_p = 0.5\,\mathrm{J/(g\,K)},\ L = 77\,\mathrm{J/g}.$$

The heat transfer on the upper and lower boundary of the sample is described by the Newton's cooling law in the boundary condition (6.1b), where θ_w is the temperature of the coolant water, the function β a water distribution over the surface of the steel slab in direction x. The function u denotes a time-dependent heat transfer coefficient. According to the special nozzle geometry described in Lechler documentation, the water profile function β can be roughly approximated by the Gaussian function whose general form is

$$\beta(x) = ae^{-\frac{(x-b)^2}{2c^2}} + d,$$

where a, b, c and d are real constants.

In particular, as was investigated by the mechanical engineers at the IMF in a series of cooling experiments at pilot plant, the water distribution over the surface of the steel slab in direction x can be assumed as a constant, i.e., $\beta \equiv const$.

A common approach for the modelling of the heat transfer coefficient is to use various functions whose parameters are to be determined through the fitting to the experimental data. The influence factors on the heat transfer coefficient by the water spray cooling, such as the surface temperature, water impact density and strip velocity, have been investigated thoroughly in many studies (see, e.g., Puschmann [61], Sun et al. [72] and Viščorová [85]). At the higher temperatures, above approximately 600 °C, it is well established that the heat transfer coefficient becomes less temperature dependent.

To describe the heat transfer coefficient, the model proposed by Sun et al. [72] is applied:

$$u(t) = \zeta(z_0 + vt) \left(\frac{v}{v_0}\right)^{\lambda} \left(\frac{w(t)}{w_0}\right)^{\gamma}, \tag{6.2}$$

where v is a strip velocity, $w(t)$ is a flow-rate of water and v_0, w_0 are the reference strip velocity and flow-rate of water, respectively. The constants λ, γ define the effect of the strip velocity and the flow-rate of water on the heat transfer coefficient. These factors can

be determined by solving an inverse problem from the measurements of the temperature during the water spray cooling. To this purpose, a series of experiments at the hot rolling mill at the IMF have been carried out.

The heat transfer coefficients as a function of time were identified from the temperature measurements in 9 experiments for the strip speeds of 0.85 m/s, 1 m/s, 2 m/s and different flow-rates of water in cooling line, namely, 100 l/min, 200 l/min, 300 l/min, 400 l/min. The results of the identification process are shown in Figure 6.5.

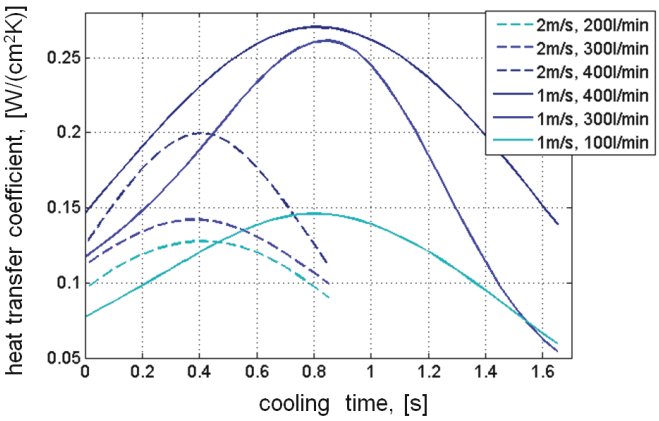

Figure 6.5: Calculated heat transfer coefficients as a function of time for the experiments with strip speed of 1 m/s and 2 m/s. The flow-rate of water varies from 100 l/min to 400 l/min.

Using the information about the strip velocity v in each experiment and the fact, that $z = vt$, the heat transfer coefficients can be represented as a function of z , i.e. the space coordinate along the cooling line (see Figure 6.6).

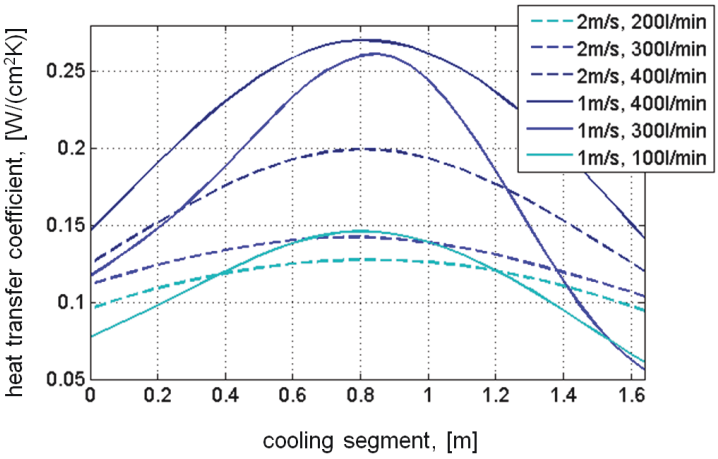

Figure 6.6: Heat transfer coefficients as a function of the space coordinate along the cooling line.

It can be realized by observing Figures 6.5 and 6.6 that the lower the strip speed, the higher the values of the heat transfer coefficients. Moreover, the maximum values of the

heat transfer coefficients are directly proportional to the flow-rate of water in cooling line. It also can be seen from Figure 6.6 that the heat transfer coefficients can be represented by the Gaussian function. The optimal values for λ, γ in (6.2) fitted to the curves of heat transfer coefficients are the following:

$$\lambda = -0.63,\ \gamma = 0.45.$$

At the end, we obtain a model for the heat transfer coefficient dependent on the process parameters like strip velocity v and the flow-rate of water $w(t)$ in cooling line:

$$u(t) = e^{-(1.48-0.28v^2)(t\cdot v-0.8)^2} \left(\frac{v}{0.05}\right)^{-0.63} \left(\frac{w(t)}{100}\right)^{0.45} \tag{6.3}$$

More details about the identification of the heat transfer coefficients from the measurements of temperature at IMF can be found in [24].

After the model for the heat transfer in the cooling line has been established, we are able to formulate the optimal control problem for the production of dual phase steel.

6.3 Optimal control problem for dual phase steel

We will now set up an optimal control problem for the cooling line to produce a desired dual phase microstructure. Our aim is to compute an optimal flow-rate of water for the cooling line to achieve a desired distribution of ferrite f_d in the steel slab at the end time T. At the same time, we want to realize a desired end temperature θ_d. This will be done in a two-stage approach. Firstly, we solve an optimal control problem to obtain an optimal time-dependent heat transfer coefficient $u(t)$ as it was discussed in the previous chapter. Then, we use equation (6.3) to compute the corresponding optimal flow-rate of water $w(t)$, which serves as the control quantity at the pilot mill. For this purpose, we consider an optimal boundary control problem (P), which was analyzed in previous chapter: *minimize*

$$J(\theta, f, u) = \frac{\alpha_1}{2} \int_\Omega (f(x,T) - f_d(x))^2\, dx + \frac{\alpha_2}{2} \int_\Omega (\theta(x,T) - \theta_d(x))^2\, dx + \frac{\alpha_3}{2} \int_0^T u^2 dt$$

subject to

$$\begin{aligned}
f_t &= (f_{eq}(\theta) - f)\mathcal{H}(f_{eq}(\theta) - f) g_1(\theta) g_2(D_\gamma, \varepsilon) && \text{in } Q, && (6.4a)\\
f(0) &= 0 && \text{in } \Omega, && (6.4b)\\
\rho c_p \theta_t - \kappa \Delta\theta &= \rho L f_t && \text{in } Q, && (6.4c)\\
-\kappa \frac{\partial \theta}{\partial n} &= u(t)\beta(x)(\theta - \theta_w) && \text{on } \Sigma_1, && (6.4d)\\
-\kappa \frac{\partial \theta}{\partial n} &= 0 && \text{on } \Sigma_2, && (6.4e)\\
\theta(0) &= \theta_0 && \text{in } \Omega, && (6.4f)
\end{aligned}$$

and

$$u \in U_{ad} = \{u \in L^\infty(0,T) : u_a \leq u \leq u_b,\ u_a, u_b \geq 0\},$$

where α_i, $i = 1, \ldots, 3$ are positive constants, $Q = \Omega \times (0,T)$, $\Sigma_1 = \Gamma_1 \times (0,T)$, $\Sigma_2 = (\partial\Omega \setminus \Gamma_1) \times (0,T)$. Here again, the third term in the cost functional represents the Tikhonov regularization term that can also be interpreted as an indicator for the costs of the control. The control is bounded by two positive constants u_a and u_b since we consider only cooling process and because of the restrictions on the maximal amount of coolant. The ordinary differential equation (6.4a) with initial condition (6.4b) represents the model for the kinetics of ferrite transformation, which was derived in Chapter 3, Section 3.2.1.

In the next section we present the numerical solution of the control problem formulated above for the hot rolling of Mo-Mn dual phase steel.

6.4 Numerical results

We will consider two problems. In the first, denoted by (P_1), the aim is to calculate an optimal heat transfer coefficient for the water spray cooling such that, at the end of the cooling line, the desired microstructure of the steel slab is realized. The second problem (P_2) is formulated according to the experimental set-up on the ROT of pilot hot rolling mill at the IMF of the TU Bergakademie Freiberg. Here we consider two steps of the entire process: water spray cooling into a ferrite transformation region and subsequent isothermal holding on the ROT. These results were validated in the hot rolling experiments and already discussed in the recent paper [9].

In order to solve the control problems (P_1) and (P_2) numerically, we apply the rSQP method with active-set strategy discussed in Chapter 5. As mentioned before, for a globalization of the rSQP method, we use a gradient projection algorithm introduced in Section 5.2.1 of Chapter 5. We also note that the physical parameters necessary for the numerical computations in this section are taken from Section 4.5.2.

6.4.1 Control problem (P_1)

Let us choose a two-dimensional domain $\Omega = (0, 7.5) \times (0, 0.69)\,\mathrm{cm}^2$. This corresponds to the vertical cross section of the steel slab moving through the cooling segment with a fixed strip speed.

The aim is to compute the optimal cooling strategy for the DP steel with a desired ferrite fraction $f_d(x) = 85\,\%$ and a temperature $\theta_d(x) = 660\,^\circ\mathrm{C}$ at the final time $T = 7\,\mathrm{s}$. The cooling strategy is obtained by solving the optimal control problem (P). In the model for ferrite growth, $\mathcal{H}$ is chosen as the following monotone approximation of the Heaviside function

$$\mathcal{H}(x) = \begin{cases} 1, & \text{for } x \geq \delta, \\ 10(\frac{x}{\delta})^6 - 24(\frac{x}{\delta})^5 + 15(\frac{x}{\delta})^4, & \text{for } \delta > x \geq 0, \\ 0, & \text{for } x < 0. \end{cases}$$

with $\delta = 0.01$.

The factor representing the effect of austenite conditioning and deformation is given by $g_2 = 10$. The initial condition for the temperature is $\theta_0 = 860\,^\circ\mathrm{C}$ and $\theta_w = 20\,^\circ\mathrm{C}$. The

bounds for the control are taken as $u_a = 0$ and $u_b = 0.3$. The water profile in the cooling segment is given by

$$\beta(x) = e^{-0.01(x-3.75)^2}$$

as depicted in Figure 6.7.

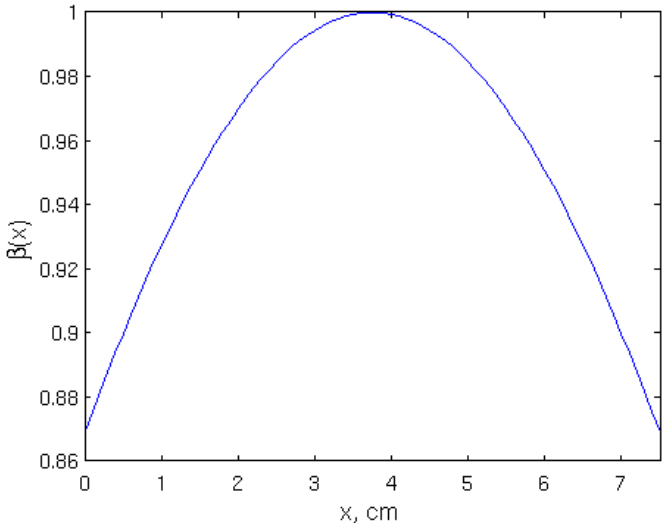

Figure 6.7: The water profile $\beta(x)$.

It should be mentioned that the choice of weighting factors $\alpha_1, \alpha_2, \alpha_3$ in the cost functional of optimal control problem (P) is of crucial importance for the numerical computations. The volume phase fraction f takes values in $[0, 1]$, while the temperature θ is in the range of 20 °C–1200 °C. Therefore, in order to obtain useful results, an equilibrating of these two terms in cost functional is necessary. In the subsequent computations, we set $\alpha_1 = 1$ and $\alpha_2 = 5 \cdot 10^{-6}$. The factor α_3 is a Tikhonov regularization parameter and is chosen as 0.1.

The finite element triangulation for the computational domain Ω is done by a uniform mesh with $N = 561$ degrees of freedom. For the time step, we take $\Delta t = 0.0125$. We approximate the control function u with piecewise constant functions on the time grid.

As explained above, we use the gradient projection method for the globalization of the rSQP algorithm. As an initial guess for the gradient projection method we take $u^0 \equiv 0$. The algorithm was terminated after 7 iterations, provided the relative error $\|u^{k+1} - u^k\|_{L^2(0,T)}/\|u^k\|_{L^2(0,T)}$ is smaller than $tol = 0.01$. The obtained control function, which is denoted by $\hat{u}$, and corresponding state variables $\hat{\theta}$ and $\hat{f}$ with adjoint variables $\hat{p}, \hat{q}$ serve as the initial iteration of the rSQP method.

Table 6.1 shows the convergence history of the rSQP steps. It contains the value of the objective function J_k, the relative error τ_k that was used for the termination criterion

$$\tau_k = \frac{1}{5}\Big(\frac{\| u^{k+1} - u^k \|_{L^2(0,T)}}{\| u^k \|_{L^2(0,T)}} + \frac{\| \theta^{k+1} - \theta^k \|_{L^2(Q)}}{\| \theta^k \|_{L^2(Q)}} + \frac{\| f^{k+1} - f^k \|_{L^2(Q)}}{\| f^k \|_{L^2(Q)}} + \frac{\| p^{k+1} - p^k \|_{L^2(Q)}}{\| p^k \|_{L^2(Q)}} + \frac{\| q^{k+1} - q^k \|_{L^2(Q)}}{\| q^k \|_{L^2(Q)}}\Big) < tol$$

and the number of PDAS-Loops in k iterations of rSQP method. As expected, the rSQP method converges in a few steps to the optimal solution with $tol = 10^{-3}$ in termination condition.

Iter	J_k	τ_k	# PDAS-Loops
1	0.01669	0.1350	8
2	0.01438	0.01077	4
3	0.01434	$6 \cdot 10^{-4}$	2

Table 6.1: Value of objective function J_k, relative error τ_k and number of PDAS loops in k^{th}-iteration of rSQP method.

In Figure 6.8, some iterations of the gradient projection algorithm and rSQP method are represented.

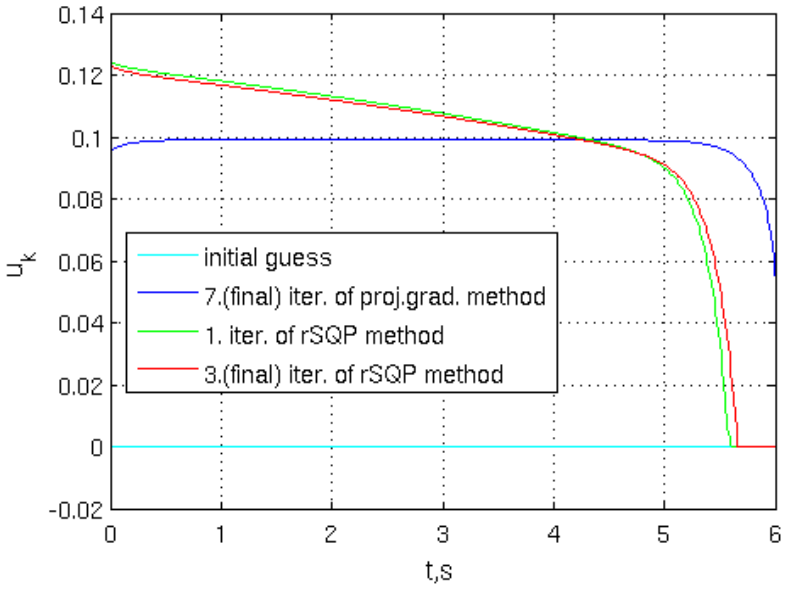

Figure 6.8: Some iterations of optimization procedure.

The optimal control u is depicted in Figure 6.9. Closer to the end of the time interval, the optimal control decreases to zero, which is the lower bound of the control. This fact also reflects the presence of the box constraints and the functioning of the active set method.

Figure 6.10 shows the simulated final temperature (left) and the phase distribution (right) in the cross section of the steel slab in selected iterations of the optimization procedure. At each iteration of the rSQP method, the temperature distribution in the steel slab becomes more homogeneous and closer to the desired value $\theta_d = 660\,°\text{C}$. On the other hand, the maximal difference of the ferrite values at the final time is about of 17 %. However, at each iteration of the rSQP method, the ferrite phase fraction in the largest part of the cross section is close to 85 %.

We additionally plot the temperature and ferrite growth during the cooling in the middle of the cross section of the steel slab. The simulation results are shown in Figure 6.11.

The desired temperature of 660 °C and ferrite fraction of 85 % are reached very accurately in the middle of the cross section.

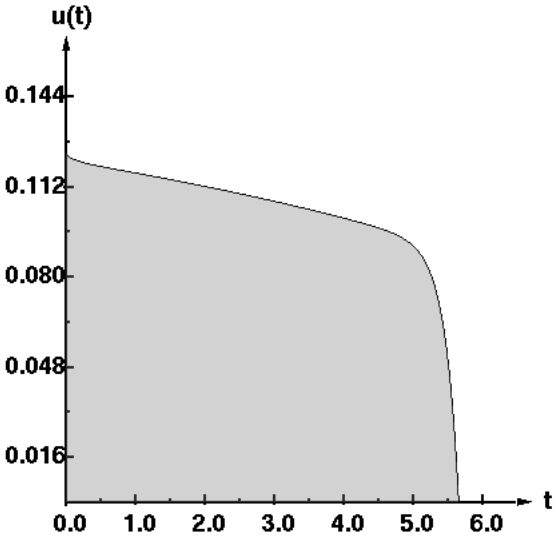

Figure 6.9: Optimal control $u(t)$.

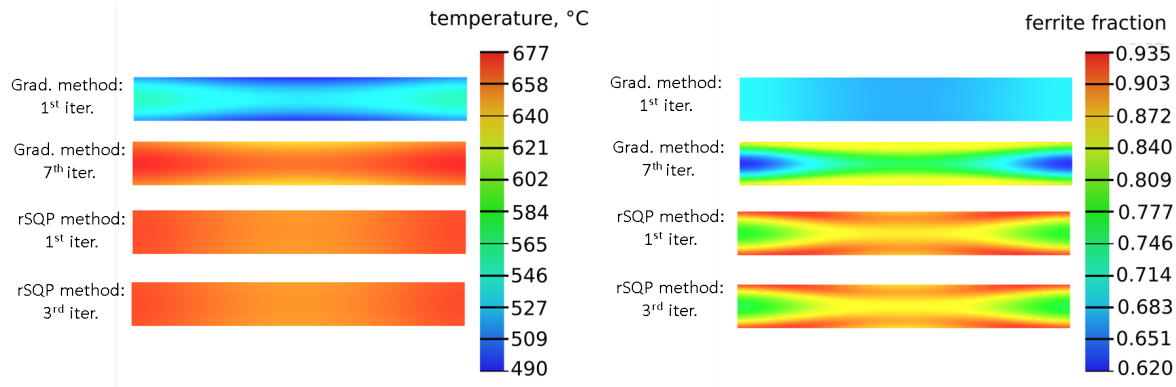

Figure 6.10: The simulated final temperature (left) and phase distribution (right) in the cross section of the steel slab in certain number of iterations of the optimization procedure. In both pictures the 1^{st} and 7^{th}(final) iteration of the gradient projection method, and 1^{st} and 3^{rd}(final) iterations of the rSQP method are depicted in order from top to bottom.

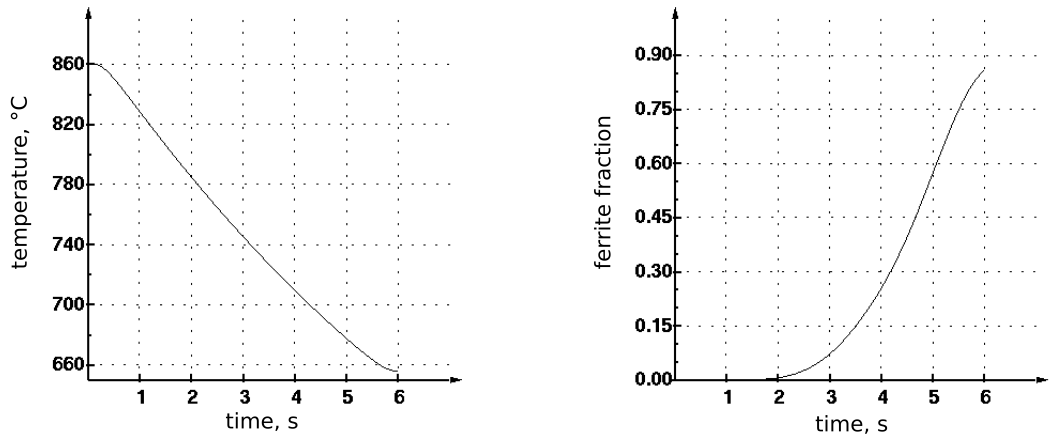

Figure 6.11: The simulated temperature (left) and ferrite fraction evolution (right) in the middle of the cross section of the steel slab.

In order to highlight the influence of the weighting factors α_1, α_2 in the cost functional on the numerical solution of the optimal control problem, we solve the problem again with the same parameter set as before, except for the values of the weighting factors. Let α_1, α_3 remain the same, and let α_2 be reduced by a factor of 10, i.e., $\alpha_1 = 1$, $\alpha_2 = 5 \cdot 10^{-7}$ and $\alpha_3 = 0.1$. In other words, the target condition for the temperature will be weakened in the cost functional. As an initial guess for the optimization procedure, $u^0 \equiv 0$ was taken. After 7 iterations of the gradient projection method and subsequent 3 steps of the rSQP method, the algorithm was terminated with relative error $\tau_k = 9.24 \cdot 10^{-5}$. The cost functional takes the value of 0.01637 in the third iteration.

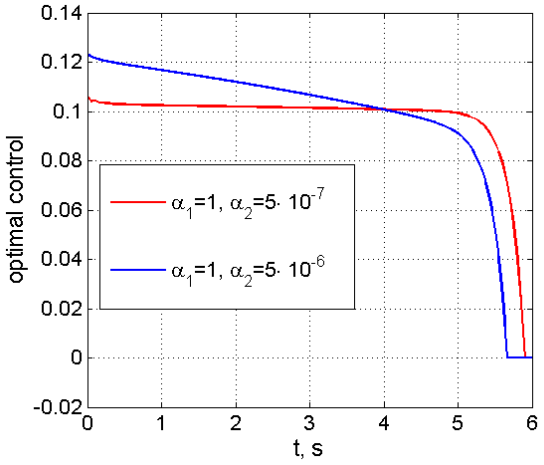

Figure 6.12: The comparison of the optimal solutions of two control problems with different values of weighting factors: 1) $\alpha_1 = 1, \alpha_2 = 5 \cdot 10^{-6}, \alpha_3 = 0.1$ and 2) $\alpha_1 = 1, \alpha_2 = 5 \cdot 10^{-7}, \alpha_3 = 0.1$.

Figure 6.12 shows a comparison of the optimal control functions of two control problems with different values for the weighting factors. It can be seen from Figure 6.12 that

the time interval in which the control is switched off at the end of the cooling is different. In comparison to the red curve, which corresponds to the control problem with a decreased weight of the temperature in the cost functional, the blue one has a longer time interval where the control is equal to zero.

The corresponding temperature and phase distribution in the cross section of the steel slab are depicted in Figure 6.13. From the left figure, we can observe that the temperature distribution is more homogeneous in the first case. The same phenomenon can be seen for the phase distribution, as the phase kinetic strongly depends on the temperature. Moreover, the desired end temperature is reached more accurately in the first case, where the factor $\alpha_2 = 5 \cdot 10^{-6}$ (which corresponds to the temperature) is greater as in the second case with $\alpha_2 = 5 \cdot 10^{-7}$. These observations demonstrate the influence of weighting factors in the cost functional on the results of optimization procedure.

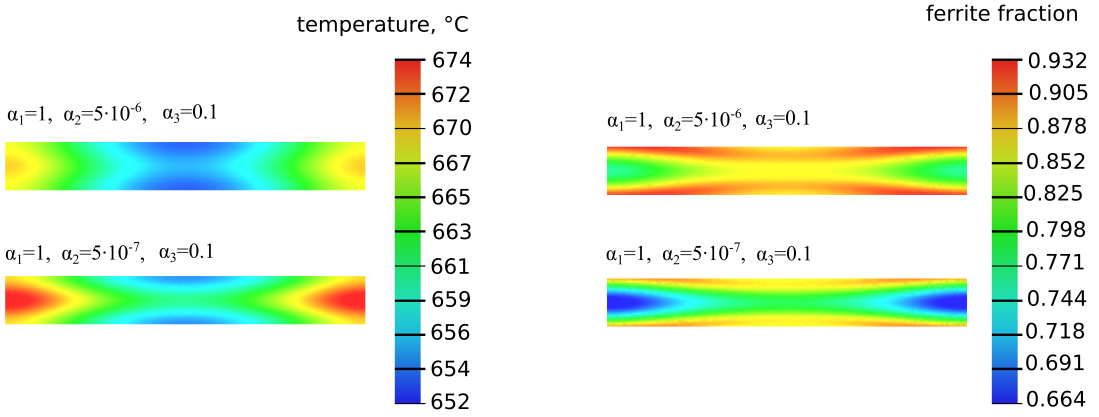

Figure 6.13: The comparison of the optimal final temperature and phase distribution in the cross section of the steel slab for two cases: 1) $\alpha_1 = 1$, $\alpha_2 = 5 \cdot 10^{-6}$, $\alpha_3 = 0.1$ and 2) $\alpha_1 = 1$, $\alpha_2 = 5 \cdot 10^{-7}$, $\alpha_3 = 0.1$.

6.4.2 Control problem (P_2)

Let us consider an optimal control problem for production of dual phase steel at the pilot hot rolling mill at the IMF of the TU Bergakademie Freiberg. In order to follow up the hot rolling process described in Section 6.1 as precisely as possible, some modification have to be made to the optimal control problem (P). As previously stated, we focus on a two-stage process route which is depicted in Figure 6.14: The first step is the controlled cooling into a ferrite transformation region; the second step is the subsequent isothermal holding on the ROT.

The isothermal holding at ferrite transformation region temperatures is approximately realized by keeping the steel sheets on the ROT for 7 s–10 s, where a natural convection and radiation are entering into force. In contrast to the control problem (P_1) from the previous subsection, the isotherm holding in ferrite region is taken into account. Thus, the time interval $[0, T]$ is split into two subintervals: $[0, t_{\text{cool}}]$ for the continuous water

spray cooling and $(t_{\text{cool}}, T]$ for the isotherm holding on the ROT. The boundary condition for the heat equation (5.2d) must then be modified as follows

$$-\kappa \frac{\partial \theta}{\partial n} = u(t)(\chi_{\text{cool}} + \chi_{\text{hold}})\beta(x)(\theta - \theta_w) \quad \text{on } \Sigma_1 = \Gamma_1 \times (0, T),$$

where

$$\chi_{\text{cool}} = \begin{cases} 1, & 0 \le t \le t_{\text{cool}}, \\ 0, & t_{\text{cool}} < t \le T, \end{cases} \qquad \text{and} \qquad \chi_{\text{hold}} = \begin{cases} 0, & 0 \le t \le t_{\text{cool}}, \\ 0.005, & t_{\text{cool}} < t \le T. \end{cases}$$

The indicator function χ_{cool} turns off the control function u on the time interval $(t_{\text{cool}}, T]$. In its turn, the function χ_{hold} serves for the roughly approximation of the isothermal holding of the steel slab on ROT.

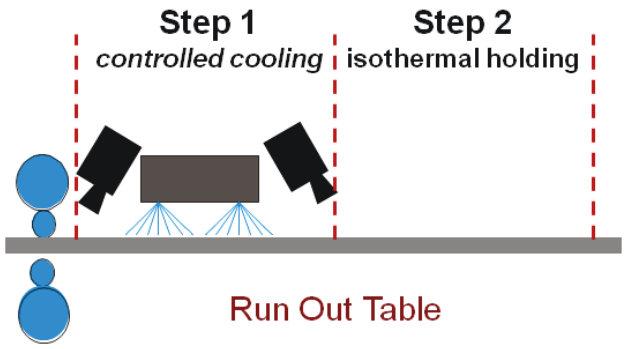

Figure 6.14: Run out table of the pilot hot rolling mill at the IMF. Two-stage process route.

In the control problem (P_2), we consider a thin steel plate, which comes from the last rolling mill with a thickness of 0.2 cm. Let the two-dimensional domain Ω be $(0, 7.5) \times (0, 0.2)\,\text{cm}^2$. As for the previous example, the aim is to compute the optimal cooling strategy for a DP steel with a desired ferrite fraction $f_d(x) = 90\,\%$ and a temperature $\theta_d(x) = 680\,^\circ\text{C}$ at the final time $T = 12\,\text{s}$. The strip velocity in the cooling line is fixed by $v = 0.85\,\text{m/s}$. Thus, the time in the cooling segment has been calculated as 2 s. The phase equation for the ferrite growth as well as the values θ_0 and θ_w in the heat equation remain the same as in control problem (P_1).

The spatial domain Ω is discretized with triangular finite elements whose maximal edge length h is equal to 0.05. The time interval $[0, 12]$ is discretized uniformly with step size $\Delta t = 0.0125$. For the globalization of the rSQP algorithm, we use again the gradient projection method. As an initial guess for this method, we take $u^0 \equiv 0$. After 10 iterations, the gradient projection method provides the initial iteration for the rSQP algorithm. Table 6.2 shows the convergence history of the rSQP steps. Only 3 iterations are needed to get the optimal solution.

The optimal control function $\bar{u}$ is depicted in Figure 6.15. This function represents the time dependent heat transfer coefficient and is nearly constant during the first 2 s in the cooling line.

Figure 6.16 shows the evolution of the temperature and ferrite fraction in the middle of the steel cross section. It can be seen, that the sample has been cooled down to the

temperature of 680 °C in the cooling line during the first 2 seconds. Then, we observe an increase in the temperature for the short time interval after water spray cooling is switched off and $u = 0.005$. This effect can be explained by the fact that the latent heat becomes free during the phase transformation. For the rest of the time interval, the temperature has a decreasing behaviour due to the natural convection and radiation. The austenite-ferrite phase transformation starts after 1 s of the cooling process at the temperature of 760 °C. At the end time $T = 12$ s, the ferrite volume fraction reaches the value of 91 %, which approximates the desired value 90 % quite precisely.

Iter	J_k	τ_k	# PDAS-Loops
1	0.0010592	0.225716	2
2	0.0010213	0.009207	2
3	0.0010212	$2.7 \cdot 10^{-4}$	2

Table 6.2: Value of the objective function J_k, relative error τ_k and number of PDAS loops in k^{th}-iteration of the rSQP method.

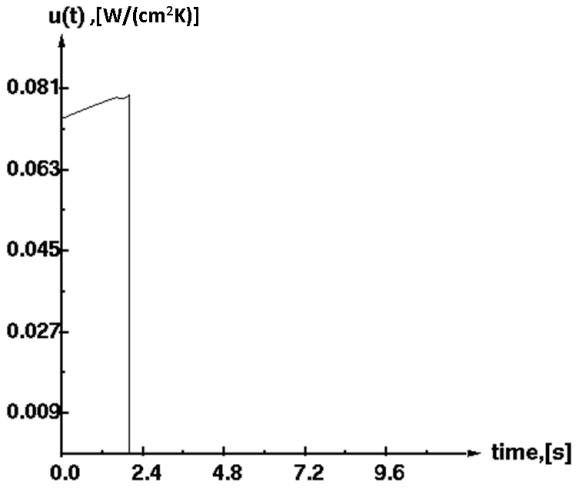

Figure 6.15: Optimal control u.

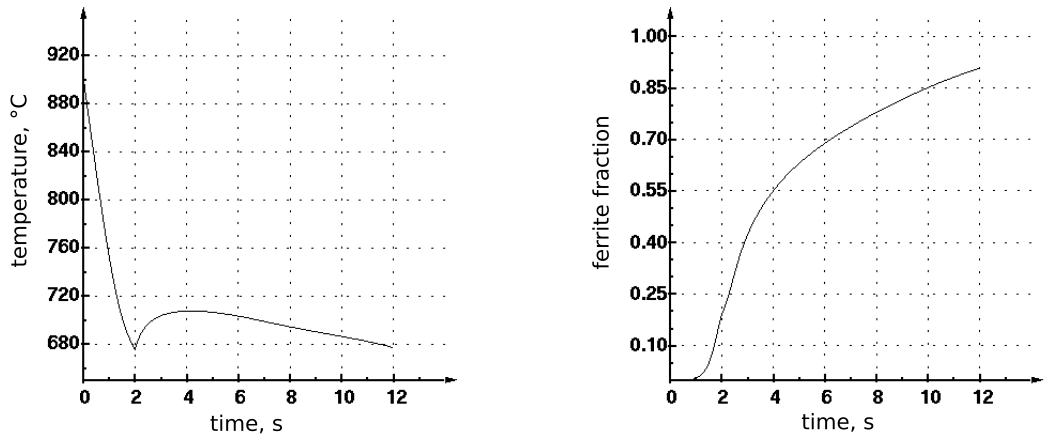

Figure 6.16: The optimal temperature (left) and phase evolution (right) simulated in the middle of the steel cross section.

Experimental validation

To validate our approach, experiments have been carried out at the IMF. Here, the defining control parameter is the flow-rate of cooling water w, which is related to the heat transfer coefficient u via (6.3). We recall that the strip speed $v = 0.85\,\mathrm{m/s}$ is fixed during the cooling. After the optimal control u has been determined, the flow-rate of water w can be recalculated from equation (6.3) with a fixed strip speed v as follows

$$w(t) = 100u(t)^2 e^{2(1.48-0.28v^2)(tv-0.8)^2} \left(\frac{v}{0.05}\right)^{1.4}. \tag{6.5}$$

Figure 6.17 depicts the resulting optimal flow-rate of water. Due to the construction of the cooling line at the IMF only a constant value of the flow-rate can be adjusted. Thus, we derived the average amount of water

$$\bar{w}(t) = \frac{1}{t_{\mathrm{cool}}} \int_0^{t_{\mathrm{cool}}} w(t)dt = 70\,\mathrm{l/min}.$$

This quantity can be prescribed in the cooling line. This is of course only an average of the optimal solution. Since the state system is nonlinear, the simulation result for this quantity fed back into the state equation will differ from the optimal one as computed before. Indeed, Figure 6.18 shows a resulting end temperature of 617 °C and a ferrite fraction of 82.7 %, respectively. These values differ from the computed ones in optimization procedure, however, a ferrite fraction of this order is satisfactory for dual phase steel.

Further, we compare the numerical results with the experimental ones. To this end, the samples have been investigated at the IEHK Aachen in terms of phase fractions by means of light optical metallography. Here, the microsections of the processed sample have been analyzed using automatic picture analysis system based on black-white contrast.

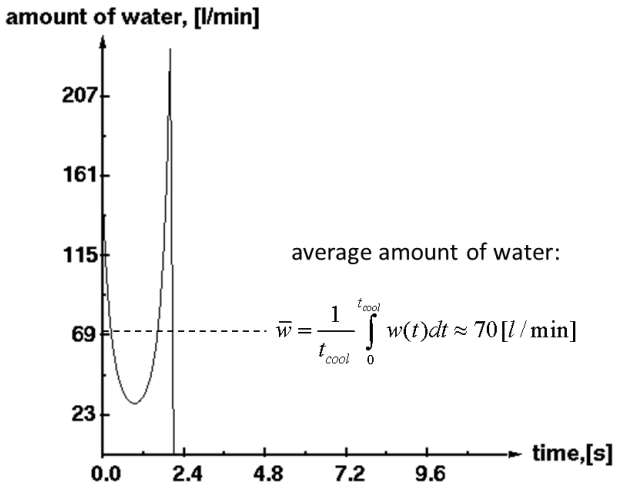

Figure 6.17: Optimal flow-rate of water in the cooling line calculated from the optimal heat transfer coefficient u.

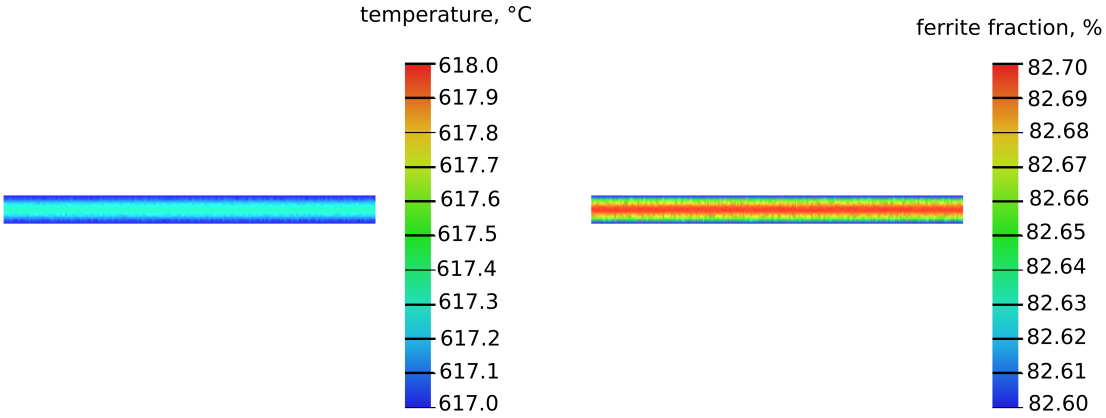

Figure 6.18: The simulated final temperature and ferrite fraction in the cross section of the slab.

Figure 6.19 shows a microsection of the sample for the Mo-Mn DP steel and the final ferrite distribution in the cross section. The quantitative analysis yields a ferrite fraction of 87 % and 13 % martensite. Hence, the difference between the experimentally achieved ferrite fraction and the numerically predicted one of 82.7 % is of order 5 % which, in view of many uncertainties in the semi-manual process guidance at the pilot plant, is a very satisfactory result.

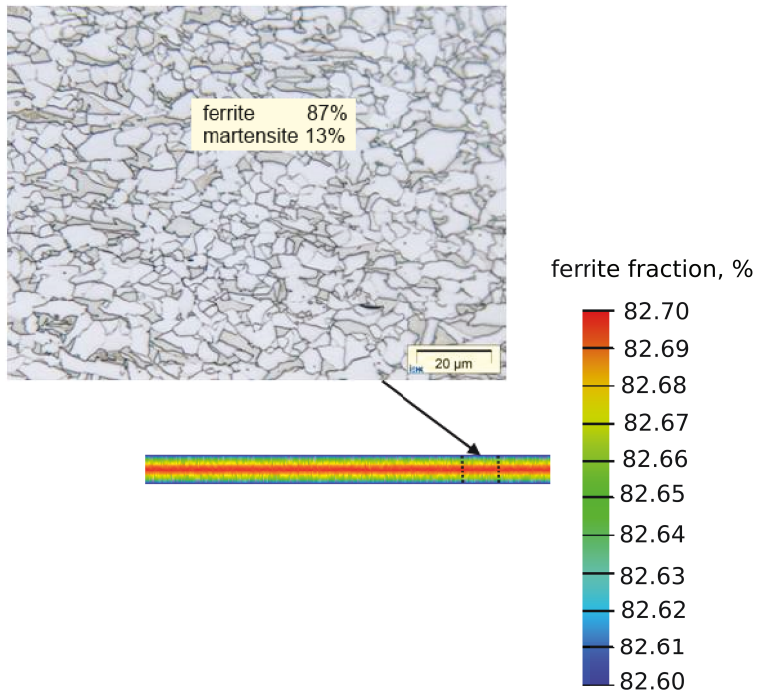

Figure 6.19: Microsection of the sample for the Mo-Mn steel and the final phase distribution in the cross section of the slab.

Chapter 7

Conclusions

In this thesis, we have considered several mathematical problems related to the production of multiphase steels. The main focus was on the phase transformations in multiphase steels since the microstructure of the final product strongly depends on the phase mixture in steel.

For hot-rolled dual phase steel, a model for the austenite-ferrite and austenite-martensite phase transformations which occur during controlled cooling on the run out table has been derived. In this model, the factors that accelerate the growth of ferrite were taken into account, namely, retained strain from the last finishing stand and austenite grain size before cooling line. The derived model could be used for the simulations of ferrite and martensite growth on the run out table of the hot rolling mill. Particularly, the model allowed us to predict the preferable degree of retained strain and the holding temperature on the run out table for the required ferrite fraction.

One of the problems investigated in this work was an inverse problem for identifying the kinetics of the phase transformations from the dilatometer measurements. The mathematical analysis of the inverse problem has shown that in the case of at most two product phases, the complete transformation kinetics of these phases should be uniquely determined by the two dilatometer measurements of length change and temperature evolution at a single point on the specimen surface.

The parameter identification problem for the phase transformations in Mo-Mn dual phase steel was solved numerically using the Matlab Optimization Toolbox. In the optimization process, the phase fraction functions to be determined were represented as cubic splines. The numerical results presented for the fast-cooling curve are in good agreement with the experimental data, with a relative error of less than 8 %. The results of the parameter identification have clearly demonstrated that the dilatometer data contain plenty of information in addition to the start and end temperatures of the related phase transformations. In other words, the complete kinetics of the phase transformations can be identified from the dilatometer curve. Moreover, the parameter identification procedure provides a good alternative to the expensive and time-consuming metallographic investigations.

The other problem concerned the optimal control of the cooling line in the hot rolling mill in order to produce the desired dual phase microstructure. We have carried out the mathematical analysis of the optimal control problem, formulated for this application. It is the boundary optimal control problem governed by the semilinear parabolic system, where

the heat transfer coefficient serves as a control function. We have proven the existence of the optimal solution and derived necessary and sufficient optimality conditions, which are the basis for the efficient application of second-order numerical algorithms such as the SQP method. In order to solve the control problem numerically, we applied the reduced SQP method with a primal-dual active set strategy. The numerical optimization algorithm was implemented using the finite element/finite volume toolbox WIAS-pdelib. The advantage of the discussed optimal control problem for the cooling line of the hot rolling mill is that the phase transformations are taken into account and the final phase distribution in steel can be optimized.

In order to validate our optimal control approach, we have considered an optimal control problem for the production of Mo-Mn dual phase steel related to the real process route on the pilot hot rolling mill at the Institute for Metal Forming of the TU Bergakademie Freiberg. For that purpose, it was necessary to investigate the heat transfer during the water spray cooling at the pilot hot rolling mill. The plant-specific heat transfer coefficient has been identified from the temperature measurements by solving an inverse problem. The control quantity at the pilot mill at the IMF of the TU Bergakademie Freiberg, the flow-rate of water, was computed by solving the control problem numerically. The numerical results have been compared with experimental data. This comparison has shown that the proposed optimal control approach could be used for the offline-controlled cooling on the run out tables of hot rolling mills.

Future research

Naturally, there remain open problems and challenging directions of future research.

One interesting direction of research on the production of hot-rolled multiphase steels is the modelling of bainitic phase transformation. This is particularly relevant for the hot rolling of TRIP steels. In this case, the model for the phase transformations on the run out table has to be complemented with an additional equation for the growth of bainite. From a materials science perspective, it is important to account for the carbon enrichment in the remaining austenite before the bainitic transformation. For the production of TRIP steels, a second isothermal holding step or a controlled cooling strategy for the formation of bainite has to be implemented in the run out table processing strategy (see Figure 7.1 below). This research direction requires further close cooperation with engineering institutes.

Concerning the evaluation of dilatometer experiments, there are also some open questions. We have considered the identification of the phase transformations derived from the dilatometer experiments with fast and moderate cooling. In the case of slow cooling, further investigations are still needed. To decelerate the cooling in dilatometer experiments, the specimens are heated by electromagnetic induction, and the electric power is measured for each cooling curve. The induction heating complicates the identification of phase transformations from dilatometer measurements of the temperature, since the information about latent heats will be lost in this case. For the parameter identification, the effect of electromagnetic induction has to be taken into account by possibly including an additional source term on the right-hand side of the energy balance equation. A precise model of this effect requires further study.

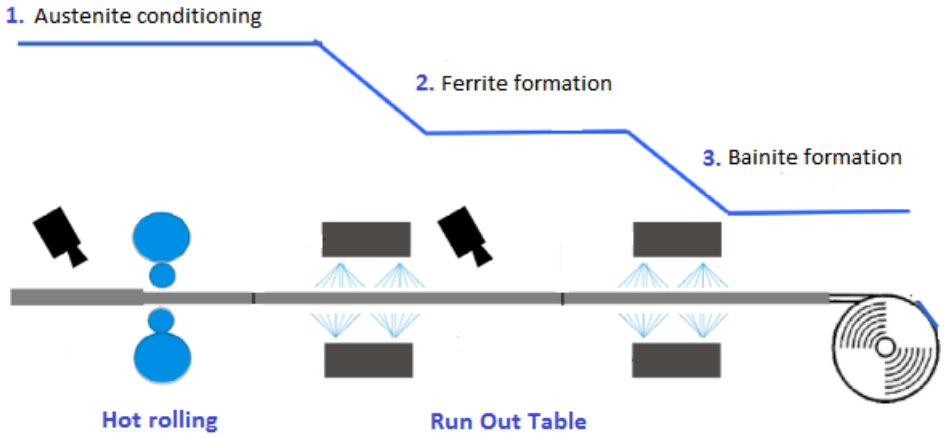

Figure 7.1: Three steps of a production route for TRIP steel. The first step is austenite conditining; the second step is isothermal ferritic phase transformation; the third step is bainite formation.

Regarding the industrial employment, the development of real-time process control strategies based on the control approach discussed in this thesis is a very important task. Although the optimal control problem has only been considered for two-dimensional domains, the calculation time needed for the numerical solution is within the range of hours. For the reduction of computation time, recent developments in model reduction techniques seem to be a promising tool. The application of the efficient model reduction methods, such as the Proper Orthogonal Decomposition and the Discrete Empirical Interpolation Method, allows us to significantly reduce the computational complexity of the proposed optimization algorithms.

Appendices

Appendix A

Notations

Ω	bounded open subset of $\mathbb{R}^n,\ n = 1, 2, 3$
$\partial\Omega$	boundary of Ω
$Q := \Omega \times (0, T)$	space-time cylinder
θ	temperature
f	volume fraction of ferrite
m	volume fraction of martensite
D_γ	austenite grain size
ε	strain
w	vector of phase fractions y, z, $w = (y, z)^T$
u	displacement
σ	(Cauchy) stress tensor
δ_i	thermal expansion coefficient for phase i
L_i	latent heat for evolution of phase i
θ^i_{ref}	constant reference temperature for the expansion of phase i
ρ	mass density
c_p	specific heat capacity (scalar constant)
κ	heat conductivity (scalar constant)
θ^e	temperature of coolant
Λ_1	first Lamé parameter
Λ_2	second Lamé parameter
Λ	$\Lambda := \Lambda_1 + 2\Lambda_2$
λ	dilatometer measurement of temperature
τ	dilatometer measurement of displacement
$[f]_+$	positive part of function f, $[f]_+ = \max\{f, 0\}$
X	Banach space with norm $\|\cdot\|_X$
$C^k(0, T)$	space of k-times continuously differentiable functions on $[0, T]$
$C(\bar{Q})$	space of uniformly continuous functions on $\bar{Q} = \bar{\Omega} \times [0, T]$
$L^p(\Omega)$	set of all measurable functions having finite norm $\|f\|_{L^p(\Omega)} = \left(\int_\Omega |f(x)|^p dx \right)^{1/p}$
$L^\infty(\Omega)$	set of all measurable functions for which $\|f\|_{L^\infty(\Omega)} = \operatorname{ess\,sup}_{x\in\Omega} \|f(x)\|$ is finite

$W^{k,p}(\Omega)$	Sobolev space $W^{k,p}(\Omega) := \Big\{ f \in L^p(\Omega) : D^\alpha f \in L^p(\Omega), \lvert\alpha\rvert \le k \Big\}$ with norm $\|f\|_{W^{k,p}(\Omega)} = \Big(\sum\limits_{\lvert\alpha\rvert \le k} \int\limits_\Omega \lvert D^\alpha f\rvert^p dx \Big)^{1/p}$
$H^1(\Omega)$	Sobolev space $H^1(\Omega) := W^{1,2}(\Omega)$
$H^1(\Omega)^*$	dual space of $H^1(\Omega)$, i.e., space of bounded linear functionals on $H^1(\Omega)$
$(\cdot,\cdot)_\Omega$	inner product in $L^2(\Omega)$
$(\cdot,\cdot)_Q$	inner product in $L^2(0,T;L^2(\Omega))$
$(\cdot,\cdot)_{(0,T)}$	inner product in $L^2(0,T)$
$L^p(0,T;X)$	Banach space of equivalence classes of Bochner integrable functions $f : [0,T] \to X$ with norm $\|f\|_{L^p(0,T;X)} = \Big(\int\limits_0^T \|f\|_X^p dt \Big)^{1/p}$
$W^{k,p}(0,T;X)$	Sobolev space $W^{k,p}(0,T;X) = \Big\{ f \in L^p(0,T;X) : f^{(s)} \in L^p(0,T;X), s \le k \Big\}$
$W(0,T)$	Hilbert space $W(0,T) = \Big\{ f \in L^2(0,T;H^1(\Omega)) : f' \in L^2(0,T;H^1(\Omega)^*) \Big\}$
$\mathcal{L}(X,Y)$	space of linear bounded operators $A : X \to Y$ equipped with the operator norm $\|A\| = \sup\limits_{\|x\|_X = 1} \|Ax\|_Y$
χ_Σ	indicator function of the set Σ
$o(h)$	$f = o(h)$ as $x \to x_0$ means that $\lim_{x \to x_0} \frac{\lvert f(x)\rvert}{\lvert h(x)\rvert} = 0$

Appendix B

Utilized definitions and theorems

Definition B.1 (Bochner Integral)**.** *The space*

$$L^p(0,T;X)$$

consist of all measurable functions $\boldsymbol{u}:[0,T]\to X$ *with*

(i)

$$\|\boldsymbol{u}\|_{L^p(0,T;X)} := \left(\int_0^T \|\boldsymbol{u}(t)\|_X^p dt\right)^{1/p} < \infty$$

for $1 \le p < \infty$*, and*

(ii)

$$\|\boldsymbol{u}\|_{L^\infty(0,T;X)} := \operatorname*{ess\,sup}_{0\le t\le T} \|\boldsymbol{u}(t)\|_X < \infty.$$

Definition B.2. *The space*

$$C([0,T];X)$$

comprises all continuous functions $\boldsymbol{u}:[0,T]\to X$ *with*

$$\|\boldsymbol{u}\|_{C([0,T];X)} := \max_{0\le t\le T} \|\boldsymbol{u}(t)\|_X < \infty.$$

Definition B.3. *(i) The Sobolev space*

$$W^{1,p}(0,T;X)$$

consist of all functions $\boldsymbol{u}\in L^p(0,T;X)$ *such that* $\boldsymbol{u}'$ *exists in the weak sense and belongs to* $L^p(0,T;X)$*. Furthermore,*

$$\|\boldsymbol{u}\|_{W^{1,p}(0,T;X)} := \begin{cases} \left(\int_0^T \|\boldsymbol{u}(t)\|_X^p + \|\boldsymbol{u}'(t)\|_X^p dt\right)^{1/p}, & 1\le p<\infty \\ \operatorname*{ess\,sup}_{0\le t\le T}(\|\boldsymbol{u}(t)\|_X + \|\boldsymbol{u}'(t)\|_X), & p=\infty. \end{cases}$$

(ii) We write $H^1(0,T;X) = W^{1,2}(0,T;X)$*.*

Definition B.4. *Let V be a Banach space and V^* be a dual space of V. We denote by $W(0,T)$ the linear space of all $y \in L^2(0,T;V)$ having a (distributional) derivative $y' \in L^2(0,T;V^*)$, equipped with the norm*

$$\|y\|_{W(0,T)} = \left(\int_0^T (\|y(t)\|_V^2 + \|y'(t)\|_{V^*}^2) dt \right)^{1/2}.$$

The space $W(0,T) = \left\{ y \in L^2(0,T;V) : y' \in L^2(0,T;V^*) \right\}$ is a Hilbert space with the scalar product

$$(u,v)_{W(0,T)} = \int_0^T (u(t),v(t))_V dt + \int_0^T (u'(t),v'(t))_{V^*} dt.$$

Theorem B.1 (Calculus in an abstract space)**.** *Let $\boldsymbol{u} \in W^{1,p}(0,T;X)$ for some $0 \le p \le \infty$. Then*

(i) $\boldsymbol{u} \in C([0,T];X)$ (after possibly being redefined on a set of measure zero), and

(ii) $\boldsymbol{u}(t) = \boldsymbol{u}(s) + \int_s^t \boldsymbol{u}'(\tau) d\tau$ for all $0 \le s \le t \le T$

(iii) Furthermore, we have the estimate

$$\max_{0 \le t \le T} \|\boldsymbol{u}(t)\| \le C \|\boldsymbol{u}\|_{W^{1,p}(0,T;X)},$$

the constant C depending only on T.

Theorem B.2 (Sobolev embedding theorem)**.** *Let $\Omega \subset \mathbb{R}^N$ be a bounded Lipschitz domain, $1 < p < \infty$, and m a non-negative integer. Then the following embeddings are defined and continuous:*

$$W^{m,p}(\Omega) \hookrightarrow \begin{cases} L^q(\Omega) \text{ for all } 1 \le q \le \frac{Np}{N-mp}, & \text{if } mp < N, \\ L^q(\Omega) \text{ for all } 1 \le q < \infty, & \text{if } mp = N, \\ C(\overline{\Omega}), & \text{if } mp > N. \end{cases}$$

In particular, for $H^1(\Omega) = W^{1,2}(\Omega)$ we obtain

$$\begin{aligned} &\text{if } \Omega \subset \mathbb{R}^2 \ : \quad H^1(\Omega) \hookrightarrow L^q(\Omega) \quad \text{for all } 1 \le q < \infty \\ &\text{if } \Omega \subset \mathbb{R}^3 \ : \quad H^1(\Omega) \hookrightarrow L^6(\Omega). \end{aligned}$$

Theorem B.3. *(Rellich–Kondrachov Compactness Theorem). Assume U is a bounded open subset of $\mathbb{R}^n$ and ∂U is C^1. Suppose $1 \le p < n$. Then*

$$W^{1,p}(U) \subset\subset L^q(U) \quad (\subset\subset \text{ denotes compact embedding})$$

for each $1 \le q < p^*$ where $p^* = \frac{np}{n-p}$ is the Sobolev conjugate of p.
Since $p^* > p$ and $p^* \to \infty$ as $p \to n$, we have in particular

$$W^{1,p}(U) \subset\subset L^p(U)$$

for all $1 \leq p \leq \infty$.
(If $n < p \leq \infty$*, this follows from Morrey's inequality and the Arzela–Ascoli compactness criterion.)*

Even if ∂U *is not assumed to be* C^1 *one achieves*

$$W_0^{1,p}(U) \subset\subset L^p(U).$$

(See e.g. Evans [19].)

Theorem B.4. *(Trace theorem). Assume* U *is bounded and* ∂U *is* C^1*. Then there exists a bounded linear operator*

$$T : W^{1,p}(U) \to L^p(\partial U)$$

such that
(i) the trace of u *on* ∂U *is defined by* $Tu = u|_{\partial U}$ *if* $u \in W^{1,p}(U) \cap C(\bar{U})$
(ii)

$$\|Tu\|_{L^p(\partial U)} \leq C\|u\|_{W^{1,p}(U)}$$

for each $u \in W^{1,p}(U)$*, with the constant* C *depending only on* p *and* U.
(See e.g. Evans [19].)

Theorem B.5. *(Carathéodory's Theorem) Let* $I = [0, T]$ *for fixed* $T > 0$ *and* $f : I \times \mathbb{R}^k \to \mathbb{R}^k$ *satisfying the following conditions:*

(Carathéodory mapping)

$$f(\cdot, \zeta) \text{ is measurable for all } \zeta \in \mathbb{R}^k \tag{B.1}$$

$$f(t, \cdot) \text{ is continuous for almost all } t \in I \tag{B.2}$$

(Growth condition)

$$|f(t, z)| \leq \gamma(t) + C|z| \text{ with some } \gamma \in L^1(I). \tag{B.3}$$

Then:

(i) The initial-value problem

$$\frac{dz}{dt} = f(t, z(t)) \text{ for almost all } t \in I, z(0) = z_0 \tag{B.4}$$

has a solution $z \in W^{1,1}(I; \mathbb{R}^k)$ *on the interval* $I = [0, T]$.

(ii) If $f(t, \cdot)$ *is also Lipschitz continuous in the sense*

$$|f(t, z_1) - f(t, z_2)| \leq L(t)|z_1 - z_2|$$

with $L \in L^1(I)$*, then the solution is unique.*

(This variant e.g. in Roubíček [66].)

Lemma B.1. *(Gronwall's Lemma) Let $c \in L^\infty(0,t_E)$ and $a \in L^1(0,t_E)$ denote non-negative functions. If a function $u \in L^\infty(0,t_E)$ satisfies*

$$0 \leq u(t) \leq c(t) + \int_0^t a(s)u(s)ds, \quad t \in (0,t_E)$$

then

$$0 \leq u(t) \leq c(t) + \int_0^t c(s)a(s)\exp\left(\int_s^t a(\tau)d\tau\right)ds, \quad t \in (0,t_E).$$

In particular, if $c(t) = c$ and $a(t) = a$ for almost every $t \in (0,t_E)$, then

$$0 \leq u(t) \leq ce^{at}, \quad t \in (0,t_E).$$

(This variant e.g. in Brokate and Sprekels [13].)

Theorem B.6 (Young's inequality)**.** *Let $1 \leq p,\, q \leq \infty$ with $\frac{1}{p} + \frac{1}{q} = 1$. Then*

$$ab \leq \varepsilon a^p + C(\varepsilon)b^q, \quad (a,b>0,\ \varepsilon>0)$$

for $C(\varepsilon) = (\varepsilon p)^{(-q/p)}q^{-1}$.

Theorem B.7 (Hölder's inequality)**.** *Let $1 \leq p,\, q \leq \infty$ with $\frac{1}{p}+\frac{1}{q} = 1$. Then if $f \in L^p(U)$ and $g \in L^q(U)$*

$$\int_U fgdx \leq \|f\|_{L^p(U)}\|g\|_{L^q(U)}.$$

Theorem B.8 (Banach's Fixed Point Theorem)**.** *Consider the nonlinear equation*

$$x = Tx, \qquad x \in M. \tag{$*$}$$

Suppose that

1. *$T\colon M \subseteq X \to M$, i.e. M is mapped into itself be an operator T;*
2. *M is a closed non-empty set in a complete metric space (X,d);*
3. *T is k-contractive, i.e.*
$$d(Tx,Ty) \leq kd(x,y)$$
for all $x,y \in M$ and for a fixed k, $0 \leq k < 1$.

Then we may conclude the following:

- *Existence and uniqueness: Equation $(*)$ has exactly one solution, i.e. T has exactly one fixed point on M;*
- *Convergence of the iteration: The sequence (x_n) of successive approximations converges to the solution x for an arbitrary choice of initial points x_0 in M;*

- *Error estimates: For all $n = 1, 2, 3, \ldots$ we have the a priori error estimate*

$$d(x_n, x) \leq k^n (1-k)^{-1} d(x_0, x_1),$$

and the a posteriori error estimate

$$d(x_{n+1}, x) \leq k(1-k)^{-1} d(x_n, x_{n+1});$$

- *Rate of convergence: For all $n = 1, 2, 3, \ldots$ we have*

$$d(x_{n+1}, x) \leq k d(x_n, x).$$

Theorem B.9 (Riesz Representation Theorem)**.** *Let X be a real Hilbert space. X^* can be canonically identified with X. More precisely, for each $\phi \in X^*$ there exists a unique element $u \in X$ such that*

$$\langle \phi, v \rangle = (u, v) \qquad \text{for all } v \in X^*.$$

The mapping $\phi \to u$ is a linear isomorphism of X^* onto X.

Definition B.5. *Let X and Y be two normed linear spaces, $A \in \mathcal{L}(X, Y)$. There exists a unique bounded linear operator $A^* \in \mathcal{L}(Y^*, X^*)$, named adjoint operator of A and defined by*

$$\langle Au, v \rangle_{X, X^*} = \langle u, A^* v \rangle_{Y, Y^*}$$

for all $u \in X$ and $v \in Y^*$. Note A is symmetric if $A^* = A$.

If X and Y are Hilbert spaces, then an adjoint operator of A can be defined using the inner product

$$(Au, v)_Y = (u, A^* v)_X$$

for all $u \in X$ and $v \in Y$.

Definition B.6. *Let X be a real Banach space. We say a sequence $\{u_k\}_{k=1}^{\infty} \subset X$ converges weakly to $u \in X$, written $u_k \rightharpoonup u$, if*

$$\langle \phi, u_k \rangle_{X^*, X} \to \langle \phi, u \rangle_{X^*, X}$$

for each bounded linear functional $\phi \in X^*$.

Theorem B.10 (Weak compactness)**.** *Let X be a reflexive Banach space, i.e. $X^{**} = X$, and suppose the sequence $\{u_k\}_{k=1}^{\infty} \subset X$ is bounded. Then there exists a subsequence $\{u_{k_j}\}_{j=1}^{\infty} \subset \{u_k\}_{k=1}^{\infty}$ and $u \in X$ such that $u_{k_j} \rightharpoonup u$.*

Theorem B.11 (Mazur's theorem)**.** *A convex, closed subset of the real Banach space X is weakly closed.*

Theorem B.12 (Weak lower semicontinuity)**.** *Let C be a Hilbert space and $C \subset X$ be a non-empty convex and closed subset of a normed space X and $f \colon C \to \mathbb{R}$ be continuous and convex. Then f is weakly lower semicontinuous, i.e. if $u_n \rightharpoonup u$ in C implies that $\liminf_{n \to \infty} f(u_n) \geq f(x)$.*

Definition B.7 (Nemytskii-operator)**.** *Let $E \subset \mathbb{R}^n$ be a bounded and measurable set, and let $\phi = \phi(x, y)\colon E \times \mathbb{R} \to \mathbb{R}$ a real valued function. The mapping Φ defined by*

$$\Phi(y) := \phi(\cdot, y(\cdot)),$$

which assigns to a function $y = y(x)\colon E \to \mathbb{R}$ the function $z\colon E \to \mathbb{R},\ z(x) = \phi(x, y(x))$, is called a Nemytskii-operator or superposition-operator.

Definition B.8. *Let $E \subset \mathbb{R}^m$, $m \in \mathbb{N}$, be a bounded set, and let $\varphi = \varphi(x, y) : E \times \mathbb{R} \to \mathbb{R}$ denote a function of the domain variable x and the function variable y. Let φ be k-times differentiable with respect to y for almost every $x \in E$. We say that φ satisfies the boundedness condition of order k if there exists some $K > 0$ such that*

$$\left|D_y^l \varphi(x, 0)\right| \leq K \quad \forall 0 \leq l \leq k, \qquad \text{for a.e.} \quad x \in E.$$

We say that φ satisfies the local Lipschitz condition of order k if for every $M > 0$ there is some (Lipschitz) constant $L(M) > 0$ such that

$$\left|D_y^k \varphi(x, y_1) - D_y^k \varphi(x, y_2)\right| \leq L(M)\,|y_1 - y_2|$$

for all $y_i \in \mathbb{R}$ such that $|y_i| \leq M$, $i = 1, 2$.

Theorem B.13 (Differentiability of Nemytskii operators)**.** *Suppose that function $\varphi = \varphi(x, y) : E \times \mathbb{R} \to \mathbb{R}$ is measurable with respect to $x \in E$ for all $y \in \mathbb{R}$ and twice differentiable with respect to y for almost every $x \in E$. Let φ satisfy the boundedness and local Lipschitz condition of order $k = 2$ from Definition B.8. Then the Nemytskii operator Φ generated by φ is twice continuously Fréchet differentiable in $L^\infty(E)$, and the second derivative can be evaluated through*

$$\left(\Phi''(y)[y_1, y_2]\right)(x) = \varphi_{yy}\big(x, y(x)\big) y_1(x) y_2(x).$$

Bibliography

[1] W. Alt. *Nichtlineare Optimierung: Eine Einführung in Theorie, Verfahren und Anwendungen*. Vieweg Studium: Aufbaukurs Mathematik. Vieweg+Teubner Verlag, 2002.

[2] *ArcelorMittal Corporation, Dual Phase Steels, Product Sheet.* URL: `http://www.arcelormittal.com/automotive/saturnus/sheets/A1_EN.pdf`.

[3] *Atlas of isothermal transformation and cooling transformation diagrams*. American Society for Metals, 1977.

[4] L. Bäcke. "Modeling the Microstructural Evolution during Hot Deformation of Microalloyed Steels". PhD thesis. KTH, Materials Science and Engineering, 2009.

[5] M. Bergounioux, K. Ito, and K. Kunisch. "Primal-dual strategy for constrained optimal control problems". In: *SIAM J. Control and Optimization* 37 (1999), pp. 1176–1194.

[6] H. Bhadeshia and R. Honeycombe. *Steels: Microstructure and Properties: Microstructure and Properties*. Elsevier Science, 2011.

[7] S. K. Biswas, S.-J. Chen, and A. Satyanarayana. "Optimal temperature tracking for accelerated cooling processes in hot rolling of steel". In: *Dynamics and Control* 7.4 (1997), pp. 327–340.

[8] W. Bleck. *Werkstoffkunde Stahl für Studium und Praxis*. Wissenschaftsverlag Mainz, 2001.

[9] W. Bleck, D. Hömberg, U. Prahl, P. Suwanpinij, and N. Togobytska. "Optimal Control of a Cooling Line for Production of Hot Rolled Dual Phase Steel". In: *Steel Research Int.* 85 (2014), pp. 1328–1333.

[10] S. Boettcher. "Modelling, Analysis and Simulation of Thermo-Elasto-Plasticity with Phase Transitions in Steel". PhD thesis. University of Bremen, 2012.

[11] D. Braess. *Finite Elemente: Theorie, Schnelle Löser und Anwendungen in der Elastizitätstheorie*. Springer London, Limited, 2007.

[12] B. Bramfitt and A. Benscoter. *Metallographer's Guide: Practice and Procedures for Irons and Steels*. EngineeringPro collection. ASM International, 2001.

[13] M. Brokate and J. Sprekels. *Hysteresis and Phase Transitions*. Applied Mathematical Sciences 121. Springer, 1996.

[14] K. Chelminski, D. Hömberg, and D. Kern. "On a thermomechanical model of phase transitions in steel". In: *Adv. Math. Sci. Appl.* 18 (2008), pp. 119–140.

[15] S.-X. Chen, J. Zou, and X. Fu. "Coupled models of heat transfer and phase transformation for the run-out table in hot rolling". In: *Journal of Zhejiang University Science A* 9.7 (2008), pp. 932–939.

[16] J. Dieudonne. *Foundations of Modern Analysis*. Pure and Applied Mathematics. Read Books, 1960.

[17] B. Donnay, J. C. Herman, V. Leroy, U. Lotter, R. Grossterlinden, and H. Pircher. "Microstructure evolution of C-Mn steels in the hot deformation process: The stripcam model". In: *Proc. of 2nd Int. Conf. on Modelling of Metal Rolling Processes, ed. by J. H. Beynon, P. Ingham, H. Teichert and K. Waterson, The Institute of Materials, London (UK)* 23 (1996).

[18] J. Edgar. *Steel identification using hardness testing*. URL: `http://prolinesystems.net/files/Steel-Identification-Using-Hardness-Testing.pdf`.

[19] L. C. Evans. *Partial Differential Equations*. Graduate studies in mathematics. American Mathematical Society, 2010.

[20] J. Fuhrmann et al. *pdelib*. URL: `http://www.wias-berlin.de/software/pdelib`.

[21] H. Goldberg and F. Tröltzsch. "Second-order sufficient optimality conditions for a class of nonlinear parabolic boundary control problems". In: *SIAM Journal on Control and Optimization* 31.4 (1993), pp. 1007–1025.

[22] H. Goldberg and F. Tröltzsch. "On a Lagrange–Newton method for a nonlinear parabolic boundary control problem". In: *Optimization Methods and Software* 8.3-4 (1998), pp. 225–247.

[23] H. Goldberg and F. Tröltzsch. "On a SQP-multigrid technique for nonlinear parabolic boundary control problems". In: *Optimal Control: Theory, Algorithms, and Applications* (1998), pp. 154–177.

[24] M. Graf, D. Hömberg, R. Kawalla, N. Togobytska, and W. Weiss. "Identification, simulation and optimal control of heat transfer in cooling lines of hot strip rolling mills". In: *WIAS preprint* (2013).

[25] W. Grever, A. Binder, H. W. Engl, and K. Mörwald. "Optimal cooling strategies in continuous casting of steel with variable casting speed". In: *Inverse Problems in Engineering* 2.4 (1996), pp. 289–300.

[26] W. Gruver and E. Sachs. *Algorithmic Methods in Optimal Control*. Research Notes in Mathematics Series. Pitman Pub., 1981.

[27] T. Hashimoto, Y. Yoshioka, and T. Ohtsuka. "Model predictive control for hot strip mill cooling system". In: *Proceedings of the IEEE International Conference on Control Applications*. 2010, pp. 646–651.

[28] F. Hengerer, B. Strässle, and P. Bremi. *Berechnung der Abkühlungsvorgänge beim Öl- und Lufthärten zylinder- und plattenförmiger Werkstücke aus legiertem Vergütungsstahl mit Hilfe einer elektronischen Rechenanlage: Calcul, à l'aide d'une calculatrice électronique, des processus de refroidissement se déroulant lors de la trempe à l'huile et à l'air de cylindres et de plaques en acier allié*. Bericht des Werkstoffausschusses des Vereins deutscher Eisenhüttenleute. Verl. Stahleisen, 1969.

[29] M. Hintermüller, S. Volkwein, and F. Diwoky. "Fast Solution Techniques in Constrained Optimal Boundary Control of the Semilinear Heat Equation". In: *Control of Coupled Partial Differential Equations* 155 (2007), pp. 119–147.

[30] M. Hinze, R. Pinnau, M. Ulbrich, and S. Ulbrich. *Optimization with PDE Constraints*. Mathematical Modelling: Theory and Applications. Springer, 2010.

[31] B. Hofmann. *Mathematik inverser Probleme*. Mathematik für Ingenieure und Naturwissenschaftler. Teubner B.G. GmbH, 1999.

[32] D. Hömberg. "A mathematical model for induction hardening including mechanical effects". In: *Nonlinear Analysis: Real World Applications* 5.1 (2004), pp. 55–90.

[33] D. Hömberg. "A numerical simulation of the Jominy end-quench test". In: *Acta Materialia* 44.11 (1996), pp. 4375–4385.

[34] D. Hömberg. "Irreversible phase transitions in steel". In: *Mathematical Methods in the Applied Sciences* 20.1 (1997), pp. 59–77.

[35] D. Hömberg and J. Sokolowski. "Optimal shape design of inductor coils for surface hardening". In: *SIAM Journal on Control and Optimization* 42.3 (2003), pp. 1087–1117.

[36] D. Hömberg, N. Togobytska, and M. Yamamoto. "On the evaluation of dilatometer experiments". In: *Applicable Analysis* 88.5 (2009), pp. 669–681.

[37] D. Hömberg and W. Weiss. "PID control of laser surface hardening of steel". In: *Control Systems Technology, IEEE Transactions on Control Systems Technology* 14.5 (2006), pp. 896–904.

[38] D. Hömberg and S. Volkwein. "Control of laser surface hardening by a reduced-order approach using proper orthogonal decomposition". In: *Mathematical and Computer Modelling* 38.10 (2003), pp. 1003–1028.

[39] V. Isakov. *Inverse Problems for Partial Differential Equations*. Applied Mathematical Sciences 127. Springer, 1998.

[40] S. Kabanikhin. "Definitions and examples of inverse and ill-posed problems". In: *Journal of Inverse and Ill-Posed Problems* 16.4 (2008), pp. 317–357.

[41] C. Kelley. *Iterative Methods for Optimization*. Frontiers in Applied Mathematics. Society for Industrial and Applied Mathematics, 1999.

[42] D. Kern. "Analysis and numerics for a thermomechanical phase transition model in steel". PhD thesis. TU Berlin, 2011.

[43] P. Knabner and L. Angermann. *Numerik Partieller Differentialgleichungen/Numerical Analysis of Partial Differential Equations: Eine Anwendungsorientierte Einführung/An Application-oriented Introduction*. Springer Lehrbuch. Springer Berlin Heidelberg, 2000.

[44] D. Koistinen and R. Marburger. "A general equation prescribing the extent of the austenite-martensite transformation in pure iron-carbon alloys and plain carbon steels". In: *Acta Metallurgica* 7.1 (1959), pp. 59–60.

[45] F.-S. Kupfer. "An infinite-dimensional convergence theory for reduced SQP methods in Hilbert space". In: *SIAM Journal on Optimization* 6.1 (1996), pp. 126–163.

[46] F.-S. Kupfer and E. W. Sachs. "A prospective look at SQP methods for semilinear parabolic control problems". In: *Optimal Control of Partial Differential Equations*. Ed. by K. H. Hoffmann and W. Krabs. Vol. 149. Lect. Notes in Control and Inform. Sciences. Springer, 1991, pp. 143–157.

[47] F.-S. Kupfer and E. W. Sachs. "Numerical solution of a nonlinear parabolic control problem by a reduced SQP method". In: *Computational Optimization and Applications* 1.1 (1992), pp. 113–135.

[48] T. Kvackaj and L. Mamuzic. "A quantitative characterization of austenite microstructure after deformation in nonrecrystallization region and its influence on ferrite microstructure after transformation". In: *ISIJ International* 38.11 (1998), pp. 1270–1276.

[49] G. Landl, H. W. Engl, J. Chen, and K. Zeman. "Optimal strategies for the cooling of steel strips in hot strip mills". In: *Inverse Problems in Engineering* 2.2 (1995), pp. 103–118.

[50] J.-B. Leblond and J. Devaux. "A new kinetic model for anisothermal metallurgical transformations in steels including effect of austenite grain size". In: *Acta Metallurgica* 32.1 (1984), pp. 137–146.

[51] S. Lenhart and D. Wilson. "Optimal control of a heat transfer problem with convective boundary condition". In: *Journal of Optimization Theory and Applications* 79.3 (1993), pp. 581–597.

[52] R. Lezius and F. Tröltzsch. "Theoretical and numerical aspects of controlled cooling of steel profiles". In: *Progress in Industrial Mathematics at ECMI 94*. Springer, 1996, pp. 380–388.

[53] U. Lorenz. "Anwendung von Werkstoffmodellen auf die Phasenumwandlung und die Austenitkonditionierung von Stählen". PhD thesis. RWTH Aachen, 2003.

[54] P. Mallick. *Materials, Design and Manufacturing for Lightweight Vehicles*. Woodhead Publishing Series in Composites Science and Engineering. Elsevier Science, 2010.

[55] M. Militzer, E. Hawbolt, and T. Meadowcroft. "Microstructural model for hot strip rolling of high-strength low-alloy steels". In: *Metallurgical and Materials Transactions* 31A.4 (2000), pp. 1247–1259.

[56] J. Nocedal and S. Wright. *Numerical Optimization*. Springer Series in Operations Research and Financial Engineering. Springer, 2006.

[57] L. Panizzi. "On a mathematical model for case hardening of steel". PhD thesis. TU Berlin, 2010.

[58] A. Pazy. *Semigroups of Linear Operators and Applications to Partial Differential Equations*. Applied Mathematical Sciences 44. Springer, 1992.

[59] H. Petersen. *The properties of helium: density, specific heats, viscosity, and thermal conductivity at pressures from 1 to 100 bar and from room temperature to about 1800 K*. Tech. rep. 1970.

[60] A. Prilepko, D. Orlovsky, and I. Vasin. *Methods for Solving Inverse Problems in Mathematical Physics*. CRC Press, 2000.

[61] F. Puschmann. "Experimentelle Untersuchung der Spraykühlung zur Qualitätsverbesserung durch definierte Einstellung des Wärmeübergangs". PhD thesis. Otto-von-Guericke-Universität Magdeburg, Universitätsbibliothek, 2003.

[62] A. Quarteroni, R. Sacco, and F. Saleri. *Numerical Mathematics*. Texts in Applied Mathematics. Springer, 2007.

[63] M. Rathore and R. Kapuno. *Engineering Heat Transfer*. Jones & Bartlett Learning, 2011.

[64] J.-P. Raymond and F. Tröltzsch. "Second order sufficient optimality conditions for nonlinear parabolic control problems with state constraints". In: *Discrete and Continuous Dynamical Systems* 6.2 (2000), pp. 431–450.

[65] J. Rödel. *Beitrag zur Modellierung des Elektronenstrahlhärtens von Stahl*. Flux-Verlag, 1997.

[66] T. Roubíček. *Nonlinear Partial Differential Equations with Applications*. Vol. 153. International Series of Numerical Mathematics. Birkhäuser, 2013.

[67] S. Serajzadeh. "Prediction of temperature distribution and phase transformation on the run-out table in the process of hot strip rolling". In: *Applied Mathematical Modelling* 27.11 (2003), pp. 861–875.

[68] P. Spellucci. *Numerische Verfahren der nichtlinearen Optimierung*. ISNM Lehrbuch. Birkhäuser Verlag AG, 1993.

[69] M. Spittel and T. Spittel. *Metal Forming Data of Ferrous Alloys - deformation behaviour*. Ed. by H. Warlimont. Vol. 2C1. Landolt-Börnstein - Group VIII Advanced Materials and Technologies. Springer Berlin Heidelberg, 2009.

[70] K. Strehmel, R. Weiner, and H. Podhaisky. *Numerik gewöhnlicher Differentialgleichungen: Nichtsteife, steife und differential-algebraische Gleichungen*. Vieweg+Teubner Verlag, 2012.

[71] M. Suehiro, T. Senuma, T. Oda, and S. Konishi. *Development of mathematical model for predicting transformation of high-carbon steel during cooling on runouttable and its application to on-line temperature control of hot strip mill*. Nippon Steel Technical report. Nippon Steel, 1995.

[72] C. Sun, H. Han, J. Lee, Y. Jin, and S. Hwang. "A finite element model for the prediction of thermal and metallurgical behavior of strip on run-out-table in hot rolling". In: *ISIJ International* 42.4 (2002), pp. 392–400.

[73] W. Sun, M. Militzer, E. Hawbolt, and T. Meadowcroft. "Analysis and modeling of austenite grain refinement and growth during hot rolling". In: *Iron and steelmaker* 25.5 (1998), pp. 85–94.

[74] P. Suwanpinij. "Multi-scale modelling of hot rolled dual-phase steels for process design". PhD thesis. RWTH Aachen, 2012.

[75] P. Suwanpinij, N. Togobytska, C. Keul, W. Weiss, U. Prahl, D. Hömberg, and W. Bleck. "Phase Transformation Modelling and Parameter Identification from Dilatometric Investigations". In: *Steel Research Int.* 10 (2008), pp. 793–799.

[76] P. Suwanpinij, N. Togobytska, U. Prahl, W. Weiss, D. Hömberg, and W. Bleck. "Numerical Cooling Strategy Design for Hot Rolled Dual Phase Steel". In: *Steel Research Int.* 11 (2010), pp. 1001–1009.

[77] H. Tanabe. *Equations of evolution*. Monographs and studies in mathematics. Pitman, 1979.

[78] G. Totten and M. Howes. *Steel Heat Treatment Handbook*. CRC Press, 1997.

[79] F. Tröltzsch. *Optimal Control of Partial Differential Equations: Theory, Methods, and Applications*. Graduate Studies in Mathematics. American Mathematical Society, 2010.

[80] F. Tröltzsch. "An SQP Method for the Optimal Control of a Nonlinear Heat Equation". In: *Control and Cybernetics* 23 (1994), pp. 268–288.

[81] ULSAB-AVC. *Advanced Vehicle Concepts, Overview report*. January 2002.

[82] A. Unger and F. Tröltzsch. "Fast solution of optimal control problems in the selective cooling of steel". In: *ZAMM-Journal of Applied Mathematics and Mechanics/Zeitschrift für Angewandte Mathematik und Mechanik* 81.7 (2001), pp. 447–456.

[83] *VDI-Wärmeatlas. Buch-Version: Berechnungsblätter für den Wärmeübergang*. VDI-Buch. Springer-Verlag GmbH, 2002.

[84] Verein Deutscher Eisenhüttenleute. *Steel: A Handbook for Materials Research and Engineering*. Springer, 1992.

[85] R. Viščorová. "Untersuchung des Wärmeübergangs bei der Spritzwasserkühlung unter Berücksichtigung des Einflusses der Verzunderung". PhD thesis. Institut für Metallurgie, TU Clausthal, 2007.

[86] A. Visintin. "Mathematical models of solid-solid phase transitions in steel". In: *IMA Journal of Applied Mathematics* 39.2 (1987), pp. 143–157.

[87] B.-X. Wang, D.-H. Zhang, J. Wang, M. Yu, N. Zhou, and G.-M. Cao. "Application of neural network to prediction of plate finish cooling temperature". In: *Journal of Central South University of Technology* 15 (2008), pp. 136–140.

[88] S. Whitaker. *Fundamental principles of heat transfer*. Pergamon Press, 1977.

[89] M. Wolff and M. Böhm. *Phasenumwandlungen und Umwandlungsplastizität bei Stählen im Konzept der Thermoelasto-Plastizität*. Tech. rep. ZeTeM Reports, Universität Bremen, 2002.

[90] M. Wolff, S. Boettcher, and M. Böhm. *Phase transformations in steel in the multiphase case–general modelling and parameter identification*. Report 07–02. Zentrum für Technomathematik, Univ. Bremen, 2007.

[91] M. Wolff, F. Frerichs, and N. Lysenko. *Bewerten von Modellen der Martensitbildung bei nichtmonotoner Abkühlung für den Stahl 100Cr6*. Zentrum für Technomathematik, Univ. Bremen, 2007.

[92] Y. Zheng, N. Li, and S. Li. “Hot-rolled strip laminar cooling process plant-wide temperature monitoring and control”. In: *Control Engineering Practice* 21.1 (2013), pp. 23–30.